Synthesis and Biological Evaluation of Trimeric 2,5-Disubstituted Benzimidazoles and Related Trinuclear Ruthenium(II) Organometallic Complexes

Athi Welsh

University of Cape Town

November 2019

Synthesis and Biological Evaluation of Trimeric 2,5-Disubstituted Benzimidazoles and Related Trinuclear Ruthenium(II) Organometallic Complexes

by

Athi Welsh

Dissertation presented for the degree

Master of Science

Supervisors: **Associate Professor Gregory S. Smith**

Professor Sharon Prince

Department of Chemistry

University of Cape Town

Rondebosch

Cape Town

7701

November 2019

Declaration

I know the meaning of plagiarism and declare that "***Synthesis and biological evaluation of trimeric 2,5-disubstituted benzimidazoles and related trinuclear ruthenium(II) organometallic complexes"*** is my own work and has not been previously presented for the award of any degree at any university. All sources of information are cited and fully referenced at the end of each chapter.

Signed by candidate

SIGNATURE: …….

DATE: 29/ 11/ 2019

Acknowledgements

First and foremost, I would like to extend my sincerest gratitude and appreciation to my supervisors, Associate Professor Gregory S. Smith and Professor Sharon Prince. Their invaluable guidance, insight, constructive criticism and encouragement throughout the course of this project were imperative to my development as a researcher and as an individual. I would also like to thank our collaborator, Professor Vladimir Arion (Institute of Inorganic Chemistry, University of Vienna).

I would like to thank Mrs. Deirdre Brooks for the unmatched administrative work and encouragement throughout my career. Further thanks extend to the UCT analytical staff, namely Mr. Pete Roberts for running NMR experiments and Dr. Hong Su for single crystal X-ray diffraction studies. A special thanks to Dr. Marietjie Stander (University of Stellenbosch) running ESI-MS experiments.

A special thanks to my friends and colleagues, Fatima-Zahra Abrahams, Diana Melis, Richard Ferger and Allan Huysamen for useful discussions and friendship. A special thanks to the members of the Organometallic Research group and the T-Box Lab for helpful discussions and assistance. My sincerest appreciation is extended to my mentors and friends, Dr. Siyabonga Ngubane, Mr. Thato Medupe and Mr. Shepherd Siangwata, for guidance, support, discussion and most importantly friendship.

I would like to thank the National Research Foundation (NRF) and the University of Cape Town for their financial support throughout my degree.

Lastly, I would like to thank my family and close friends for their unparalleled support throughout this journey and in life. A special thanks to the Nate Dogg to my Warren G, Stephen De Doncker, your support, insight and encouragement throughout my university career has left a mark on me. To my family, especially my mother and my sisters, I thank them for the inspiration, love and support throughout my life and this journey.

Publications

Journal article:

Published in *Dalton Transactions*,

Athi Welsh, Laa-iqa Rylands, Vladimir B. Arion, Sharon Prince and Gregory S. Smith, ***Synthesis and antiproliferative activity of benzimidazole-based, trinuclear neutral cyclometallated and cationic, N^N-chelated ruthenium(II) complexes,*** 2020, DOI: 10.1039/c9dt03902c.

Conference/ Symposia Contributions

***Oral Presentation**: Athi Welsh, Sharon Prince and Gregory S. Smith,* Biological studies of multinuclear hybrid organometallic complexes as anticancer and antiplasmodial agents*, presented at the Austrian-Slovak mini-symposium at the Institute of Inorganic Chemistry, University of Vienna*, **2018**.

***Poster Presentation**: Athi Welsh, Sharon Prince and Gregory S. Smith,* Synthesis, characterization and preliminary cell proliferation studies of multinuclear benzimidazole-based cyclometallated and cationic ruthenium(II) complexes*, presented at the 9th International Symposium of Bioorganometallic Chemistry (ISBOMC) at the University of York, England,* **2019**.

***Poster Presentation**: Athi Welsh, Sharon Prince and Gregory S. Smith,* Synthesis and antiproliferative studies of multinuclear benzimidazole-based cyclometallated and cationic ruthenium(II) complexes*, presented at the 12th Annual Science Postgraduate Symposium at Stellenbosch University, South Africa,* **2019**.

***Poster Presentation**: Athi Welsh, Sharon Prince and Gregory S. Smith,* Synthesis, characterization and preliminary cell proliferation studies of multinuclear benzimidazole-based cyclometallated and cationic ruthenium(II) complexes*, presented at the 2nd Annual UCT Chemistry PhD Symposium at the University of Cape Town, South Africa,* **2019**.

***Poster Presentation**: Athi Welsh, Sharon Prince, Gregory S. Smith,* Synthesis, characterization and biological studies of trinuclear benzimidazole-based *C^N*- and *N^N*-chelated ruthenium(II) complexes*, presented at the Cape Organometallic Symposium (COS) at the University of Cape Town, South Africa,* **2019**.

Abstract

Cancer remains a global epidemic, with millions affected by the Non-Communicable Disease (NCD) annually. While cisplatin and its platinum(II) derivatives remain widely used chemotherapeutic agents, the undesirable side effects associated with the use of these metallodrugs and the evolution of resistance by cancers limit the scope of use of these platinum(II) complexes. Working towards addressing these issues, research has focused on the development of chemotherapeutic agents based on alternate platinum-group metals (PGMs), with ruthenium metallodrugs being among the most successful in this category. The combination of pharmacophores onto dendritic scaffolds and the combination of these scaffolds with PGMs, yielding multinuclear organometallic complexes is a strategy that has been widely used in rational drug design. However, there is limited research into multinuclear ruthenium compounds, specifically trimetallic ruthenium compounds. With this in mind, the purpose of this study was to synthesize and characterize a series of 2,5-disubstituted benzimidazole-based trimeric compounds and related trinuclear complexes bearing ruthenium(II) metal centers at the periphery. All of the synthesized compounds were screened for their *in vitro* cytotoxicity against the MCF-7 and MDA-MB-231 breast cancer cell lines and the 501 melanoma cell line.

A series of 2,5-disubstituted benzimidazole trimeric ligands were prepared from the cyclo-condensation reaction of trimeric *o*-phenylenediamines with either benzaldehyde or 2-pyridinecarboxaldehyde. Complexation of these 2,5-disubstituted tris-benzimidazole ligands with $[RuCl(\mu\text{-}Cl)(p\text{-cymene})]_2$ afforded the respective trinuclear neutral *C^N*-chelated and cationic *N^N*-chelated ruthenium(II) complexes. In addition to this, a series of 2-ferrocenyl benzimidazole trimeric compounds were synthesized as non-planar bioisosteres of the 2-aryl 5-substituted benzimidazole trimeric ligands. All of the synthesized compounds were fully characterized using an array of spectroscopic (^{1}H, $^{13}C\{^{1}H\}$, $^{31}P\{^{1}H\}$ and $^{19}F\{^{1}H\}$ NMR, FT-IR spectroscopy) and analytical (mass spectrometry and elemental analysis) techniques.

Preliminary cytotoxic screening of all of the synthesized compounds against the MCF-7 breast adenocarcinoma cell line was done. This preliminary investigation revealed that the 2-pyridyl

trimeric ligands and the corresponding trinuclear cationic complexes show superior activity relative to their respective 2-phenyl trimeric ligand counterparts and the corresponding neutral cyclometallated complexes. Consequently, the 2-pyridyl tris-benzimidazole ligands and their corresponding cationic complexes were selected for cytotoxic evaluation against additional cancer cell lines (the MDA-MB-231 breast cancer and the 501mel cancer cell lines). Overall, a 2-pyridyl tris-benzimidazole ligand and two trimetallic cationic complexes showed anticancer activity either comparable or superior to that of cisplatin against the MCF-7 breast cancer cell line ($IC_{50} \leq 35$ µM). Additionally, a 2-pyridyl trimeric benzimidazole ligand and a trimetallic cationic *N^N*-ruthenium(II) complex showed mild activity against the MDA-MB-231 and 501mel cancer cell lines, respectively ($IC_{50} < 35$ µM in both cell lines). Selectivity studies based on the non-tumorigenic MCF-12A breast epithelial cell line indicated that selected compounds had low cytotoxicity towards non-tumorigenic cells and showed enhanced selectivity towards the MCF-7 cancerous cells relative to cisplatin. Solvent stability studies of the cationic *N^N*-ruthenium(II) complexes show that these compounds are stable in DMSO for 48 hours under physiological conditions. Additionally, preliminary mechanistic studies of the most active complex indicate that the complex does not interact with guanosine 5'-monophosphate (5'-GMP), suggesting that this complex elicits cytotoxicity *via* an alternative mechanism of action.

Abbreviations, Symbols and Units

5'-GMP	Guanosine 5’-monophosphate disodium
°	Degree
µM	Micro molar (10^{-6} M)
δ	Chemical shift
501mel	Human metastatic melanoma cells
Å	Angstrom (10^{-10} m)
A2780	Human ovarian cancer cells
A2780cisR	Cisplatin-resistant Human ovarian cancer cells
ATP	Adenosine triphosphate
ATR	Attenuated total reflection
br s	Broad singlet
cisplatin	*cis*-dichloridodiammineplatinum(II)
COSY	Homonuclear correlation spectroscopy
CSC	Cancer stem cell
d	Doublet
DCM	Dichloromethane
DMF	Dimethylformamide
DMSO (d6)	Deuterated dimethylsulfoxide
DNA	Deoxyribonucleic acid
EPR	Enhanced permeability and retention
eq.	Equivalent
ESI-MS	Electrospray ionization mass spectrometry
EtOAc	Ethyl acetate
EtOH	Ethanol
FT-IR	Fourier-transform infrared spectroscopy
HCT116	Human colorectal cancer cells
HeLa	Human cervical cancer cells

HepG2	Human liver cancer cells
HMBC	Heteronuclear multiple-bond correlation spectroscopy
HMLER	Human breast cancer stem cells
HPLC	High-performance liquid chromatography
h	Hours
HSQC	Heteronuclear single-quantum correlation spectroscopy
IC_{50}	50% cell viability concentration
J	Coupling constant
LNCap	Human prostate cancer cells
m	Multiplet
MCF-12A	Human breast epithelial cells
MCF-7	Human breast adenocarcinoma cells
MDA-MB-231	Human breast cancer cells
MeCN	Acetonitrile
MeOH	Methanol
MHz	MegaHertz
mL	Millilitre(s)
MP	Melting point
MTT	3-(4,5-dimethylthiazol-2-yl)-2,5 diphenyltetrazolium bromide
NAMI-A	New anti-tumour metastasis inhibitor
NMR	Nuclear magnetic resonance
PC3	Human epithelial teratocarcinoma cells
PDT	Photodynamic therapy
Pet. Ether	Petroleum ether
PGM	Platinum group metal
ppm	Parts per million
PT	Proton transfer
PTA	1,3,5-triaza-7-phospaadamantane
RAED	Ruthenium arene ethylenediamine
RAPTA	Ruthenium arene PTA

ROS	Reactive oxygen species
RT	Room temperature
s	Singlet (NMR), Strong (IR)
S.I.	Selectivity index
sept.	Septet
t	Triplet
TFA	Trifluoroacetic acid
TLC	Thin layer chromatography
TMS	Tetramethylsilane
TNBC	Triple negative breast cancer
t_R	Retention time (minutes)
v/v%	Volume percentage
WHCO1	Human oesophageal cancer cells
XRD	X-ray diffraction

Table of Contents

Chapter 1

Advances in the Development of Multinuclear Organometallic Complexes as Anticancer Agents

1.1 Introduction

1.1.1 Cancer prevalence and mortality

Cancer remains one of the major causes of death both in developed and developing countries, including South Africa. The non-contagious disease affects approximately 600 000 people and accounts for approximately 41 000 deaths annually in South Africa alone.[1,2] The term cancer is used to describe a large group of diseases that affect any part of the body. The main defining characteristic of cancer is the abrupt evolution of abnormal cells which overgrow and may spread to other organs using either the lymphatic or bloodstream systems.[3] Due to cancer being one of the leading causes of mortality globally,[4] a thorough understanding of its biology is of utmost importance for effective drug development.

1.1.2 Cell cycle and the biology of cancer

Cancer cells are a result of an accumulation of mutations of various genes that control cell proliferation, thus, allowing the cancerous cell to grow, divide, and become increasingly independent of controls that maintain normal cells.[5] These mutated cells divide and replicate faster than their non-cancerous counterparts and congregate to form a tumour; which can either be benign or malignant. Benign tumours are tumours which are localised within tissue boundaries, and they are the easiest to treat. On the other hand, malignant tumours comprise of cancerous cells that can migrate from the primary tumour, *via* either the lymphatic or the bloodstream systems, to other parts of the body or organs (called secondary sites) to form secondary tumours.[6,7] This process of migration is termed metastasis (Figure 1.1)[7] and is the most fearsome aspect of cancer, as majority of cancer-related mortalities are due to

metastatic cancer cells which may be resistant to conventional therapies. There are several conventional therapies that have been developed to manage and treat cancer, these include radiation therapy, immunotherapy, surgery and chemotherapy. However, each cancer therapy option is accompanied by several specific side effects which may range in severity from slight headaches to nephrotoxicity.[8]

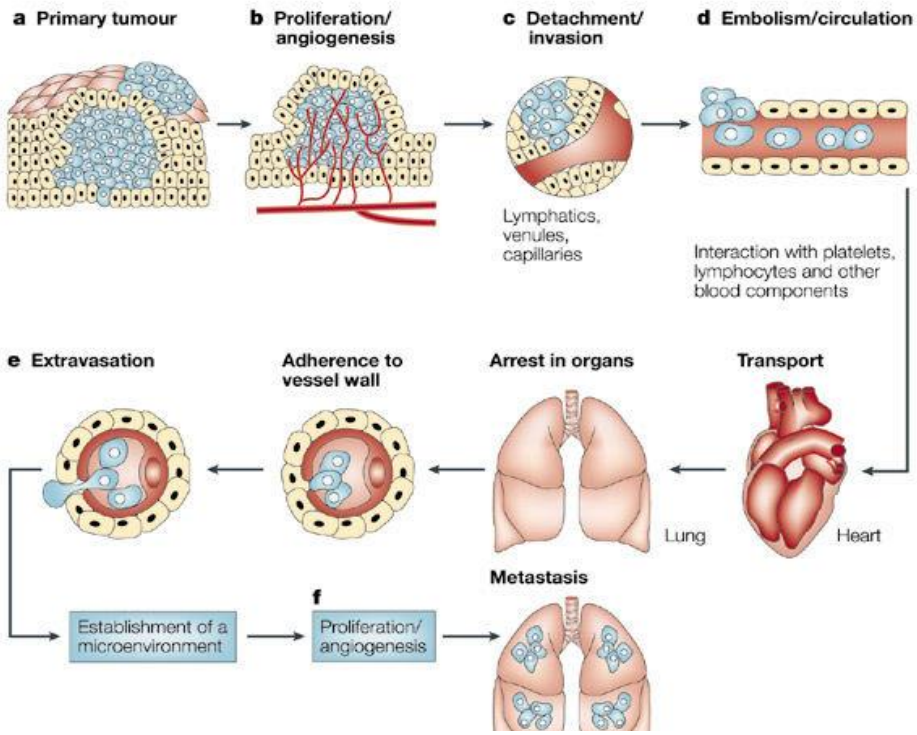

Figure 1.1*: The main steps in the process of metastasis.*[7]

1.1.3 Cancer therapies

In the early stages of cancer, the disease can be treated by one or more therapies, including surgery, radiotherapy or systemic chemotherapy. Surgery and radiotherapy are the primary therapies used to treat cancers that are localized in tissue (benign tumours).[9] To reduce the chances of the development of recurring localized tumours and the development of secondary tumours, these primary therapies are used in tandem with cytotoxic chemotherapeutic agents.[9,10] This is when chemotherapy is applied in combination with

surgery or radiotherapy as either an adjuvant (chemotherapy used after curative surgery) or a neoadjuvant (chemotherapy used as treatment before planned curative surgery).[10]

In the unfortunate case of the tumour advancing to its metastatic stage, combination chemotherapy is the recommended treatment. This is whereby several agents from different chemotherapy classes are used in combination (Figure 1.2). The main rationale behind this treatment is that the combined chemotherapy drugs have differing mechanisms of action and dose-limiting toxicities, which allow for additive anticancer effects with minimal toxic side effects.

Chemotherapeutic agents may be cell cycle-specific (such as anti-tumour antibiotics) or cell cycle non-specific (such as alkylating agents), as shown in Figure 1.2; but they all induce apoptosis by damaging DNA and/or preventing mitotic division.[11] The currently available chemotherapeutic agents, however, entail considerable adverse effects, with the most common immediate side effects being myelosuppression (bone marrow suppression), hair loss, and chemotherapy-induced-nausea and vomiting (CINV).[12] These undesirable side effects arise from the non-selective killing of rapidly growing cells by chemotherapeutic agents.[9–11]

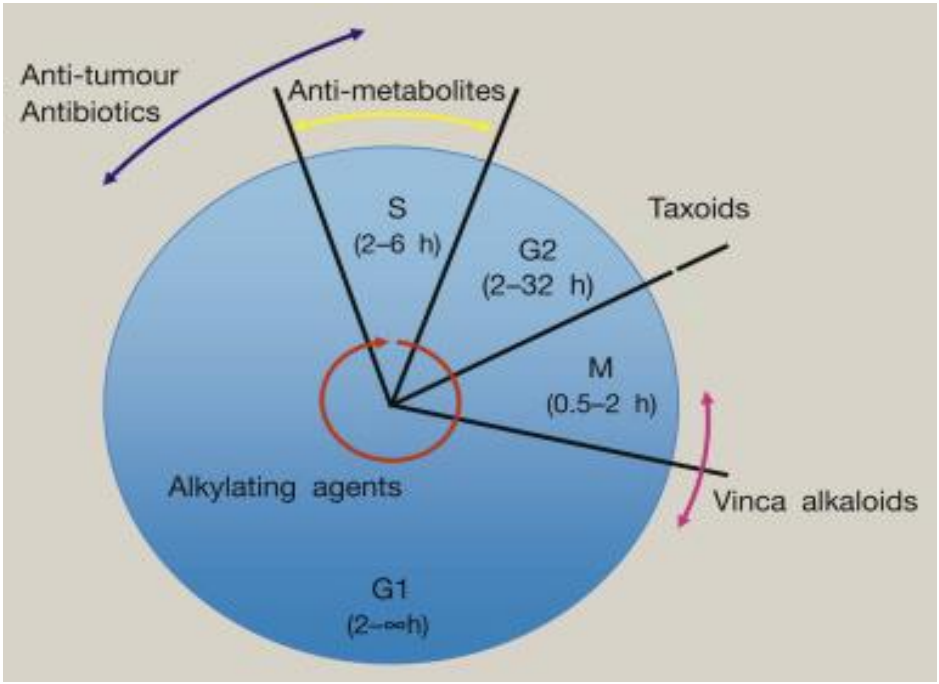

***Figure 1.2**: Actions of chemotherapy agents on various stages of the cell cycle.[9]*

These therapies do not always provide a curative treatment for cancer, as tumours often develop resistance to chemotherapy through a combination of mechanisms. This

chemoresistance is the main reason for the failure in the treatment and management of cancer.

1.1.4 Chemoresistance

Despite chemotherapy being an important treatment option, and the several classes of chemotherapeutic agents available, chemotherapeutic agents frequently miscue slow-dividing and non-dividing cancer cells.[13] Although these pharmacological factors may contribute to the development of chemoresistance, cellular factors play a major role in chemoresistance.[14] Resistance to chemotherapy, or chemoresistance, accounts for approximately 90% of drug failures in the treatment of metastatic cancers.[15]

Chemoresistance is multifactorial and is caused by multiple interconnected or independent mechanisms.[13–15] Chemoresistance manifests itself in two primary forms; acquired resistance and intrinsic (natural) resistance. In both cases, cancer cells tend to show resistance to numerous chemotherapeutic agents from different classes. The main mechanisms for chemoresistance can be grouped into three main categories:

- Decrease of chemotherapeutic drug concentration at the target cancer cells, due to the activation of transporter proteins and/or detoxifying agents (such as the activation of ATP-dependant transporter domains on cancer cell membranes).
- Alterations affecting the drug-target interactions (such as the altering of the structure of DNA polymerase in cancer cells).
- Factors influencing cellular response that affect tumour cell survival (such as the upregulation of DNA repair mechanisms in cancer cells).[14]

Chemoresistance remains a major challenge in the treatment of metastatic cancers. The benzimidazole pharmacophore is extensively investigated for its potential as an anticancer agent and researcher's interests in this pharmacophore are further cultivated by the promising results observed in these investigations.

1.2 Benzimidazoles

1.2.1 Chemical structure

The benzimidazole ring system has been of interest to researchers since the 1950s when it was established that 5,6-dimethyl-1-(α-D-ribofuranosyl) benzimidazole is an integral part of the vitamin B_{12} structure.[16] This spawned interest and extensive studies on the benzimidazole core as a potential therapeutic agent.

A benzimidazole is a heterocyclic aromatic ring system formed by the fusion of a benzene ring onto the 4- and 5-positions of an imidazole ring (Figure 1.3).[17] Studies have shown that modifications of the 2- and 5-position of the benzimidazole scaffold yields a number of biologically active compounds. [16]

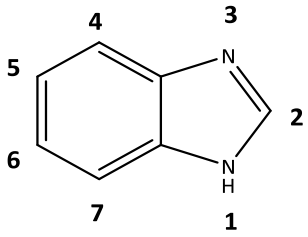

Figure 1.3*: The structure of 1H-benzimidazole.*[17]

The prevalence of the benzimidazole core in biologically active molecules has stimulated systematic investigations of this class of heterocyclic compounds. It is well established in literature that benzimidazole derivatives show an array of biological activity, including antiviral, antihistaminic, antiparasitic, antimalarial and anticancer activity.[18] Due to their vast medicinal value, research into benzimidazole-based compounds as potential anticancer agents is an active and attractive field in medicinal chemistry.

1.2.2 Anticancer activity

Despite improvements in chemotherapy treatments, the development of resistance remains a major hurdle in the treatment of cancer. The success of clinically approved benzimidazole derivatives, such as omeprazole, lansoprazole and albendazole, has resulted in increased interest into the medicinal use of benzimidazoles as chemotherapeutic agents.[19]

In a study, Wu *et al.*[19] assayed a series of benzimidazole-2-substituted phenyl or pyridine propyl ketenes for their *in vitro* antiproliferative activity against the colon cancer (HCT116), breast cancer (MCF-7) and liver cancer (HepG2) cell lines. It was observed that the antiproliferative activities of compounds **1** and **2** (Figure 1.4) were in the ranges of 0.06 – 1.53 µM and 0.04 – 9.80 µM, respectively, against all the tested cancer cell lines. This activity is significantly better than that of 5-fluorouracil (IC_{50} = 56.96 – 174.50 µM) and close to the anticancer activity of carboplatin (IC_{50} = 0.026 – 1.53 µM). Furthermore, it was shown that these compounds also inhibit tumour growth in BALB/c mice with HCT116 colon carcinoma.[19]

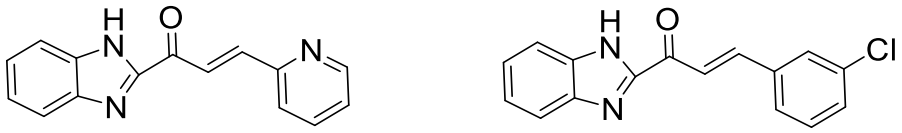

1 **2**

Figure 1.4*: The structures of promising lead compounds identified from a study by Wu et al.*[19]

In a more recent study, Sun and co-workers[20] conducted a structure-activity relationship study on novel water-soluble benzimidazole carbamates. All the compounds synthesized in the study were screened for *in vitro* anticancer activity at 1 and 10 µM concentrations against the non-small cell lung cancer (A549) and prostate cancer cell lines (PC3 and PC3MLN4). The study led to the identification of a novel oxetane-containing benzimidazole derivative (Figure 1.5), which shows potent cytotoxic activity in the range 23.19 – 50.19 µM in the tested concentrations across the assayed cell lines.[20]

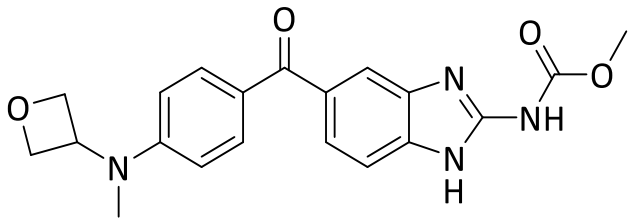

Figure 1.5*: The novel oxetane-containing benzimidazole derivative potential lead identified by Sun and co-workers.*[20]

The evaluation of benzimidazole derivatives for their anticancer activity is an ever-growing field in medicinal chemistry. This field continues to show great promise in addressing the

looming threat of chemoresistance. However, another strategy that may be useful in combating chemoresistance is the investigation of organometallic complexes.

1.3 Metals in medicine

Metal-based drugs have played a pivotal role in the diverse history of medicine, especially as anti-infective agents.[21] The main concept in the rational design of organometallic drug candidates is the use of the metal-organic drug synergism; through binding a potentially pharmacologically active organic compound to a metal center.[22] The complexation of a potentially biologically active compound to a metal center presents two distinct advantages: firstly, the enhancement of the biological activity of the organic compound; possibly by increasing solubility and bioavailability. Secondly, the reduction of the risk of toxicity of the metal center, as the metal is not available to promote and/ or undergo undesirable reactions.[23]

Organometallic complexes present the unique advantage of vast synthetic diversity for rational drug design. As the metal ion, the oxidation state of the metal ion, and the ligands coordinated to the metal center can be varied; thus allowing various characteristics of the metal complex to be altered and fine-tuned to best suit the desired biological activity.[22] This diversity may also be the key to combating drug resistance, which remains a major hurdle in the treatment of cancer.

1.3.1 Platinum-based anticancer complexes

The fortuitous discovery of *cis*-diamminedichloridoplatinum(II), commonly known as cisplatin, by Rosenberg in 1967 has cemented the path for the development of metal-based complexes as an alternative class of chemotherapeutic agents. Today, platinum-based drugs (well-known examples include cisplatin, carboplatin and oxaliplatin; Figure 1.6) constitute as much as 70% of cancer treatment regimens.[24] Cisplatin is commonly used to treat testicular and ovarian cancers and is increasingly being used for the treatment of other tumours like bladder and cervical tumours. Cisplatin and other platinum-based compounds are known to primarily target DNA, disrupting DNA replication by forming inter- and/ or intra-strand crosslinks.[11,25] This prevents DNA replication, RNA and protein synthesis in cancer cells, leading to apoptosis.

Several derivatives of cisplatin have been developed in a bid to improve efficacy and minimize side effects. Derivatives with the same *cis*-$PtX_2(amine)_2$ structure (where X = leaving anionic group; amine = any primary or secondary amine group) have been developed and some display similar or even improved anticancer activity relative to cisplatin.[25] However, due to the numerous side effects of cisplatin and its derivatives, strategies to lower toxicity of platinum-based chemotherapeutics have been employed. These strategies include the development of Pt(IV) pro-drugs and the development of multinuclear Pt(II) complexes.

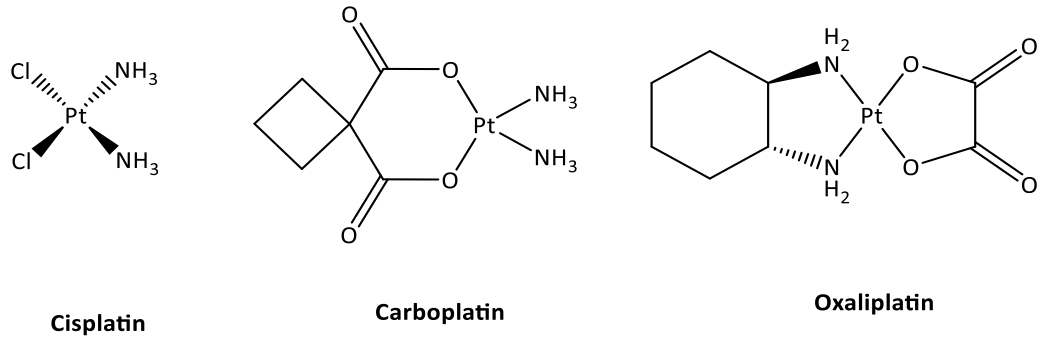

Figure 1.6*: The structures of cisplatin, carboplatin and oxaliplatin.*[25]

Cisplatin use is accompanied by severe side effects, including kidney toxicity, loss of sensation in extremities and nausea, have been major issues for cancer treatment;[24,25] and this is how platinum(IV) complexes came into the medicinal chemistry stage. The general scientific consensus is that these octahedral platinum(IV) complexes are kinetically more inert in the bloodstream and can be activated upon entry into cells, by biological reducing agents, to the cytotoxic platinum(II) species. This offers potential advantages over platinum(II) complexes regarding oral availability, reduced drug resistance and lower toxicity.[26] Two best-known examples of Pt(IV) pro-drugs are satraplatin and LA-12 (Figure 1.7). Satraplatin is currently in clinical trials for the treatment of ovarian, prostate and lung cancers.[27] The complex LA-12 is an analogue of satraplatin and contains an adamantylamine ligand, which may improve the complex's cellular uptake. The compound LA-12 displayed improved anticancer activity against cisplatin-sensitive (A2780) and cisplatin-resistant (A2780cisR) human ovarian carcinoma cells relative to cisplatin, with equitoxic concentrations that were 6- (A2780) or 18-fold (A2780cisR) lower.[28]

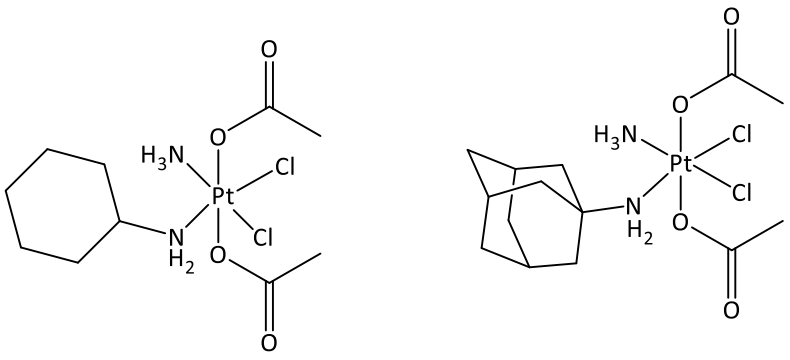

Satraplatin **LA-12**

***Figure 1.7**: The structures of satraplatin and LA-12.*[27]

The success of mononuclear chemotherapeutic agents also fuelled the investigation of multinuclear platinum(II) complexes as potential drug candidates. The most successful candidate in this category is BBR3464 (Figure 1.8), which comprises of three platinum(II) metal centres bridged by naturally occurring polyamines. The polyamine scaffold, and multinuclearity of the complex results in a slightly different mechanism when interacting with DNA; as the complex spans a long distance along DNA strands.[25] The trinuclear complex showed promising activity in pancreatic, non-small cell lung and ovarian cancers in Phase I clinical trials. However, in Phase II clinical trials, no significant responses were noted in patients treated with small cell lung, gastric and gastroesophageal cancers after treatment with BBR3464.[27]

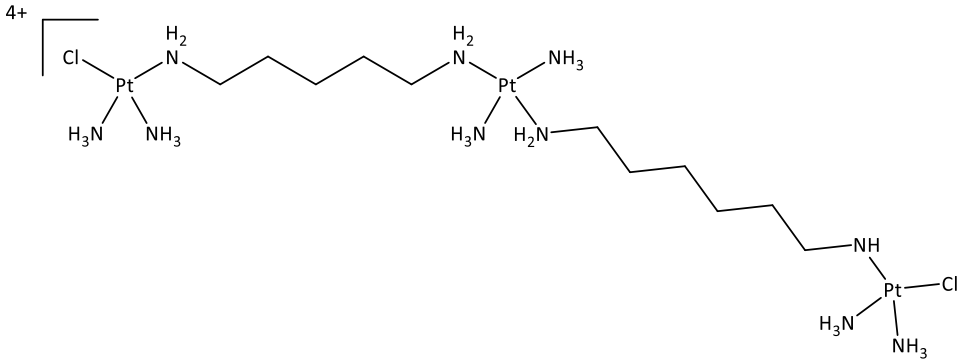

***Figure 1.8**: The structure of the trinuclear BBR3464 complex.*[27]

Platinum-based agents still constitute most of the currently used chemotherapeutic treatments. Nevertheless, their high toxicity and resistance of cancers towards these metallodrugs has prompted interest in other platinum group metals for cancer treatment.

1.3.2 Ruthenium(III) anticancer agents

Unlike platinum compounds, which display reasonably predictable biological behaviour, ruthenium complexes are known to show diverse toxicity and mechanisms of action. This diversity is even observed in very structurally similar compounds, which often display strikingly different biological properties. This diversity in biological activity is one of the factors cultivating interest into the investigation of ruthenium complexes for anticancer activity.[29] To date, the most successful ruthenium complexes are the New Anti-tumour Metastatic Inhibitor-A (NAMI-A) and NKP1339 (Figure 1.9); which have entered clinical trials.[24,30] NAMI-A possesses anti-metastatic properties, can reduce metastases mass and prevents the formation of secondary tumours. However, NAMI-A has minimal effects on primary tumour growth.[31] In Phase II clinical studies, NAMI-A was investigated in combination with gemcitabine (2',2'-difluoro-2-deoxycytidine) for the treatment of non-small cell lung cancer. The combination was noted to be less effective than gemcitabine alone, and the use of the combination was accompanied by gastrointestinal disturbances and neutropenia. As a result, the combination was deemed ineffective for further use.[32,33]

On the other hand, the Phase I clinical trials of NKP1339 were deemed a success, as the complex was noted to show effective activity against neuroendocrine tumours and colorectal tumours.[30] Furthermore, mild side effects were noted from the trial participants after treatment with NKP1339.[34] This low side effect profile may be accounted for by the metal-protein adduct formed by NKP1339 and serum albumin, as this adduct may selectively accumulate in tumour cells by exploiting the Enhanced Permeability and Retention (EPR) effect (Section 1.6, *vide infra*).[35]

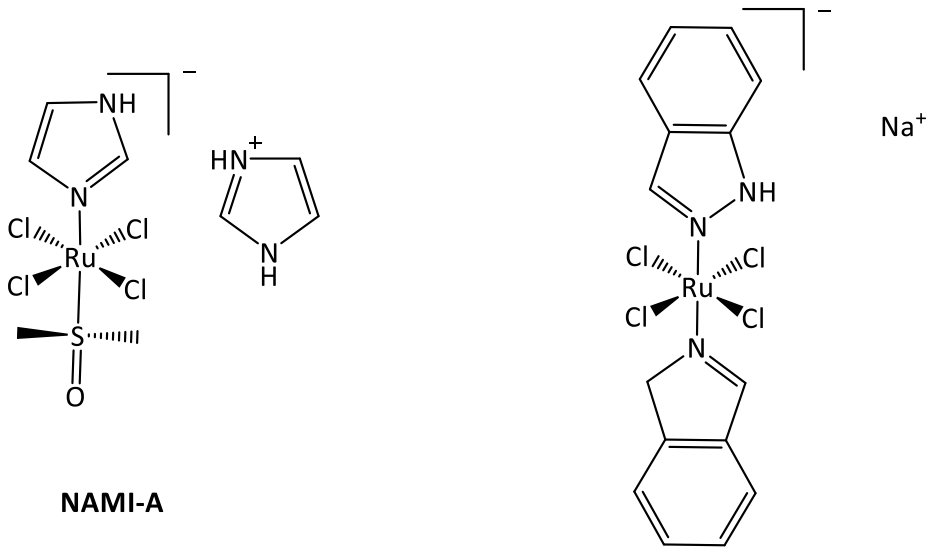

***Figure 1.9**: The structures of Ruthenium complexes which have entered clinical trials.*[15]

The aforementioned ruthenium(III) complexes are widely considered as pro-drugs, in that they are administered in their inactive form and are converted to the cytotoxic species *in situ*.[31] Similar to the reduction of platinum(IV) complexes, such as satraplatin as previously discussed (Section 1.3.1, *vide supra*), the reduction of ruthenium(III) complexes is carried out by biological reductants such as glutathione, ascorbate or nicotinamide adenine dinucleotide (NADH). The reduction from ruthenium(III) to ruthenium(II) results in a decrease of the π-acceptor properties of the metal center, subsequently leading to the increased lability of π-donor ligands, such as chlorides. Thus, resulting in the facilitation of hydrolysis, yielding the active species.[33] The interaction with actin-type proteins on cancer cell surfaces or with collagens of the extracellular matrix, leading to reduced mobility of metastatic cells, have been implicated for the possible mechanism of action of these ruthenium(III) complexes.[31]

Although NAMI-A and NKP1339 are known to show appreciable activity towards metastases, these complexes lack appreciable activity towards primary tumours.[36] The negligible activity of these ruthenium(III) complexes towards primary tumours has prompted the investigation of ruthenium(II) complexes which may be active against both metastases and primary tumours.

1.3.3 Ruthenium(II) anticancer agents

The activation by reduction hypothesis, which states that the active ruthenium(II) species is generated *in situ* by the reduction of ruthenium(III), was one of the motivations behind the direct preparation of potential anticancer ruthenium(II)-arene complexes. These ruthenium(II) complexes do not require the activation step and are relatively more stable. One class of these ruthenium(II)-arene complexes is the Ruthenium-Arene PTA (RAPTA) complexes (where PTA is the 1,3,5-triaza-7-phospaadamantane ligand). RAPTA complexes are characterized by a monodentate PTA ligand and an η^6-arene which are bound to the metal center.[37] The most widely known examples of this class of compounds are the prototype RAPTA-C and the η^6-toluene derivative, RAPTA-T (Figure 1.10). *In vivo* studies revealed that both of the aforementioned RAPTA complexes are inhibitors of lung metastasis in mice bearing MCa mammary carcinoma, inhibit tumour growth and halt the growth of solid metastatic tumours.[38,39] Due to the lability of the Ru(II)-Cl bond in RAPTA-C and RAPTA-T, these complexes were initially hypothesized to primarily target DNA.[37] However, these RAPTA complexes have been observed to target several proteins, including histidine protein cores in chromatin,[24] cathepsin B and thioxin reductase.[40] The primary targeting of proteins, instead of DNA, by these piano-stool ruthenium(II) complexes is an advantage as this characteristic attributes to the low toxicity displayed by these complexes.[32]

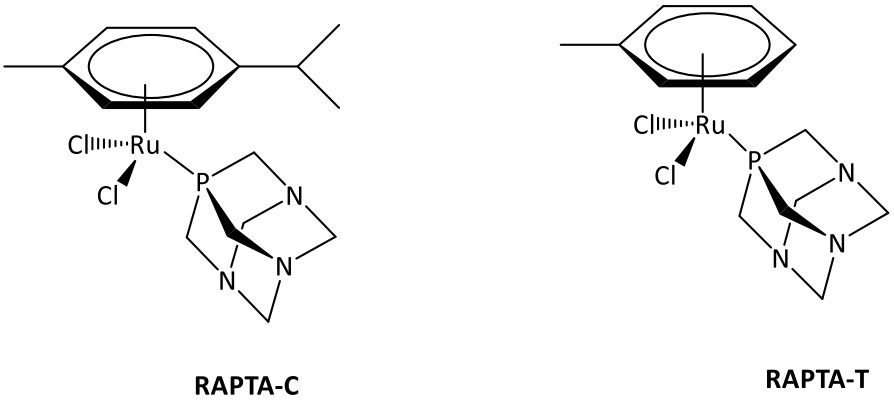

RAPTA-C **RAPTA-T**

***Figure 1.10**: The structures of Ru(II) pta containing complexes RAPTA-T and RAPTA-C.[15]*

Another well-explored class of ruthenium(II)-arene complexes is the Ruthenium(II)-Arene Ethylenediamine (RAED) complexes. These pseudo-octahedral complexes, pioneered by the Sadler group, are characterized by the general formula [Ru(II)-η^6-arene(en)Cl]$^{+,}$ where en is ethylenediamine.[41] Numerous derivatives of the prototype RAED-C complex have been developed, with the aims of fine-tuning the biological activity while minimizing off-target effects. The most widely known examples of this RAED family of complexes include RAED-C, the η^6-biphenyl derivative RM175 and the η^6-tetrahydroanthracene derivative HC11 (Figure 1.11).[42] *In vitro* evaluation of these complexes against the A2780 and A2780cisR human ovarian cancer cell lines (cisplatin-sensitive and -resistant, respectively) revealed that these complexes show antiproliferative activity either comparable or superior to that of carboplatin (2 µM < IC_{50} < 10 µM for the RAED complexes).[43] Additionally, the anticancer activity was noted to increase with the increase in the size of the arene: *p*-cymene< biphenyl< tetrahydroanthracene.[43]

RAED complexes are known to primarily target DNA, with a mechanism of action drawing similarities to that of cisplatin.[32] Although these complexes are known to bind to guanine nucleotides in DNA to form covalently bonded adducts, it is thought that the arene system in these complexes enables hydrophobic interactions with DNA, *via* intercalation between base pairs.[44] This intercalation may be used to account for the observed dependence of the anticancer activity of RAED complexes on the size of the arene moiety.

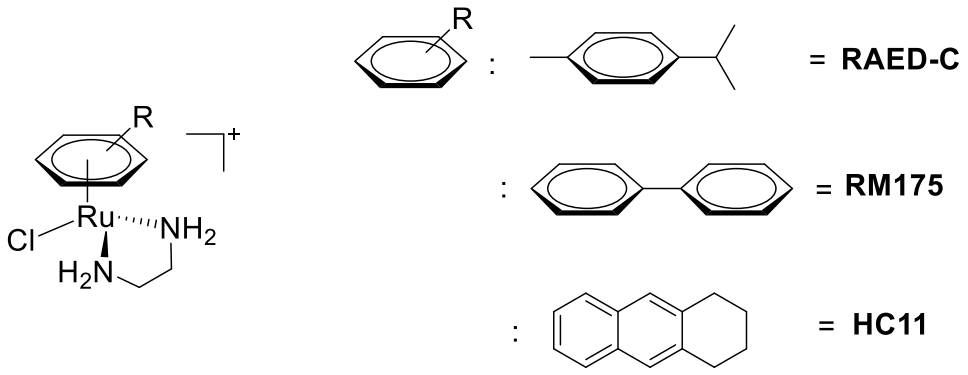

***Figure 1.11**: The structures of RAED complexes that have shown promising activity.[42]*

Another strategy that has become of recent interest is the use of ruthenium(II) complexes as photosensitizers for Photodynamic Therapy (PDT). The flagship complex in this class is TLD1443 (Figure 1.12), which is a ruthenium(II) polypyridyl complex developed by the McFarland group in 2011.[45] TLD1443 is currently in Phase IB clinical trials as a PDT agent for the treatment of non-muscle invasive bladder cancer, and is proving to be a new, alternative and non-invasive therapy.[33,46]

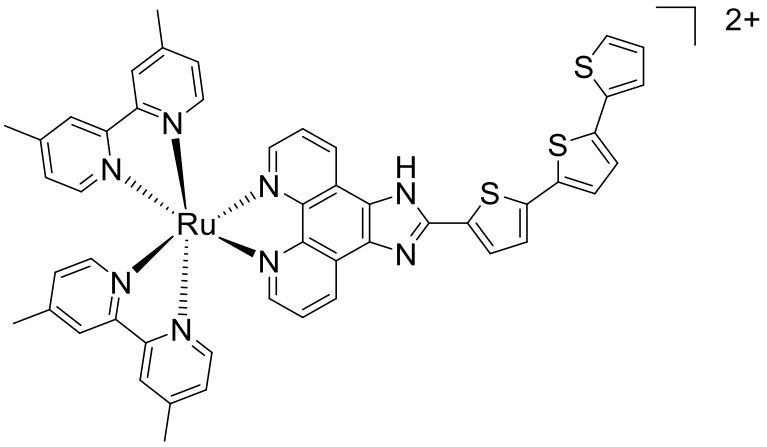

TLD1443

***Figure 1.12**: The structures of the ruthenium(II) complex in clinical trials as a PDT agent.[45]*

The success of ruthenium-based complexes and their alternate mechanisms of action suggests that they may facilitate the development and discovery of new combination chemotherapy agents. This further entices research into ruthenium-based complexes with pharmacologically active scaffolds in a bid to exploit synergism between the metal and the organic scaffold.

1.4 Transition-metal based benzimidazoles

The contribution of metal complexation to the enhancement of the biological activity of known pharmacologically active organic scaffolds is well established in literature and is highlighted by the development of ferrocifens.[47] This phenomenon is also observed when benzimidazoles are complexed to transition metal centers.

1.4.1 Benzimidazole-based anticancer agents

The design of ligands that have stand-alone therapeutic effects has proven to be beneficial and may also provide a quicker optimization of organometallic complexes.[48] This was one of the main rationales behind the study of semaxininb-inspired bispyrazole-benzimidazole ligands complexed to ruthenium(II) by Mukherjee and co-workers[48] for antiproliferative activity. Semaxinib ((3Z)-3-[(3,5-dimethyl-1H-pyrrol-2-yl)methylidene]-1,3-dihydro-*2H*-indol-2-one) inhibits the vascular endothelial growth factor receptor (VEGFR), which is imperative for the angiogenesis of cancer cells.[49] In the study, all the investigated complexes (Figure 1.13) showed potent cytotoxic activity (with IC_{50} values <15 µM) against the breast cancer (MCF-7), human hepato-carcinoma (HepG2) and the human metastatic prostate cancer (LNCaP) cell lines. Moreover, it was established that these compounds show excellent anti-cell migratory properties at almost non-toxic *in vitro* doses.[49]

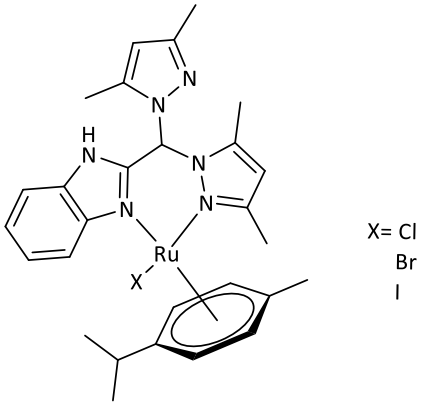

***Figure 1.13**: The general structure of Ru(II)-based benzimidazole complexes that display potent antitumour activity.[49]*

In another recent study, a series of iridium(III) complexed benzimidazoles were assayed for anticancer activity against the cisplatin-sensitive (A2780) and resistant (A2780cisR) human ovarian cancer cell lines, and breast cancer (MCF-7 and MDA-MB-23) cell lines.[50] These iridium

complexes all showed potent antitumour activity against the assayed cell lines, with the complexes with a butyl functionality attached to the benzimidazole ligand showing the highest cytotoxicity. The compounds **3** and **4** (Figure 1.14), displayed approximately 7- and 100-fold more cytotoxic activity than cisplatin, against the A2780 and MDA-MB-231 cancer cell lines, respectively. Additionally, all the complexes were found to be significantly less toxic to healthy kidney cell line (BGM) relative to cisplatin. This may contribute to overcoming the debilitating nephrotoxicity associated with cisplatin chemotherapy.[50]

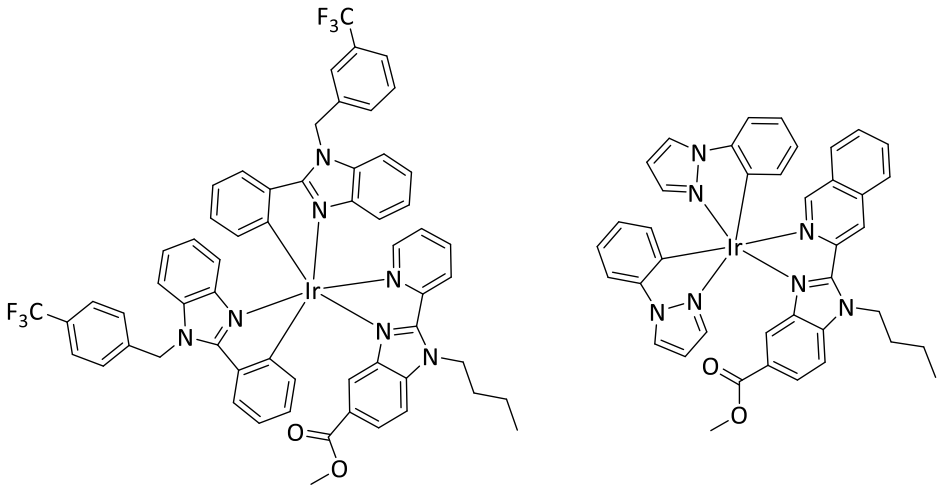

3 **4**

***Figure 1.14**: The most active Ir(III)-based benzimidazole complexes screened for antitumour activity by Yellol et al.[50]*

The investigation of antitumour activity of transition metal complexed benzimidazoles remains fruitful, with numerous studies on the potent activity of benzimidazole based organometallic complexes. However, the development of benzimidazole-based multinuclear anticancer agents remains relatively unexplored.

1.5 Multinuclear organometallic anticancer agents

With the need for the development of novel drugs in efforts to overcome increasing resistance of cancers to current chemotherapeutic agents, organometallic complexes are seen as a potential solution to this, as they offer a broad spectrum of biological activity. More recently, however, there has been a growing interest in the development of multinuclear organometallic complexes. This interest was ignited by the observation that compounds

bearing more than one metal center possess improved biological activities relative to their mononuclear counterparts.[51,52]

As previously discussed, one of the factors impeding the clinical success of cisplatin and its platinum-based derivatives are the debilitating side effects and the development of resistance. To overcome these factors, numerous polynuclear platinum-based drug candidates have been investigated, with the most successful and widely known example being Farrell's cationic complex BBR3464 (Figure 1.8, *vide supra*).[53] Despite the limited success of BBR3464 in Phase II clinical trials due to trial participant reports of adverse side effects including chemotherapy-induced nausea and vomiting (CNIV) and neutropenia,[54–56] this trinuclear complex is exemplary in illustrating the concept of exploiting multinuclear organometallic complexes as anticancer agents.

More recently, the Suntharalingam group investigated a novel triangular trinuclear platinum complex, Pt-3 (Figure 1.15) for cytotoxicity against breast cancer stem cells (CSCs). The trinuclear complex Pt-3 exhibited potent anticancer activity against the HMLER and HMLER-shEcad cells (1.26 μM < IC_{50} < 2.24 μM in both cell lines).[57] Furthermore, the activity of Pt-3 is superior to that of cisplatin and carboplatin against the aforementioned cell lines. In addition, the trinuclear complex Pt-3 was noted to show activity more potent than that of salinomycin, an established breast CSC agent, on the three-dimensional tumour-like spheroids of the HMLER-shEcad cell line. Notably, the trinuclear Pt-3 displayed approximately 3-fold greater activity relative to its corresponding mononuclear (Pt-1a) and dinuclear (Pt-2) analogues.[57] This trend reinforces the therapeutic potential of multinuclear complexes as anticancer agents.

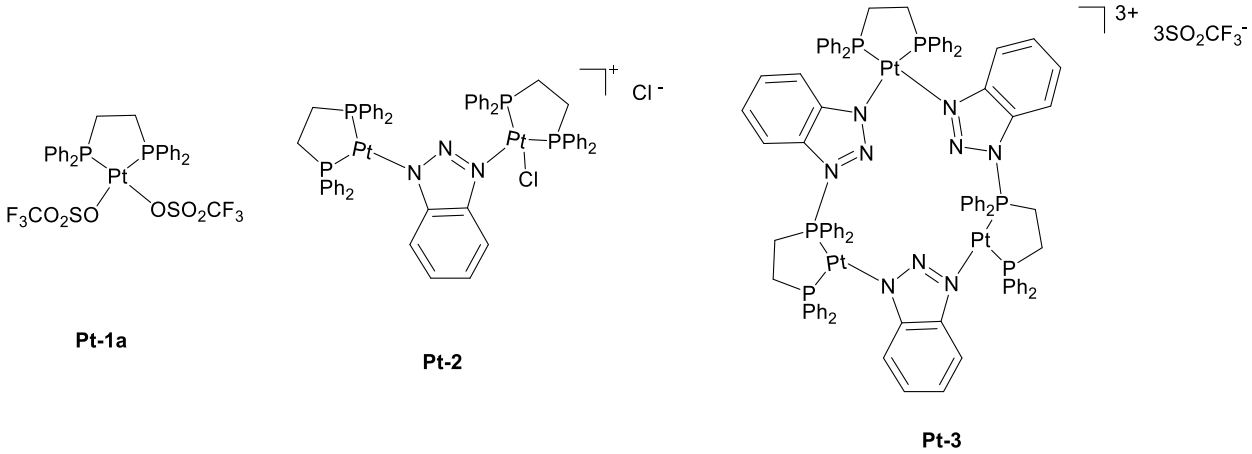

***Figure 1.15**: The novel triangular trinuclear platinum-based complex investigated by the Suntharalingam group for anticancer activity against breast CSC, along with the mononuclear and the dinuclear counterparts*

The investigation of multinuclear complexes as potential anticancer agents has also been extended to other transition metals such as rhodium, ruthenium and iridium. These PGMs have several stable oxidation states and possess an octahedral geometry; thus offering two more coordination sites relative to platinum(II).[58]

In a recent study, Burgoyne *et al.*[59] screened salicylaldiminato-sulfonate based iridium(III) and rhodium(III) mono- and trinuclear complexes (Figure 1.16) for anticancer activity against the WHCO1 oesophageal cancer cell line. A general trend was reported, in which the trinuclear complexes displayed enhanced antitumour activity (43.87 – 200 µM) relative to their corresponding monomeric complexes (with IC_{50} values ranging from 169.1 µM to >300 µM).[59]

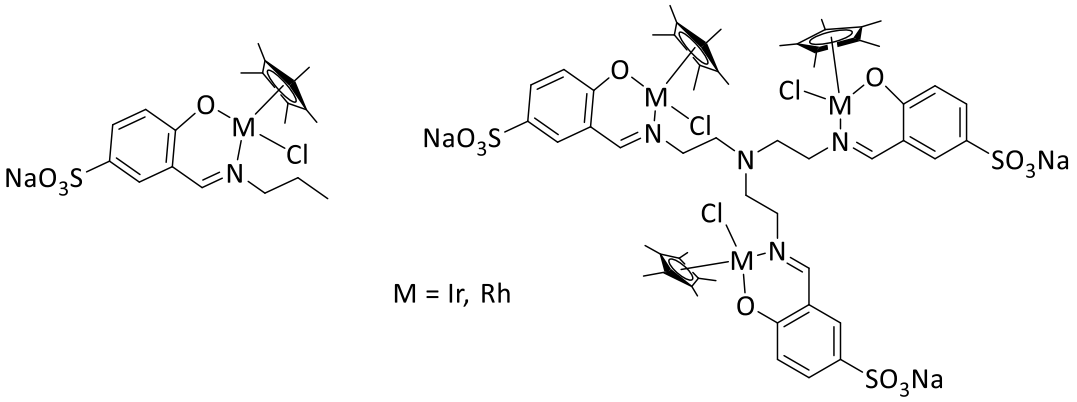

***Figure 1.16**: The novel rhodium(III) and iridium(III) half-sandwich complexes investigated by Burgoyne et al.*[59]

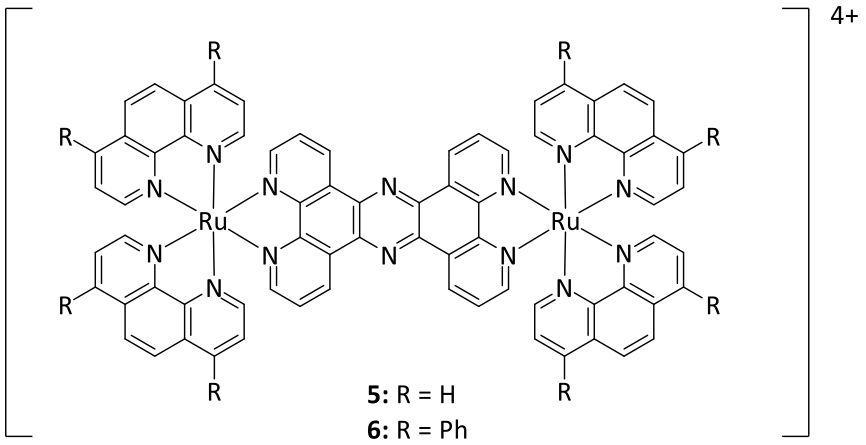

***Figure 1.17**: The dinuclear ruthenium(II) complexes **5** and **6**.*[60]

Motivated by the encouraging results obtained from a previous study of the dinuclear ruthenium(II) tppz complex $[(Ru(phen)_2)_2(tpphz)]^{4+}$ (where phen = 1,10-phenanthroline , and tpphz = tetrapyrido[3,2-*a*:2',3'-*c*:3",2"-*h*:2''',3'''-*j*]phenazine), complex **5**, Gill *et al*.[60] investigated the lipophilic derivative of **5**, $[(Ru(DIP)_2)_2(tpphz)]^{4+}$ (where DIP is 4,7-diphenyl-1,10-phenanthroline), **6**. From the study, it was observed that complex **6** (Figure 1.17) displayed approximately 2-fold higher cytotoxicity relative to the cisplatin standard, against the breast cancer (MCF-7) and HeLa human cervical cancer cell lines. Moreover, it was established that this complex (**6**) displays a localization profile that is consistent with targeting the endomembrane system, which comprises of the endoplasmic reticulum, nuclear envelope and vacuole structures.[60]

1.6 Trinuclear ruthenium arene complexes as anticancer agents

Trinuclear ruthenium arene organometallic complexes are significantly less developed and considerably less investigated relative to their dinuclear and tetranuclear counterparts.[61] An approach that is widely used in the rational design of trinuclear ruthenium complexes for application as anticancer agents is the use of branched and flexible linkers to connect three ruthenium moieties, yielding trinuclear dendritic complexes. This approach is commonly used as it confers flexibility and conformational adjustment of each ruthenium unit.[61]

The effects of different flexible linker ligands to the anticancer activity of trinuclear organoruthenium complexes have been extensively studied by the Smith group.[62–65] In a

study, Burgoyne *et al.* investigated a series of trinuclear polyester-bridged ruthenium(II)-arene complexes (Figure 1.18 a) as potential anticancer agents against human ovarian cancer cell lines (A2780 and A2780cisR).[64] This class of trinuclear ruthenium complexes showed promising antiproliferative activity against both the A2780 and A2780cisR cell lines (33.38 µM < IC_{50} < 60.50 µM), with selectivity towards these cancerous cell lines over non-tumorigenic human fibroblast cells (KMST-1).[64] Additionally, the trinuclear complexes were noted to have 2 – 4 fold enhanced activity relative to their respective mononuclear counterparts in the A2780 and A2780cisR cell lines.

In another study, the Smith group investigated a series of trinuclear ruthenium(II) complexes based on the tris-2-(salicylaldimine ethyl)amine and tris-2-(2-pyridine ethyl)amine scaffolds (Figure 1.18 b) for their potential anticancer activity.[65] Generally, it was noted that there is a correlation between the number of ruthenium centers and the cytotoxicity of the complexes. This is evidenced by the enhanced antiproliferative activity noted for the trinuclear complexes relative to their mononuclear analogues on the human osteosarcoma (MG63) and the cisplatin-resistant human ovarian cancer (A2780cisR) cell lines. However, the trinuclear complexes were noted not to be selective for cancer cells, when evaluated for cytotoxicity against non-tumorigenic human fibroblast cells (KMST-1).[65]

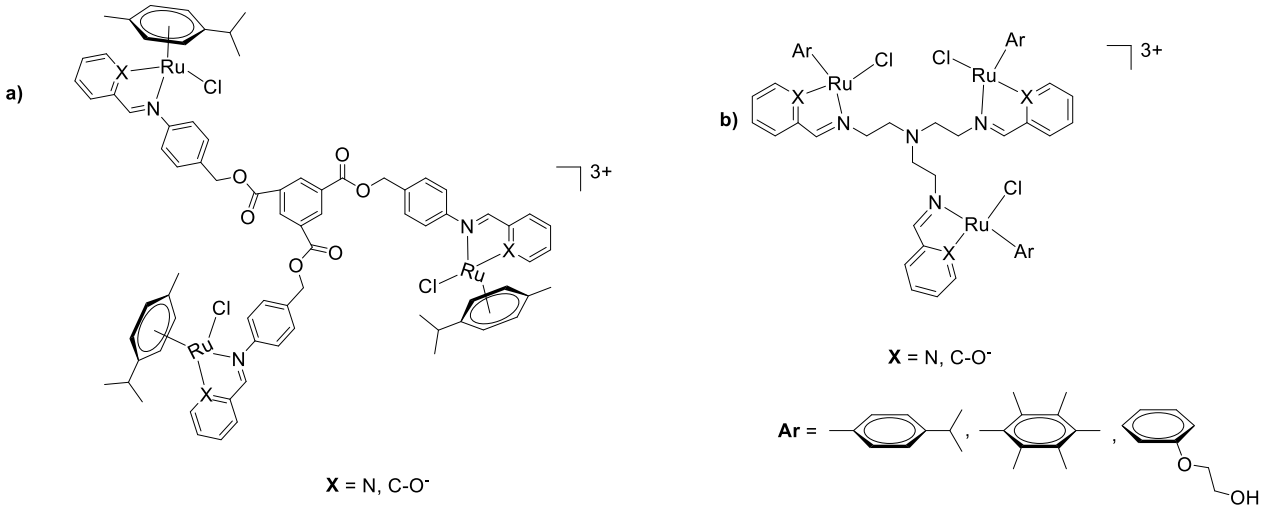

***Figure 1.18**: Some of the trinuclear ruthenium(II)-arene complexes based on either the polyester (a) or tris-2-ethylamine scaffolds (b) studies by Smith et al. as potential anticancer agents.*[64,65]

More recently, Beckford *et al.* investigated a discrete series of trinuclear ruthenium complexes based on a 2,4,6-tris(di-2-pyridylamino)-1,3,5-triazine core (Figure 1.19).[66] The investigated complexes showed very mild activity against the triple-negative HCC-1937 breast cancer cell line, with all IC_{50} values >100 µM. All the trinuclear complexes were only observed to show an appreciable reduction of HCC-1937 cell viability at 1 mM, reducing cell viability to a range between 20% and 80%. Furthermore, these complexes were noted to have stimulatory effects on the viability of MCF-10A non-tumorigenic breast epithelial cells.[66] Additional mechanistic studies suggest that DNA is the primary target of these complexes, with the trinuclear complexes either binding to DNA grooves or electrostatically interacting with DNA.

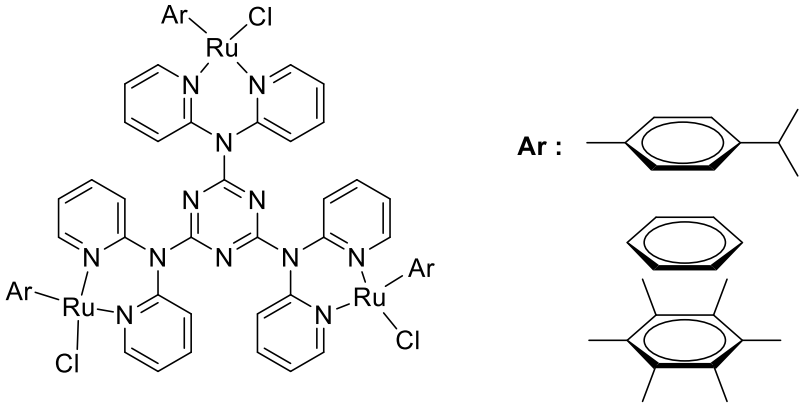

Figure 1.19*: The trinuclear ruthenium(II)-arene complexes based on a 1,3,5-triazine core investigated by Beckford and co-workers.*

The improved cytotoxicity of multinuclear macromolecules, relative to their mononuclear analogues, may also be attributed to the enhanced permeability and retention (EPR) effect.[51] This is a phenomenon in which solid tumours have defective and permeable blood vessels; this is to ensure a sufficient supply of nutrients and oxygen to tumour tissues for rapid growth (Figure 1.20). Macromolecules, such as polynuclear complexes exploit this EPR effect and selectively accumulate in tumour cells.[67]

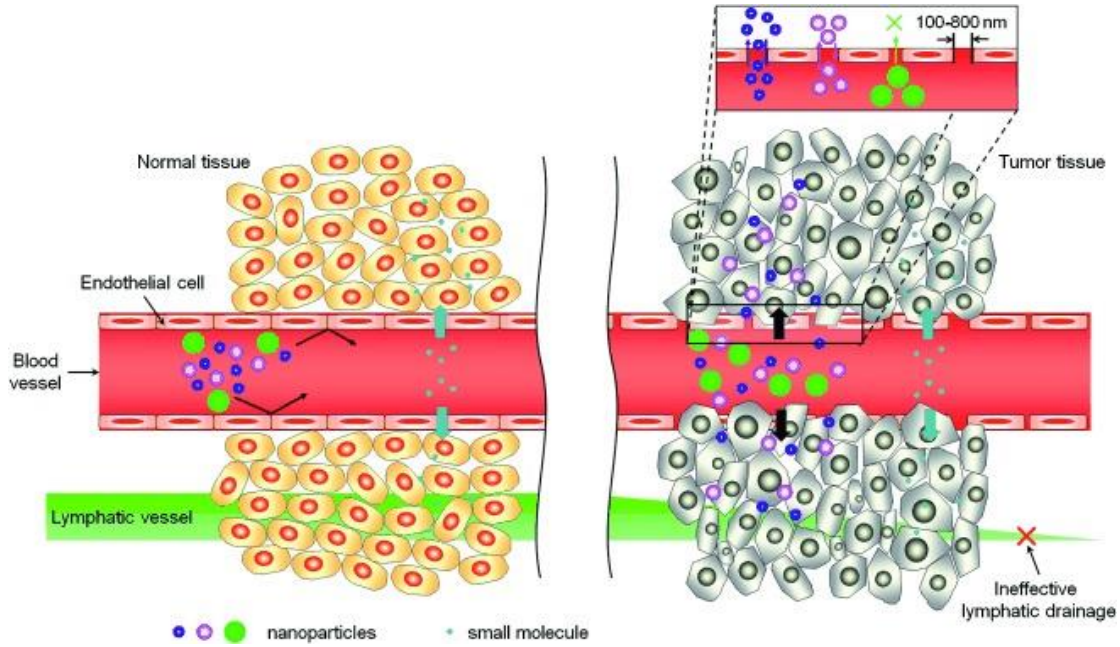

***Figure 1.20**: An illustration of the Enhanced Permeability and Retention (EPR) effect.*[68]

1.7 Rationale for the current Study

The field of bioorganometallic chemistry presents favourable biological results which cultivate interest into further development of organometallic compounds as biological agents. The incorporation of two or more metal centers onto an organic scaffold has been shown to yield multinuclear organometallic complexes with novel mechanisms of action as potential anticancer agents. These novel mechanisms of action may assist in overcoming resistance displayed by tumours to clinically used chemotherapeutic agents and improve the selectivity of metallodrugs. The incorporation of pharmacophores onto dendritic scaffolds and the combination of these dendritic ligands with PGMs, to form trinuclear complexes, is a widely used strategy in rational anticancer drug design. However, whilst interest in the development of multinuclear organometallic complexes as anticancer agents is growing, exploration into ruthenium arene trinuclear complexes remains in infancy.

As previously discussed, the benzimidazole moiety is well-documented for its appreciable anticancer activity. Moreover, the study of benzimidazole-based organometallic biological agents is ever-growing and continues to provide encouraging results, especially as anticancer agents. However, the exploration of multinuclear benzimidazole-based organometallic

complexes remains slow developing. As a result, the development of multinuclear benzimidazole-based organometallic complexes and their use as potential anticancer agents have not been systematically investigated, and thus prompts further investigation into this field.

1.8 Aims and objectives

1.8.1 General aims

As discussed in this chapter, the investigation of the less-developed trinuclear ruthenium arene benzimidazole-based organometallic complexes may result in an interesting study. As a result, the aims of the project were to:

- Synthesize a series of trimeric 2,5-disubstituted benzimidazole ligands and corresponding 2-ferrocenyl bioisosteres based on the tris(2-aminoethyl)amine scaffold.
- Complex the respective ligands to ruthenium to afford the corresponding trinuclear *N^N*-ruthenium(II) cationic and *C^N*-ruthenium(II) cyclometallated complexes bearing the ruthenium centers at the periphery.
- The evaluation of the synthesized compounds for their biological activity as potential anticancer agents.

1.8.2 Specific objectives

1. The synthesis of a series of 2,5-disubstituted trimeric benzimidazole ligands and the corresponding 2-ferrocenyl compounds as non-planar bioisosteres of the 2-aryl functionalities (Figure 1.21).

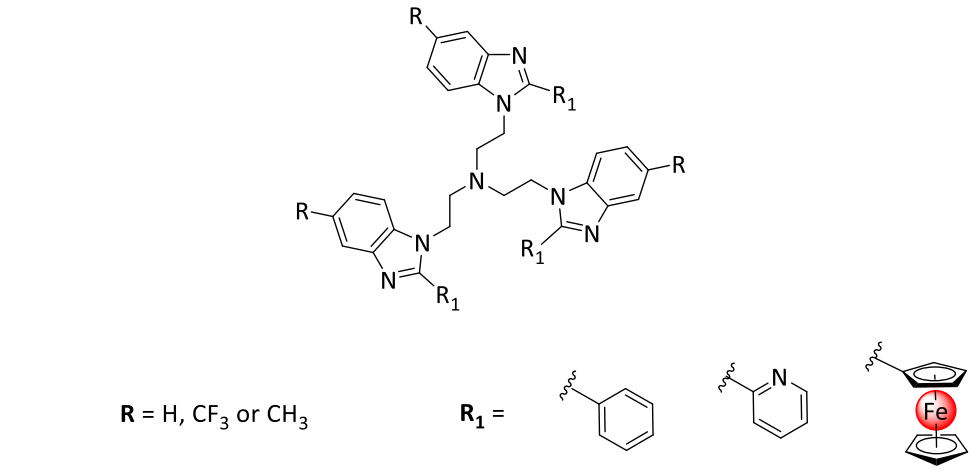

***Figure 1.21**: The general structures of the trimeric 2,5-disubstituted benzimidazole compounds synthesized in this study.*

2. The preparation of the corresponding trinuclear ruthenium(II) arene complexes as either the neutral *C^N*-Ru(II) or cationic *N^N*-Ru(II) complexes (Figure 1.22).

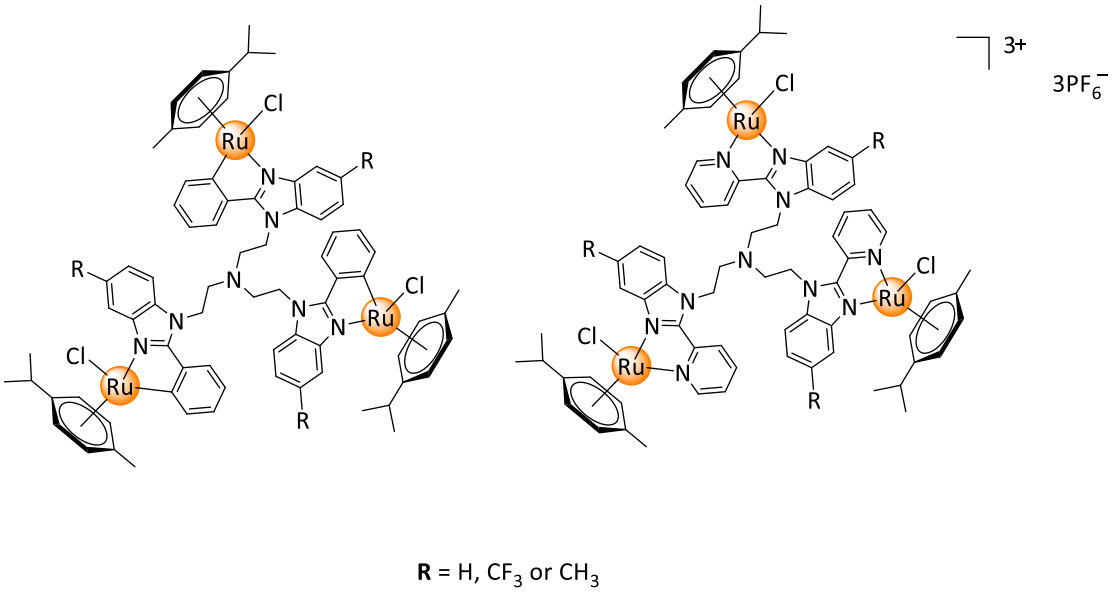

***Figure 1.22**: The general structures of the neutral cyclometallated and cationic N^N-chelated trinuclear ruthenium(II)-p-cymene complexes synthesized in this study.*

3. To characterize all of the compounds using an array of analytical and spectroscopic techniques, including Nuclear Magnetic Resonance spectroscopy (NMR), Elemental Analysis, Fourier Transform-Infrared spectroscopy (FT-IR) and Electrospray Ionisation (ESI) or Electron Impact (EI) Mass spectrometry. Single crystal X-ray diffraction (XRD)

analysis was used on single crystals to provide further evidence of the molecular structure for a ligand.

4. The investigation of the anticancer activity of the synthesized ligands and complexes against breast cancer (MCF-7 and MDA-MB-231) and skin cancer (501mel) cell lines using the MTT assay. Additionally, to conduct NMR studies to determine a potential intercellular target for the most active complex.

1.9 References

1 CANSA, CANSA: Statistics, http://www.cansa.org.za/files/2016/08/Fact-Sheet-Cancer-NCR-2011-web-Aug-2016.pdf, (accessed 20 August 2019).

2 WHO, WHO: Cancer, http://www.who.int/mediacentre/factsheets/fs297/en/, (accessed 20 August 2019).

3 A. Schroeder, D. A. Heller, M. M. Winslow, J. E. Dahlman, G. W. Pratt, R. Langer, T. Jacks and D. G. Anderson, *Nat. Rev. Cancer*, 2011, **12**, 39–50.

4 F. Bray, J. Ferlay and I. Soerjomataram, *Cancer J. Clin.*, 2018, **68**, 394–424.

5 Nature, Cell Division and Cancer, https://www.nature.com/scitable/topicpage/cell-division-and-cancer-14046590/, (accessed 1 January 2018).

6 J. A. Aguirre-Ghiso, *Nat. Rev. Cancer*, 2007, **7**, 834–846.

7 I. Fidler, *Nat. Rev. Cancer*, 2003, **3**, 1–6.

8 American Chemical Society, Chemotherapy, http://www.cancer.org/treatment/treatmentsandsideeffects/treatmenttypes/chemothera%0Apy/index%0A, (accessed 1 January 2018).

9 P. G. Corrie, *Medicine (Baltimore).*, 2007, **36**, 24–28.

10 R. Jones, *Medicine (Baltimore).*, 2016, **44**, 25–29.

11 V. Malhotra and M. C. Perry, *Cancer Biol. Ther.*, 2003, **2**, 4–6.

12 P. R. Bhandari, *J. Adv. Pharm. Technol. Res.*, 2012, **3**, 202–9.

13 J. Zhao, *Pharmacol. Ther.*, 2016, **160**, 145–158.

14 L. Gatti and F. Zunino, *Methods Mol. Med.*, 2005, **111**, 127–148.

15 L. N. Abdullah and E. K.-H. Chow, *Clin. Transl. Med.*, 2013, **2**, 3.

16 K. Shah, S. Chhabra, S. K. Shrivastava and P. Mishra, *Med. Chem. Res.*, 2013, **22**, 5077–5104.

17 N. Singh, A. Pandurangan, K. Rana, P. Anand, A. Ahamad and A. K. Tiwari, *Int. Curr. Pharm. J.*, 2012, **1**, 119–127.

18 M. Gaba and C. Mohan, *Development of drugs based on imidazole and benzimidazole bioactive heterocycles: Recent advances and future directions*, Springer US, 2016, vol. 25.

19 L. T. Wu, Z. Jiang, J. J. Shen, H. Yi, Y. C. Zhan, M. Q. Sha, Z. Wang, S. T. Xue and Z. R. Li, *Eur. J. Med. Chem.*, 2016, **114**, 328–336.

20 J. E. Cheong, M. Zaffagni, I. Chung, Y. Xu, Y. Wang, F. E. Jernigan, B. R. Zetter and L. Sun, *Eur. J. Med. Chem.*, 2018, **144**, 372–385.

21 M. Navarro, C. Gabbiani, L. Messori and D. Gambino, *Drug Discov. Today*, 2010, **15**, 1070–1078.

22 R. A. Sánchez-Delgado and A. Anzellotti, *Mini-Reviews Med. Chem.*, 2004, **4**, 23–30.

23 M. Navarro, W. Castro and C. Biot, *Organometallics*, 2012, **31**, 5715–5727.

24 C. S. Allardyce and P. J. Dyson, *Dalton Trans.*, 2016, **45**, 3201–3209.

25 J. Reedijk, *Eur. J. Inorg. Chem.*, 2009, 1303–1312.

26 N. Muhammad and Z. Guo, *Curr. Opin. Chem. Biol.*, 2014, **19**, 144–153.

27 N. J. Wheate, S. Walker, G. E. Craig and R. Oun, *Dalton Trans.*, 2010, **39**, 8113 - 8116.

28 A. Kozubík, V. Horváth, L. Švihálková-Šindlerová, K. Souček, J. Hofmanová, P. Sova, A. Kroutil, F. Žák, A. Mistr and J. Turánek, *Biochem. Pharmacol.*, 2005, **69**, 373–383.

29 E. Alessio, *Eur. J. Inorg. Chem.*, 2017, 1549–1560.

30 G. K. Gransbury, P. Kappen, C. J. Glover, J. N. Hughes, A. Levina, P. A. Lay, I. F. Musgrave and H. H. Harris, *Metallomics*, 2016, **8**, 762–773.

31 A. Levina, A. Mitra and P. A. Lay, *Metallomics*, 2009, **1**, 458 - 463.

32 J. P. C. Coverdale, T. Laroiya-McCarron and I. Romero- Canelón, *Inorganics*, 2019, **7**, 1–15.

33 S. M. Meier-Menches, C. Gerner, C. G. Hartinger and B. K. Keppler, *Chem. Soc. Rev.*, 2018, **47**, 909–928.

34 D. S. Thompson, G. J. Weiss, S. F. Jones, H. A. Burris, R. K. Ramanathan, J. R. Infante, J. C. Bendell, A. Ogden and D. D. Von Hoff, *J. Clin. Oncol.*, 2012, **30**, 3033–3033.

35 B. Schoenhacker-Alte, T. Mohr, C. Pirker, K. Kryeziu, P. S. Kuhn, A. Buck, T. Hofmann, C. Gerner, G. Hermann, G. Koellensperger, B. K. Keppler, W. Berger and P. Heffeter, *Cancer Lett.*, 2017, **404**, 79–88.

36 E. Alessio and L. Messori, *Molecules*, 2019, **24**, 1–20.

37 L. Zeng, P. Gupta, Y. Chen, E. Wang, L. Ji, H. Chao and Z. S. Chen, *Chem. Soc. Rev.*, 2017, **46**, 5771–5804.

38 A. Bergamo, A. Masi, P. J. Dyson, G. Sava, C. F. Onlus and V. A. Fleming, *Int. J. Oncol.*, 2008, **33**, 1281–1289.

39 A. Weiss, R. H. Berndsen, M. Dubois, M. Cristina, R. Schibli, A. W. Griffoen, P. J. Dyson and P. Nowak-Sliwinska, *Chem. Rev.*, 2014, **5**, 4742–4748.

40 A. Casini, C. Gabbiani, F. Sorrentino, M. P. Rigobello, A. Bindoli, T. J. Geldbach, A. Marrone, N. Re, C. G. Hartinger, P. J. Dyson and L. Messori, *J. Med. Chem.*, 2008, 6773–6781.

41 W. Han and P. J. Dyson, *Eur. J. Inorg. Chem.*, 2006, 4003–4018.

42 M. G. Mendoza-Ferri, C. G. Hartinger, M. A. Mendoza, M. Groessl, A. E. Egger, R. E. Eichinger, J. B. Mangrum, N. P. Farrell, M. Maruszak, P. J. Bednarski, F. Klein, M. A. Jakupec, A. A. Nazarov, K. Severin and B. K. Keppler, *J. Med. Chem.*, 2009, **52**, 916–925.

43 Y. K. Yan, M. Melchart, A. Habtemariam and P. J. Sadler, *Chem. Commun.*, 2005, 4764–4776.

44 R. Carter, A. Westhorpe, M. J. Romero, A. Habtemariam, C. R. Gallevo, Y. Bark and N. Menezes, *Nat. Publ. Gr.*, 2016, 1–12.

45 H. Yin, J. Roque, P. Konda, S. Monro, K. L. Colo, S. Gujar, R. P. Thummel, L. Lilge, C. G. Cameron and S. A. Mcfarland, *Chem. Rev.*, 2019, **119**, 797–828.

46 S. Thota, D. A. Rodrigues, D. C. Crans and E. J. Barreiro, *J. Med. Chem.*, 2018, **61**, 5805–5821.

47 G. Jaouen, A. Vessieres and S. Top, *Chem. Soc. Rev.*, 2015, **44**, 8802–8817.

48 S. Bhattacharyya, K. Purkait and A. Mukherjee, *Dalton Trans.*, 2017, **46**, 8539–8554.

49 A. O'Donnell, A. Padhani, C. Hayes, A. J. Kakkar, M. Leach, J. M. Trigo, M. Scurr, F. Raynaud, S. Phillips, W. Aherne, A. Hardcastle, P. Workman, A. Hannah and I. Judson, *Br. J. Cancer*, 2005, **93**, 876–883.

50 J. Yellol, S. A. Pérez, G. Yellol, J. Zajac, A. Donaire, G. Vigueras, V. Novohradsky, C. Janiak, V. Brabec and J. Ruiz, *Chem. Commun.*, 2016, **52**, 14165–14168.

51 P. Govender, B. Therrien and G. S. Smith, *Eur. J. Inorg. Chem.*, 2012, 2853–2862.

52 C. Billecke, S. Finniss, L. Tahash, C. Miller, T. Mikkelsen, N. P. Farrell and O. Bögler, *Neuro. Oncol.*, 2006, **8**, 215–226.

53 N. J. Wheate and J. G. Collins, *Coord. Chem. Rev.*, 2003, **241**, 133–145.

54 C. X. Zhang and S. J. Lippard, *Curr. Opin. Chem. Biol.*, 2003, **7**, 481–489.

55 D. I. Jodrell, T. R. J. Evans, W. Steward, D. Cameron, J. Prendiville, C. Aschele, C. Noberasco, M. Lind, J. Carmichael, N. Dobbs, G. Camboni, B. Gatti and F. De Braud, *Eur. J. Cancer*, 2004, **40**, 1872–1877.

56 T. A. Hensing, N. H. Hanna, H. H. Gillenwater, M. Gabriella Camboni, C. Allievi and M. A. Socinski, *Anticancer. Drugs*, 2006, **17**, 697–704.

57 A. Eskandari, A. Kundu, S. Ghosh and K. Suntharalingam, *Angew. Chem. Int. Ed.*, 2019, **58**, 12059–12064.

58 P. Chellan, K. M. Land, A. Shokar, A. Au, S. H. An, D. Taylor, P. J. Smith, K. Chibale and G. S. Smith, *Organometallics*, 2013, **32**, 4793–4804.

59 A. R. Burgoyne, C. H. Kaschula, M. I. Parker and G. S. Smith, *J. Organomet. Chem.*, 2017, **846**, 100–104.

60 M. R. Gill, D. Cecchin, M. G. Walker, R. S. Mulla, G. Battaglia, C. Smythe and J. A. Thomas, *Chem. Sci.*, 2013, **4**, 4512.

61 M. V Babak and W. H. Ang, eds. A. Sigel, H. Sigel, E. Freisinger and R. K. O. Sigel, *Metallodrugs: Development and Action of Anticancer Agents*, Walter de Gruyter GmbH, Berlin, Germany, 2018, pp. 171–194.

62 P. Chellan, K. M. Land, A. Shokar, A. Au, S. H. An, D. Taylor, P. J. Smith, T. Riedel, P. J. Dyson, K. Chibale and G. S. Smith, *Dalton Trans.*, 2014, **43**, 513–526.

63 A. R. Burgoyne, C. H. Kaschula, M. I. Parker and G. S. Smith, *Eur. J. Inorg. Chem*, 2016, 1267–1273.

64 A. R. Burgoyne, B. C. E. Makhubela, M. Meyer and G. S. Smith, *Eur. J. Inorg. Chem.*, 2015, **2015**, 1433–1444.

65 B. C. E. Makhubela, M. Meyer and G. S. Smith, *J. Organomet. Chem.*, 2014, **772**–**773**, 229–241.

66 F. A. Beckford, M. B. Niece, B. P. Lassiter, S. J. Beebe and A. A. Holder, *J. Biol. Inorg. Chem.*, 2018, **23**, 1205–1217.

67 J. Fang, H. Nakamura and H. Maeda, *Adv. Drug Deliv. Rev.*, 2011, **63**, 136–151.

68 T. Sun, Y. Zhang, B. Pang, D. Choon Hyun, M. Yang and Y. Xia, *Angew. Chem. Int. Ed.*, 2014, **46**, 12320–12364.

Chapter 2

Synthesis and Characterization of tris(2-aminoethyl)amine-based 2,5-disubstituted benzimidazoles

2.1 Introduction

Over the years of active research, the benzimidazole nucleus has evolved to be an important privileged heterocyclic structure in medicinal chemistry. There are several examples of benzimidazole-containing compounds that show appreciable antiparasitic, antiviral, antimalarial and anticancer activity.[1, 2] It is well documented that modification at the 2- and 5-position of the benzimidazole scaffold yields a number of biologically active compounds with varying cellular targets.[3] The wide range of pharmacological activities of benzimidazole-containing drugs is attributed to the unique fused benzene and imidazole rings which form the benzimidazole core. These fused rings may interact with an array of biological targets in a non-covalent manner, which may be attributed to the electron-rich nature of the benzimidazole heterocyclic system.[4]

Several benzimidazole-based compounds have been approved for clinical use for the treatment of various ailments.[5,6] The most commonly known examples include the anthelmintic drugs albendazole (methyl [5-(propylthio)-*1H*-benzoimidazol-2-yl]carbamate) and mebendazole (methyl *N*-(6-benzoyl-1*H*-benzimidazol-2-yl)carbamate), and the antiulcer drug lansoprazole (2-[[3-methyl-4-(2,2,2-trifluoroethoxy)pyridin-2-yl]methylsulfinyl]-1*H*-benzimidazole).[5] Despite the great success of the benzimidazole system in the clinical treatment of various diseases, the accomplishments of the heterocyclic system are not reflected in the treatment of cancer. There is only a single benzimidazole-containing drug that is currently approved for the clinical treatment of cancer, bendamustine (4-[5-[bis(2-chloroethyl)amino]-1-methylbenzimidazol-2-yl]butanoic acid) (Figure 2.1 a), which used to treat chronic lymphocytic leukemia and myeloma.[7] Additionally, there are two compounds in Phase III clinical trials that contain the benzimidazole nucleus, selumetinib[8] (6-(4-bromo-2-

chloroanilino)-7-fluoro-*N*-(2-hydroxyethoxy)-3-methylbenzimidazole-5-carboxamide) and galeterone[9] ((3*S*,8*R*,9*S*,10*R*,13*S*,14*S*)-17-(benzimidazol-1-yl)-10,13-dimethyl-2,3,4,7,8,9,11,12,14,15-decahydro-1*H*-cyclopenta[a]phenanthren-3-ol) (Figure 2.1 b and c, respectively).

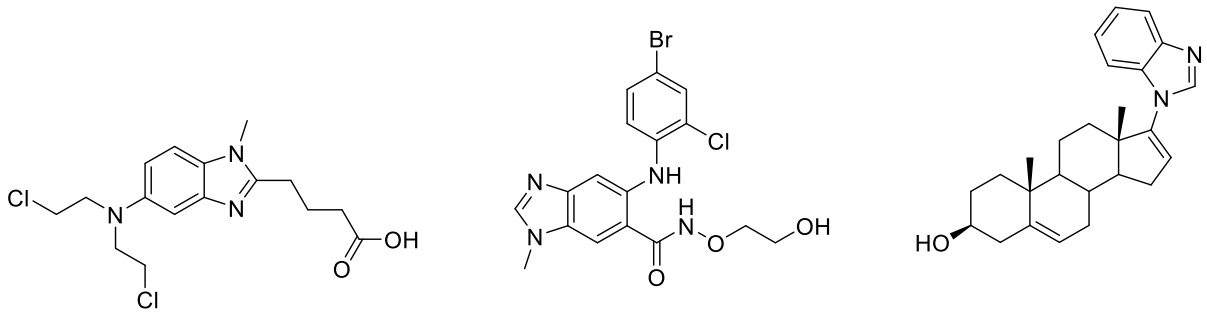

a) Bendamustine b) Selumetinib c) Galeterone

***Figure 2.1**: The chemical structures of benzimidazole-based drugs in clinical use (a) and in clinical trials (b and c).*[7 - 9]

Numerous trimeric benzimidazoles have been reported for their potential biological applications, including Hoechst 33258 DNA stain-inspired trinuclear benzimidazoles,[10] RNA-cleaving tris(2-aminobenzimidazoles),[11] citric acid-based antibacterial tris-benzimidazoles[12] and antimicrobial triazine-based tripodal tris-benzimidazoles.[13] However, there have been no reports of tris(2-aminoethyl) based benzimidazoles. The prevalence of the benzimidazole core in biological molecules and the applications of the scaffold as synthons for various biologically important compounds has stimulated the need for the development of simple and efficient methods to synthesize this heterocyclic system. To this end, the synthesis and characterization of a series of 2,5-disubstituted trimeric benzimidazole compounds, and their intermediates is reported in this chapter.

2.2 Synthesis of 2,5-disubstituted tris-benzimidazole compounds (7 – 15) and their corresponding intermediates

The synthesis of the 2,5-disubstituted tris-benzimidazoles (**7** – **15**) involved three steps: i) A nucleophilic aromatic substitution reaction (S_NAr) of tris(2-aminoethyl)amine with either *ortho*-substituted fluoro- or chloro- nitrobenzenes ii) the reduction of the nitro-functionalities to primary amine groups, and last of all, iii) the condensation-cyclisation with

either benzaldehyde, 2-pyridinecarboxaldehyde or ferrocenecarboxaldehyde to afford the desired tris-benzimidazole compounds (Scheme 2.1).

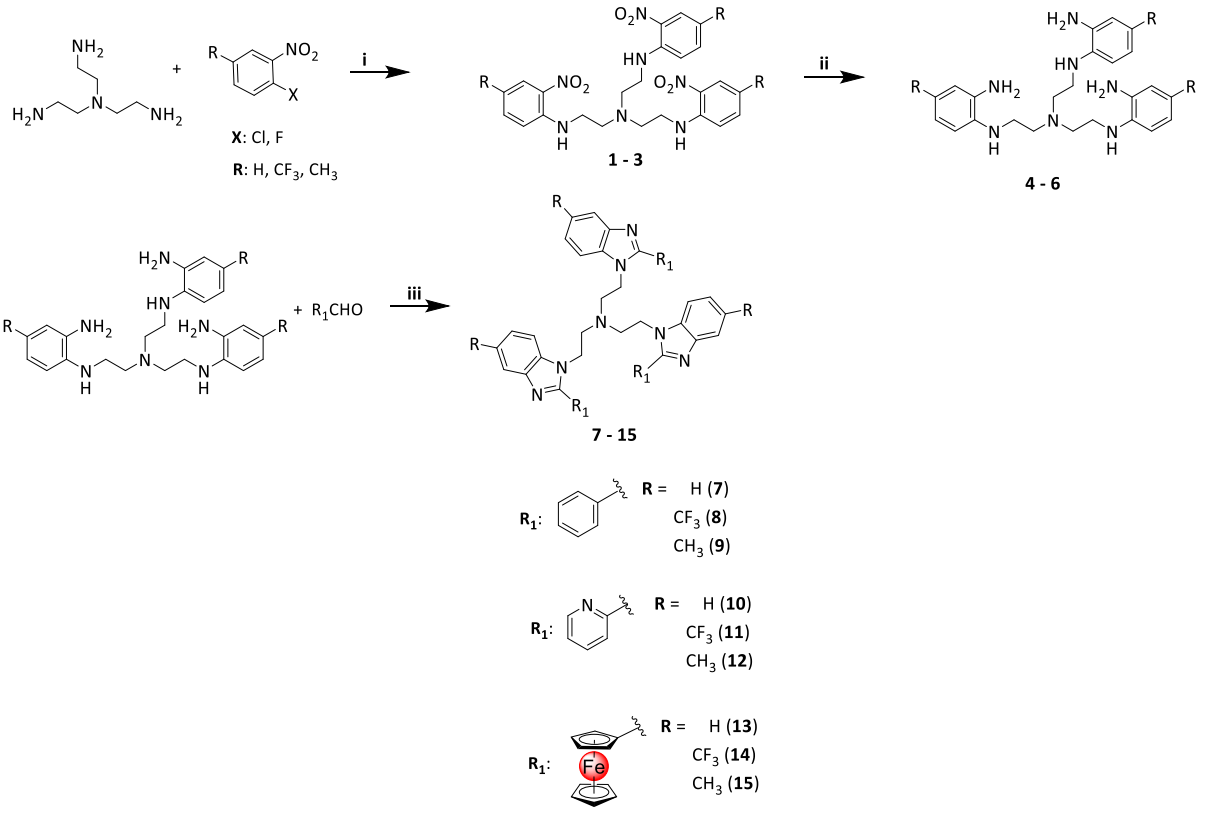

Scheme 2.1: *Synthesis of the intermediates and the 2,5-disubstituted tris-benzimidazoles. Reagents and conditions: i) DMF/ RT/ 24 h; ii) Zn/ NH_4Cl/ MeOH/ RT/ 1 h; iii) Benzaldehyde, 2-pyridinecarboxaldehyde or ferrocenecarboxaldehyde / TFA/ EtOH/ $MgSO_4$/ 80 °C or RT/ 24 h.*

There are several reported methods in which the synthesis of 2-aryl substituted benzimidazoles is described.[14–18] The reaction of *o*-phenyldiamenes with aromatic aldehydes in the presence of an acid catalyst remains one of the popular methods due to the one-pot nature and simplicity of procedures in yielding benzimidazoles.[19] The first step towards the synthesis of the tris-benzimidazole compounds reported in this chapter entails the synthesis of the tris-nitrobenzenes (**1 – 3**).

2.2.1 The synthesis of tris-nitrobenzenes (1 – 3)

2.2.1.1 Synthesis

The first step towards the synthesis of the tris-benzimidazole compounds is a S_NAr reaction, in which an excess of a commercially available *ortho*-halogenated nitrobenzene is reacted with one molar equivalent of tris(2-aminoethyl)amine (Scheme 2.2).

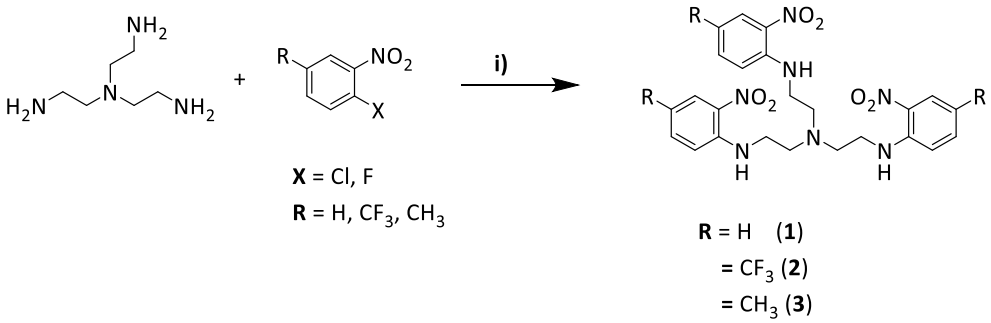

***Scheme 2.2**: The general synthetic route for the tris-nitrobenzenes (**1 – 3**). Reagents and conditions: DMF/ RT/ 24 h.*

A S_NAr reaction is described as a reaction in which a nucleophile displaces a good leaving group, commonly a halogen, on an aromatic ring. The core prerequisite of a S_NAr reaction is that a strong electron-withdrawing group is present in either the *ortho*- or *para*- positions relative to the nucleofuge. The electron-withdrawing group serves to stabilize the Meisenheimer complex, which is formed as an intermediate as the reaction proceeds, *via* a negative resonance effect (Scheme 2.3). The Meisenheimer complex is formed as a result of the nucleophilic addition of the tris(2-aminoethyl)amine nucleophile onto the aromatic ring. The subsequent elimination of the halogen from the aromatic ring and successive proton transfer yields the tris-nitrobenzene.

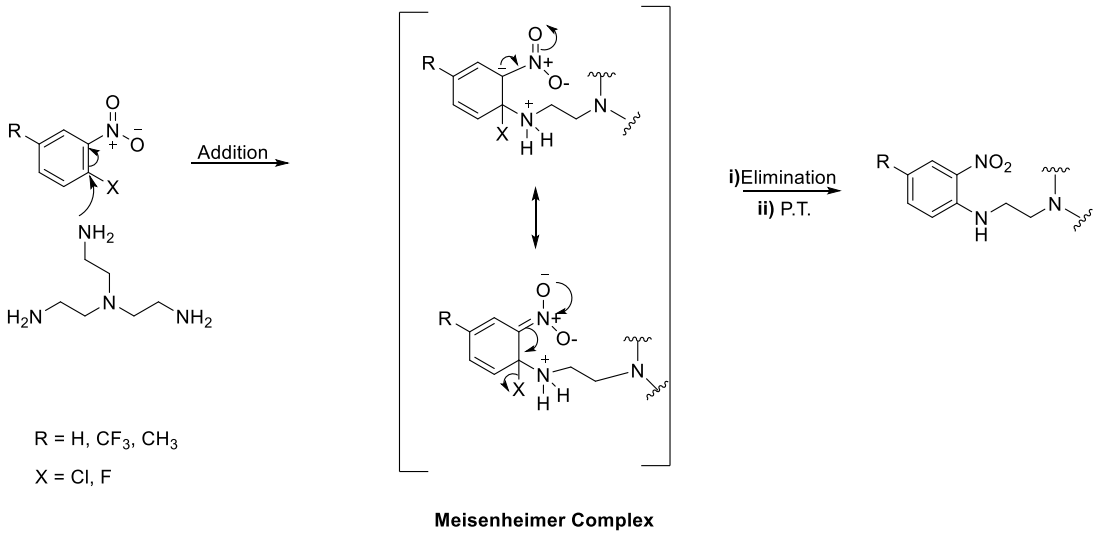

***Scheme 2.3**: The proposed general mechanism of the Nucleophilic Aromatic Substitution (S_NAr) reaction to yield the tris-nitrobenzene compounds.*

Generally, the synthesis of the tris-nitrobenzenes proceeded with ease, with the conversion of starting materials occurring under mild conditions. After 24 hours, TLC analysis showed the near-complete conversion of the starting materials to a new, more polar product. The desired compounds were isolated *via* column chromatography as bright yellow solids (**1** and **2**) or a dark orange solid (**3**) in moderate yields between 35% and 48%.

2.2.1.2 Characterization

Analysis of the ^{1}H NMR spectra of compounds **1** – **3** (Figure 2.2) confirmed the successful synthesis of the desired tris-nitrobenzenes. The presence of a triplet between δ_H 8.08 and δ_H 8.45 ppm (H-g for **1** and H-h for **2** and **3**), integrating for three protons corresponding to the secondary amine protons, and the two distinct aliphatic signals at δ_H ~3.50 ppm and δ_H ~2.90 ppm (H-h and H-i for **1**, H-i and H-j for **2** and **3**) individually integrating for six protons corresponding to the methylene protons of the tris- core, are all indicative of introduction of the tris- core onto the aromatic rings. Additionally, in the aromatic region of the spectra, either three (for **2** and **3**) or four (for **1**) distinct aromatic signals are observed and these signals collectively integrate for nine and twelve protons, respectively, and are assigned to the protons on the aromatic rings of the tris-nitrobenzenes.

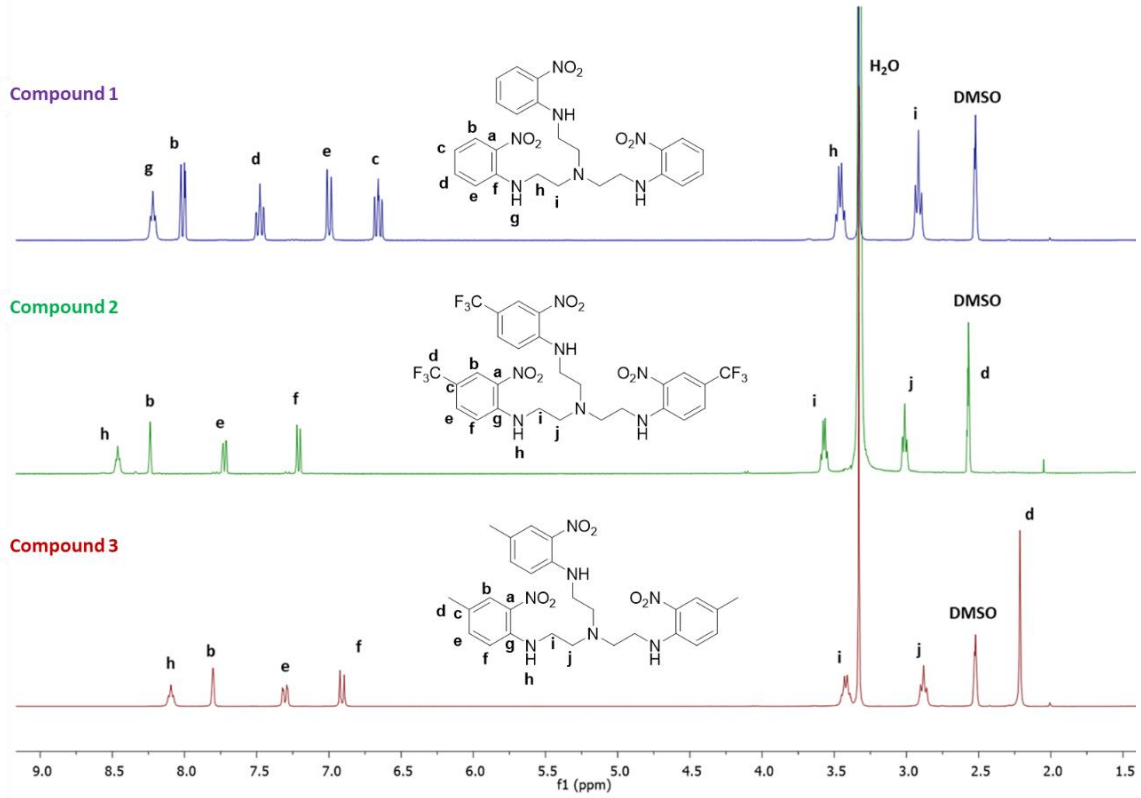

Figure 2.2: *The stacked ^{1}H NMR spectra of the tris-nitrobenzene compounds (**1** – **3**) in DMSO (d_6).*

The splitting of these aromatic signals is consistent with a splitting pattern associated with a 1,2,4-trisubstituted aromatic ring (apart from **1**, as this compound is 1,2-disubstituted) with three electronically distinct functional groups. Furthermore, in the ^{13}C{^{1}H}-NMR spectra of the tris-nitrobenzenes (**1** – **3**), the expected eight (for **1**) or nine (for **2** and **3**) signals are observed, which correlate to the proposed compounds.

2.2.2 The synthesis of tris-1,2-benzenediamines (4 – 6)

2.2.2.1 Synthesis

The synthesis of the tris-1,2-benzenediamines (**4** – **6**) from the corresponding tris-nitrobenzenes (**1** – **3**) involved the reduction of the nitro- groups to primary amine functionalities. This was achieved by the reaction of the tris-nitrobenzenes with thirty molar equivalents of ammonium chloride and sixty molar equivalents of zinc powder. This method gave the highest yields of the desired products under mild conditions (Scheme 2.4).

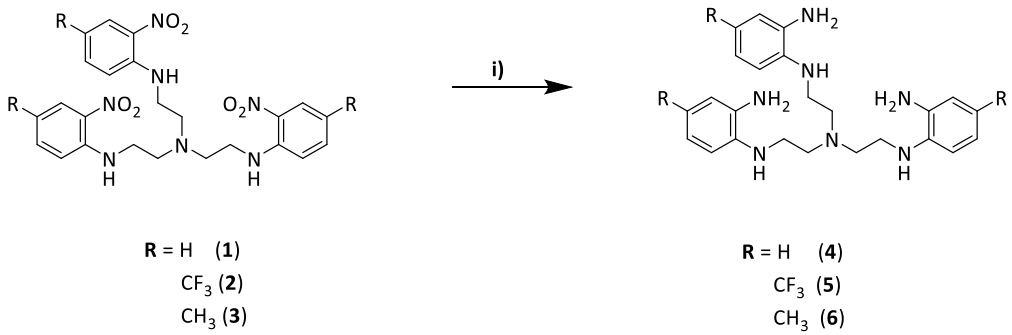

Scheme 2.4: *The general synthesis of the tris-1,2-benzenediamines (**4** – **6**). Reagents and conditions: Zn/ NH_4Cl/ MeOH/ RT/ 1 h.*

After an hour, TLC analysis showed the complete conversion of the tris-nitrobenzene limiting reagent (**1** – **3**) to a new more polar product. Purification by column chromatography, with ethyl acetate as the eluent in each instance, afforded the desired products as either dark brown solids (**4** and **6**) or a beige solid (**5**) in excellent yields ranging between 76% and 97%.

2.2.2.2 Characterization

Upon comparison of the ^{1}H NMR spectra of the tris-1,2-benzenediamines (**4** – **6**) (Figure 2.3) with the ^{1}H NMR spectra of the corresponding precursor tris-nitrobenzenes (**1** – **3**) (Figure 2.2, *vide supra*), there are several indicators of successful reduction of the nitro-functionalities to primary arylamine moieties. Firstly, in the aromatic region of the spectra, an interesting trend was observed in which the aromatic protons of the tris-1,2-benzenediamines (**4** – **6**) converge and some coalesce, relative to the aromatic protons of the corresponding tris-nitrobenzene (**1** – **3**). This is attributed to the similar electronic effects that the primary and secondary amine functionalities exert on the aromatic ring. Secondly, the presence of an additional signal which corresponds to the primary amine protons, at δ_H 4.40, δ_H 4.84 and δ_H 4.32 ppm for **4**, **5** and **6**, respectively, validates the reduction of all the aryl nitro- moieties to primary amine functionalities. However, when comparing the aliphatic regions of the spectra on the tris-1,2-benzenediamines (**4** – **6**) with the ^{1}H NMR spectra of the corresponding tris-nitrobenzene (**1** – **3**), no significant changes were observed, as two aliphatic signals with individual integrations of six are observed. These aliphatic signals correspond to the methylene protons of the tris- core.

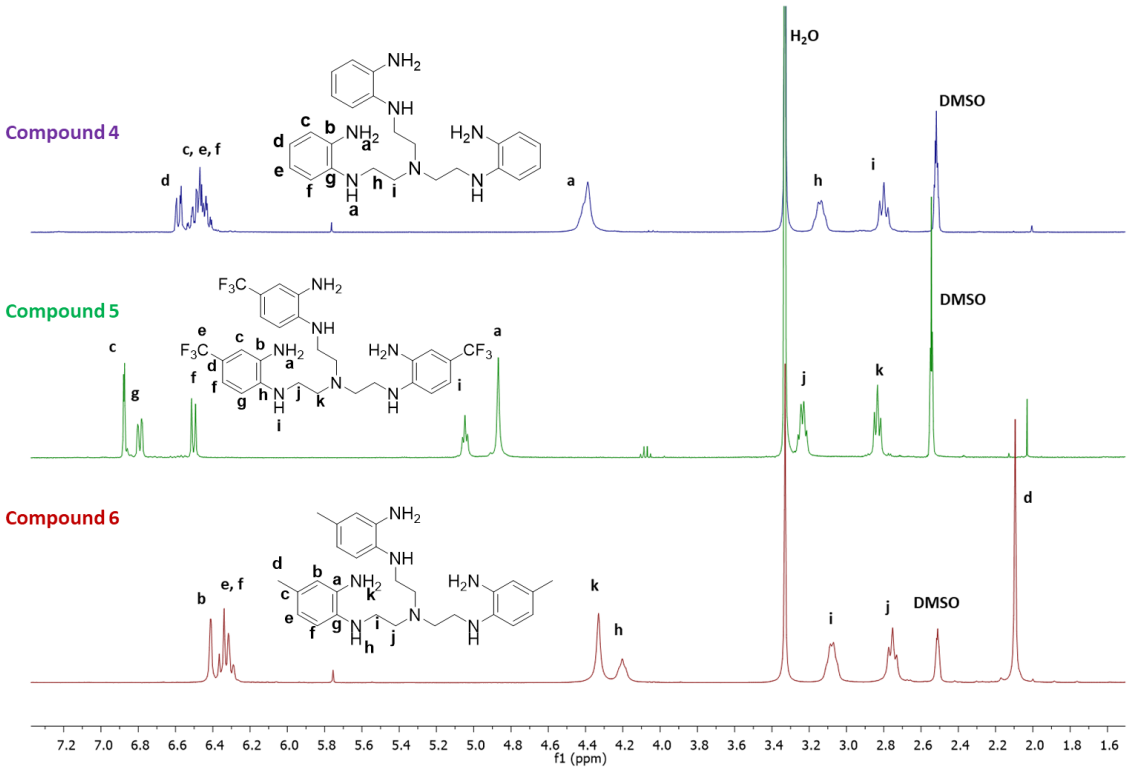

Figure 2.3: *The stacked ^{1}H NMR spectra of the tris-1,2-benzenediamine compounds (**4** – **6**) in DMSO (d_6).*

Comparison of the $^{13}C\{^1H\}$-NMR spectra of the tris-1,2-benzenediamines (**4** – **6**) to the $^{13}C\{^1H\}$-NMR spectra of the corresponding tris-nitrobenzene precursors (**1** – **3**) revealed a general upfield shift of the aromatic carbon signals of the tris-1,2-benzenediamines (**4** – **6**) is observed, shifting from δ_C 147 – 115 ppm in the tris-nitrobenzenes to δ_C 139 – 108 ppm in the tris-1,2-benzenediamines. This shift may be attributed to the electron-donating nature of the primary amine moiety on each aromatic ring resulting in increased electron density in the aromatic rings of the tris-1,2-benzenediamines, further attesting to the successful reduction of the nitro- functionalities to primary amine moieties.

Infrared spectroscopic analysis of the compounds **4** – **6** revealed two absorption bands between 3306 and 3373 cm^{-1} in each spectrum (summarized in Table 2.1). These absorption bands are diagnostic of the symmetrical and asymmetrical stretches of primary amine functionalities and are thus indicative of the presence of the primary aryl amine groups. This further corroborates the successful synthesis of the tris-1,2-benzenediamines.

***Table 2.1**: Summarised Infrared spectroscopic data for the tris-1,2-benzenediamine compounds (**4** – **6**)*

Compound	1° Amine$_{R\text{-}NH_2}$ (cm^{-1})
4	3366 and 3299
5	3342 and 3306
6	3373 and 3318

Combined, these spectroscopic analyses all attest to the successful synthesis of the tris-1,2-benzenediamine compounds (**4** – **6**) from their respective tris-nitrobenzene (**1** – **3**) precursors.

2.2.3 Synthesis of 2,5-disubstituted tris-benzimidazoles (7 – 15)

2.2.3.1 Synthesis

The synthesis of the 2,5-disubstituted benzimidazole compounds entailed a cyclization-condensation reaction of the synthesized tris-1,2-benzenediamines (**4** – **6**) with 3.6 molar equivalents of either benzaldehyde, 2-pyridinecarboxaldehyde or ferrocenencarboxaldehyde in the presence of a catalytic amount of trifluoroacetic acid (TFA) and magnesium sulfate (Scheme 2.5).

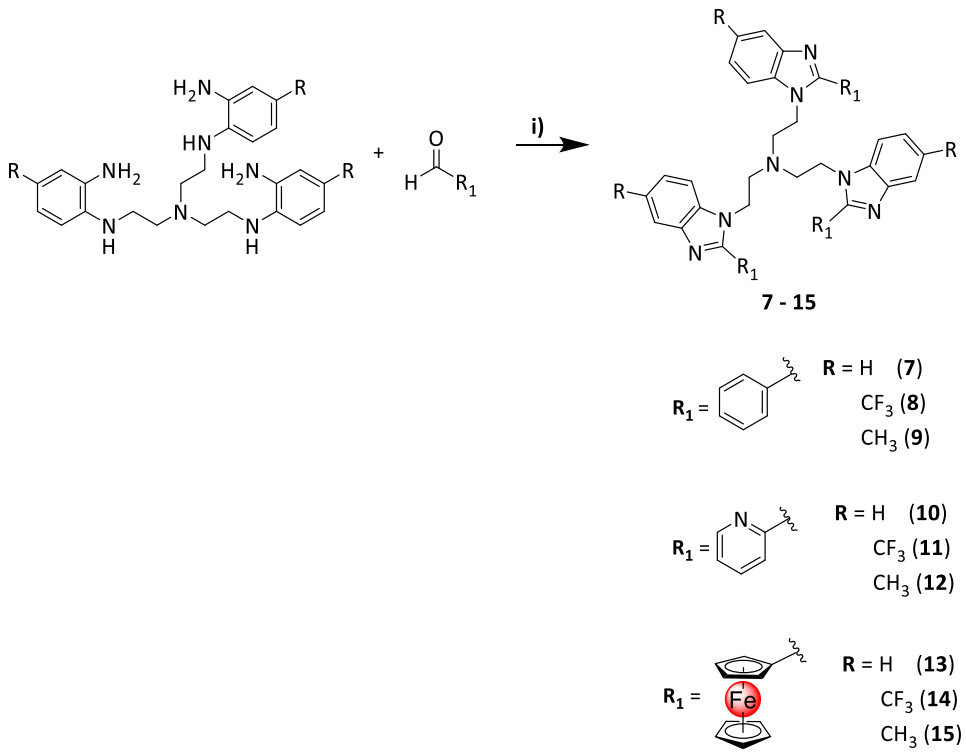

***Scheme 2.5**: The general synthesis of 2,5-disubstituted tris-benzimidazole compounds (**7** – **15**). Reagents and conditions: Benzaldehyde, 2-pyridinecarboxaldehyde or ferrocenecarboxaldehyde / TFA/ EtOH/ $MgSO_4$/ 80 °C or RT/ 24 h.*

There are numerous methods describing the synthesis of benzimidazoles from *o*-phenylenediamines and the various biological applications of these benzimidazoles.[15,20,21] However, mechanistic insights into the acid-catalyzed synthesis of 2-arylsubstituted benzimidazoles from *o*-phenylenediamines and aryl aldehydes are very limited. Recent mechanistic studies propose that the reaction occurs *via* a sequence of steps that are catalyzed by hydrochloric acid, oxalic acid or tosylic acid.[22–24] The proposed mechanism for the cyclization-condensation reactions performed in this study (Scheme 2.6) is based on these mechanisms.[22–24]

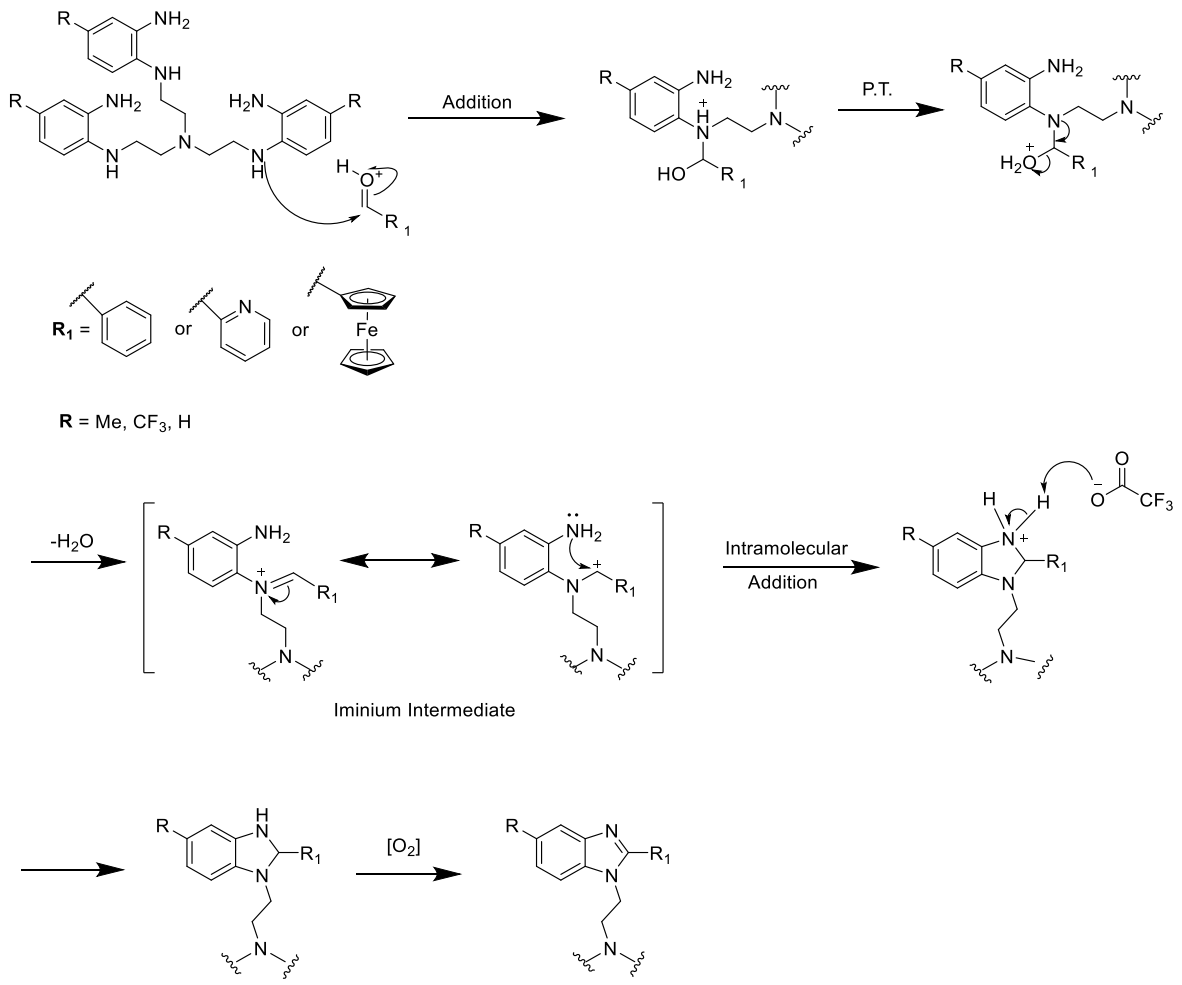

Scheme 2.6*: The proposed mechanism of the cyclization-condensation reaction for benzimidazole synthesis.*

In all the reported mechanisms,[22–24] the first step is the acid-catalyzed nucleophilic attack of the aldehyde. Here, trifluoroacetic acid plays the crucial role of protonating the carbonyl oxygen of the aldehyde, resulting in the increased electrophilicity of the carbonyl carbon, making the carbonyl carbon more susceptible to nucleophilic attack. The secondary amine of the synthesized tris-1,2-benzenediamines acts as the nucleophile in this step. This can be attributed to the inductively electron-donating methylene carbon adjacent to the secondary amine nitrogen, which results in an increased abundance of electron density on the secondary amine nitrogen relative to the primary amine nitrogen. Due to the well-reported correlation between basicity and nucleophilicity,[25–27] the secondary amine nitrogen has more nucleophilic character relative to the primary amine. Thus, the secondary amine acts as the nucleophile in the first addition (A_N) step. Furthermore, it is only the nucleophilic attack by the secondary amine nitrogen that will result in the formation of the iminium intermediate,

which forms after the elimination of water (Scheme 2.6). This is subsequently followed by intramolecular nucleophilic attack of the iminium carbon by the primary amine moiety, yielding the hydrobenzimidazole which is aerobically oxidized to afford the benzimidazole.[28] Therefore, the reactions in which the tris-benzimidazoles were synthesized were allowed to progress in air, to ensure optimal oxidation of the hydrobenzimidazole.

After 24 hours, TLC analysis showed the complete conversion of the limiting reagents (**4 – 6**) to a new more polar product. The pure products were isolated using column chromatography as various coloured solids in moderate to good yields, ranging between 33% and 71%.

2.2.3.2 Characterization

*2.2.3.2.1 Characterization of the 2-phenyl and 2-pyridyl ligands (**7** – **12**)*

Analysis of the ^{1}H NMR spectra of 2-aryl tris-benzimidazole ligands **9 – 12** (Figures 2.4 and 2.5) correlates with the proposed structures of these ligands. Comparison of the spectra corresponding previously synthesized tris-1,2-benzenediamines (**4** – **6**) (Figure 2.3, *vide supra*), the ^{1}H NMR spectra of the tris-benzimidazole ligands (**9** – **12**) did not show any significant changes in the aliphatic region, as two aliphatic signals, integrating for six protons each, are observed and correspond to the methylene protons (H-a and H-b) on the tris- core. However, in the aromatic region, additional aromatic signals collectively integrating for either fifteen (for **7** - **9**) or twelve protons (for **10** - **12**) are observed. These additional aromatic signals correspond to the protons of the phenyl or 2-pyridyl functionalities on the 2-positions of the benzimidazole cores and are indicative of the successful synthesis of the benzimidazole cores.

Furthermore, an additional five (for **7** - **9**) or six (for **10** - **12**) aromatic signals are observed in the ^{13}C{^{1}H}-NMR spectra of the tris-benzimidazole ligands (**9** – **12**) relative to their respective tris-benzenediamines (**4** – **6**). These additional carbons are indicative of the formation of the benzimidazole motif and corroborate the introduction of the phenyl or the 2-pyridyl functionalities at the 2-positions of the benzimidazole cores.

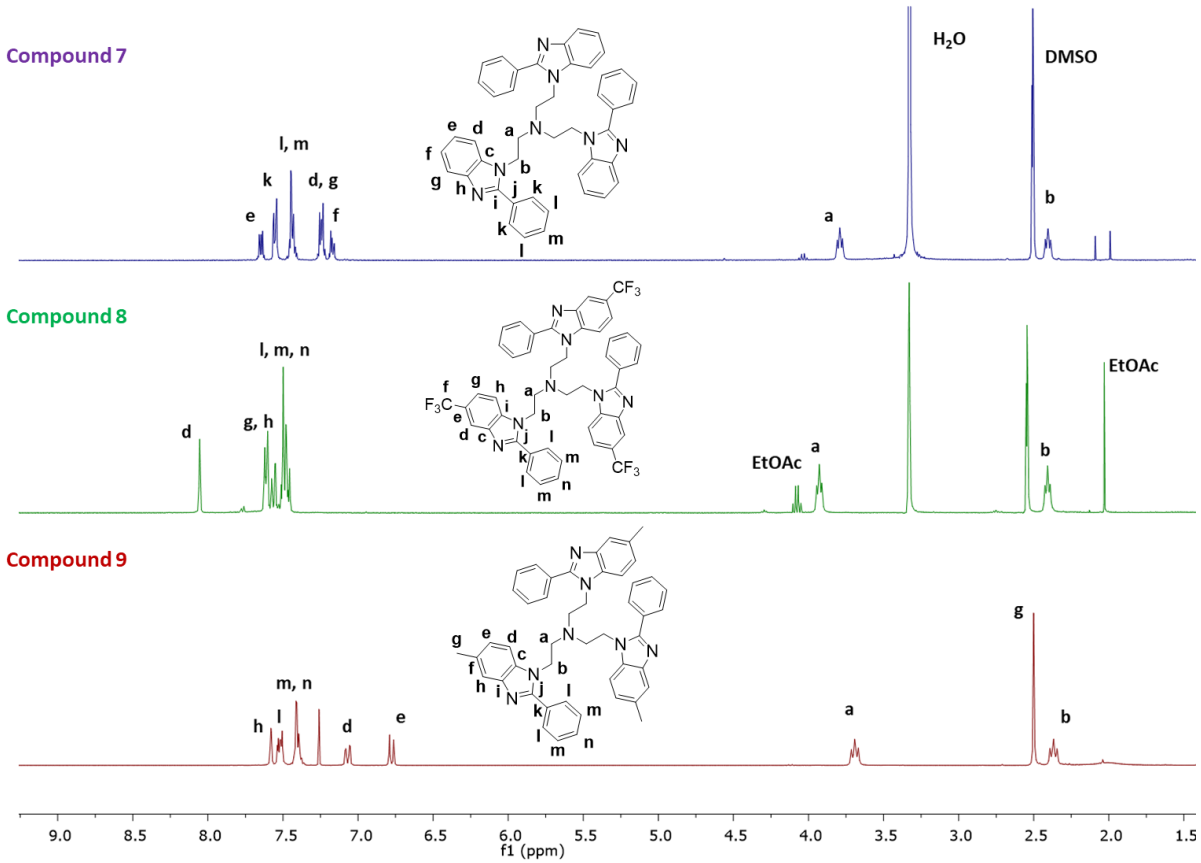

Figure 2.4: *The stacked ^{1}H NMR spectra of the 2-phenyl tris-benzimidazole ligands (**7** – **9**) in DMSO (d_6).*

Infrared spectral analysis of the tris-benzimidazole ligands (**7** – **12**) revealed a general trend. In the IR spectra of the 2-phenyl benzimidazoles (**7** - **9**), an absorption band between 1695 - 1625 cm^{-1} was observed and this absorption band corresponds to the imine (C=N) moiety. The IR spectra of the 2-pyridyl tris-benzimidazole ligands (**10** – **12**) revealed two absorption bands, one in the range 1592 - 1733 cm^{-1} and another in the range 1489 - 1587 cm^{-1}. These absorption bands correspond to imine (C=N) bond stretch on the benzimidazole core and the C=N bond stretch of 2-pyridyl functionality, respectively. This further validates the synthesis of the tris-benzimidazole ligands (**7** - **12**).

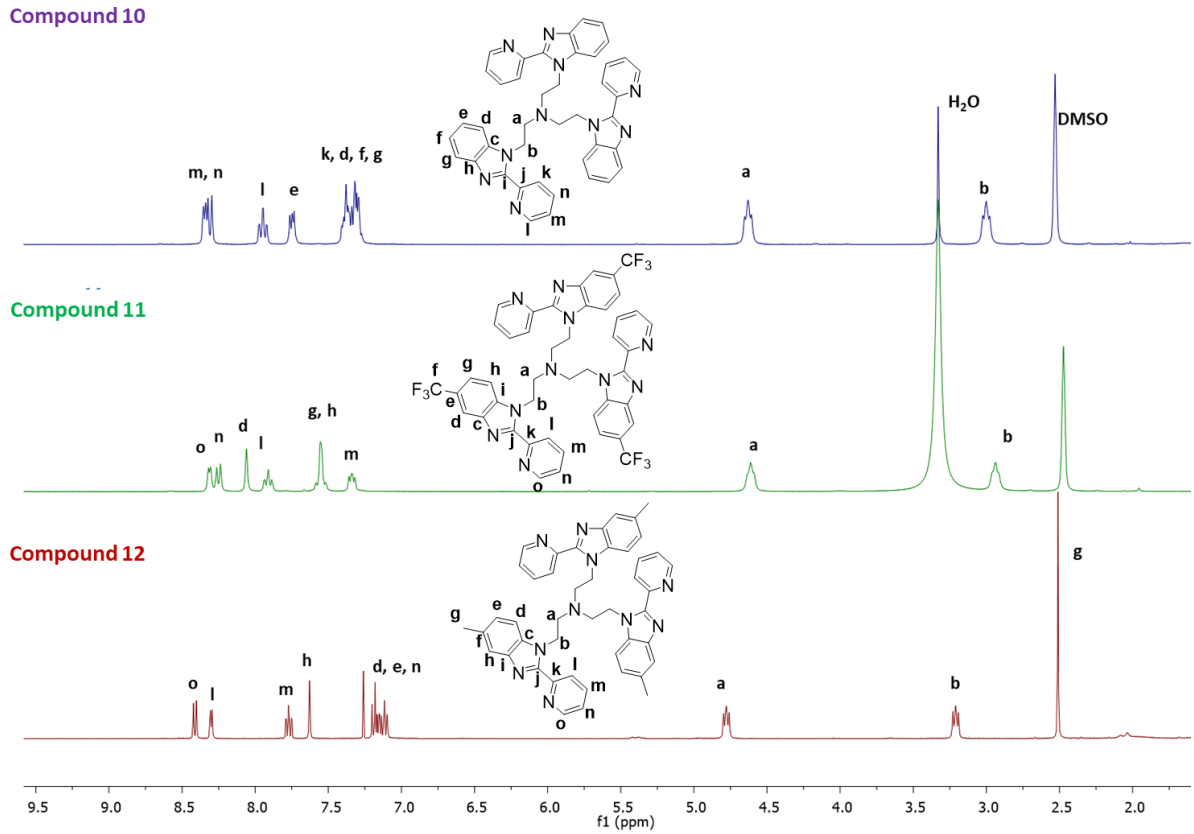

Figure 2.5: *The stacked ^{1}H NMR spectra of the 2-pyridyl tris-benzimidazole ligands (**10** – **12**) in DMSO (d_6).*

In addition, the purity of the tris-benzimidazole ligands (**7** – **12**) was attested to by High-Performance Liquid Chromatography (HPLC). From the data attained, the compounds were 94 – 99% pure, and thus sufficiently pure for *in vitro* anticancer evaluation (Chapter 4, *vide infra*).

Single crystal X-ray Diffraction (XRD) is a valuable tool in confirming the molecular structures of compounds. Single crystal XRD was used to confirm the molecular structure of compound **9** in the solid-state. Single crystals of **9** were obtained by slow diffusion of a concentrated solution of **9** in dichloromethane layered with ethyl acetate, at room temperature. The molecular structure of **9** is depicted in Figure 2.6 and further crystallographic data is available in Table 2.2.

Compound **9** crystallized in the triclinic crystal system and P_{-1} space group, with two molecules present per cell unit. The fluorine atoms of two, of the three, trifluoromethyl groups C9A and C9C are disordered over two sites, with refined site occupancy factors of 0.615(15) for F1A, F2A and F3A, 0.315(15) for F4A, F5A and F6A; 0.778(9) for F1C, F2C and F3C, 0.222(9) for F4C, F5C and F6C. The imine (C=N) bond lengths in the benzimidazole core range from 1.317 Å to 1.320 Å, which are comparable to imine bond lengths reported in literature for 2-phenyl benzimidazole compounds.[29,30]

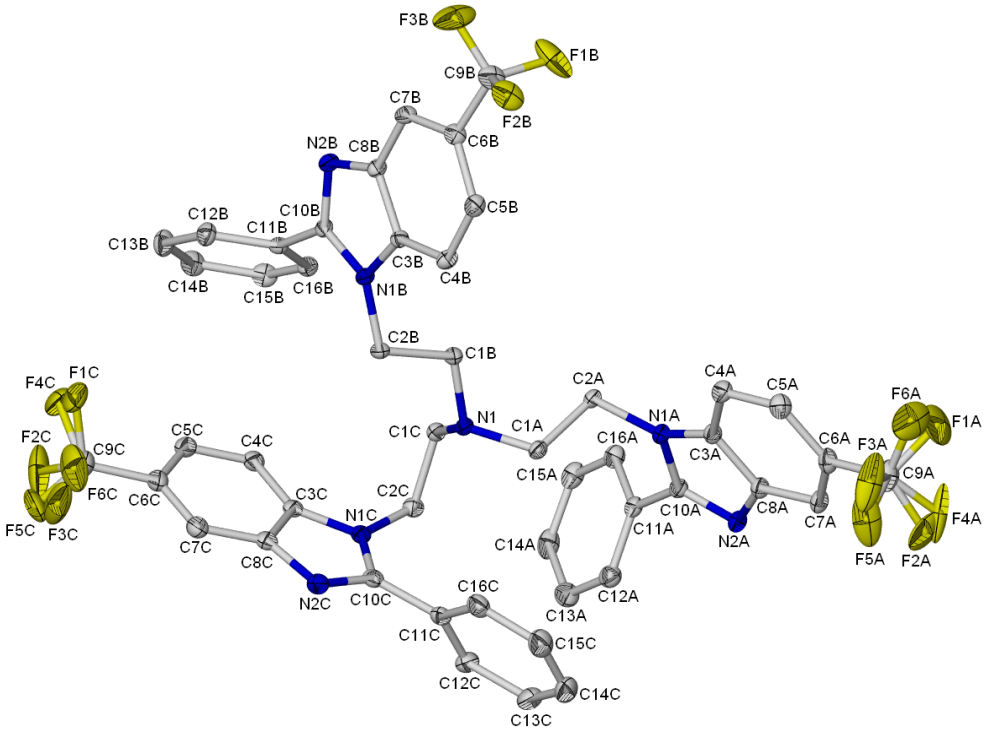

Figure 2.6: *The ORTEP drawing of the molecular structure of compound* ***9****, hydrogen atoms have been omitted for clarity. Thermal ellipsoids are at the 50% probability level.*

Table 2.2**: Selected crystallographic data for compound **9

	Compound **9**
Empirical formula	$C_{48}H_{36}F_9N_7$
Formula weight	881.85
Temperature (K)	173(2)
Crystal system	Triclinic
Space group	P_{-1}
a (Å)	12.9590(8)
b (Å)	13.5286(10)
c (Å)	14.2464(10)
α (°)	70.930(2)
β (°)	64.023(2)
γ (°)	81.799(2)
Volume ($Å^3$)	2122.1(3)
Z	2
ρ_{calc} (g/cm^3)	1.380
μ (mm^{-1})	0.111
F(000)	908.6
Crystal size(mm^3)	0.18 × 0.18 × 0.12
Radiation	MoKα (λ = 0.71073)
2Θ range for data collection (°)	3.18 to 56.62
Index ranges	-17 ≤ h ≤ 17, -18 ≤ k ≤ 18, -18 ≤ l ≤ 18
Reflections collected	55275
Independent reflections	10545 [R_{int} = 0.0656, R_{sigma} = 0.0528]
Data/restraints/parameters	10545/15/633
Goodness-of-fit on F^2	1.030
Final R indexes [I>=2σ (I)]	R_1 = 0.0504, wR_2 = 0.1011
Final R indexes [all data]	R_1 = 0.0907, wR_2 = 0.1215
Largest diff. peak/hole (e $Å^{-3}$)	0.36/-0.38

*2.2.3.2.2 Characterization of the 2-ferrocenyl compounds (**13** – **15**)*

In the ^{1}H NMR spectra for the 2-ferrocenyl tris-benzimidazole compounds (**13** – **15**) (Figure 2.7) there are several indicators of the successful synthesis of the 2-ferrocenyl tris-benzimidazole compounds. Upon comparison of the ^{1}H NMR spectra of **13** – **15** to the spectra of the respective tris-1,2-benzenediamines (**4** – **6**) (Figure 2.3, *vide supra*), three additional signals at δ_H ~4.75 ppm (H-l for **14** and **15**, H-k for **13**), δ_H ~4.50 ppm (H-m for **14** and **15**, H-l for **13**) and δ_H ~4.15 (H-Cp) ppm are observed. These additional signals correspond to the protons on the substituted and unsubstituted cyclopentadienyl (Cp) rings, respectively. This is the first indicator of the successful introduction of the ferrocenyl entity onto the 2-positions of the benzimidazole motifs. Furthermore, when comparing the ^{13}C{^{1}H}-NMR spectra of **13** – **15** to their corresponding tris-1,2-benzenediamines (**4** – **6**), five additional signals are observed, which are also indicative of the formation of the benzimidazole cores and indicate the incorporation of the ferrocenyl moiety onto the 2-positions of the benzimidazole scaffolds.

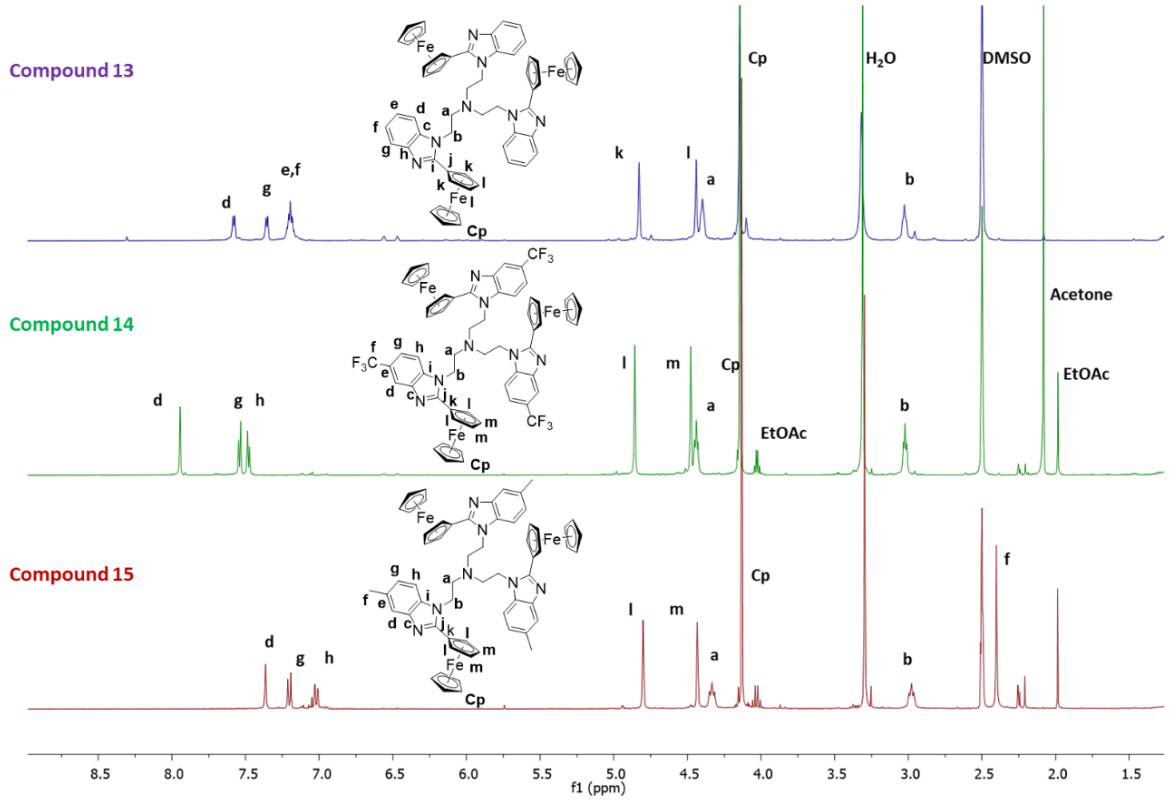

Figure 2.7: *The stacked ^{1}H NMR spectra of the 2-ferrocenyl tris-benzimidazole compounds (**13** – **15**) in DMSO (d_6).*

Analysis of the 2-ferrocenyl tris-benzimidazole compounds (**13** – **15**) using IR spectroscopy revealed an absorption band in the range 1611 – 1620 cm^{-1} corresponding to the imine (C=N) functional group (Table 2.3). This is indicative of the successful synthesis of the benzimidazole motifs present in the compounds.

High-Resolution Electrospray Ionisation (HR-ESI) mass spectrometry data was obtained for the 2-ferrocenyl tris-benzimidazole compounds (**13** – **15**). Generally, a base peak corresponding to the protonated molecular ion, $[M+H]^+$, was observed. The ESI-MS data for **13** – **15** is summarized in Table 2.3 and attests to the integrity of the compounds.

Table 2.3*: A summary of the ESI-MS and the IR spectroscopy data obtained for the 2-ferrocenyl tris-benzimidazole compounds (**13 – 15**)*

Compound	Calculated [*m/z*]	Found [*m/z*]	IR $(C=N)_{Imine}$ (cm^{-1})
13	1002.6270	1002.2359 $[M+H]^+$	1611
14	1206.1956	1206.1980 $[M+H]^+$	1613
15	1044.2804	1044.2837 $[M+H]^+$	1620

The correlation between the proposed structures and the spectroscopic and analytical results concludes that the desired 2,5-disubstituted tris-benzimidazole compounds (**7** – **15**) were indeed synthesized from their respective precursors.

2.3 Synthesis of the monomeric 2-pyridylbenzimidazole ligand (18)

2.3.1 Synthesis

The monomeric 2-pyridylbenzimidazole ligand (**18**) was synthesized after the *in vitro* anticancer evaluation of the 2,5-disubstituted tris-benzimidazole compounds (**9** – **15**), later discussed in Chapter 4 (*vide infra*). From the *in vitro* anticancer results attained, the 5-unsubstituted 2-pyridyl tris-benzimidazole ligand (**10**) was observed to show superior anticancer activity against the tested cancer cell lines (Chapter 4, Sections 4.2 and 4.3, *vide infra*). Consequentially, the mononuclear counterpart (**18**) of the trimeric ligand **10** was synthesized.

The synthesis of the 1-ethyl-2-(pyridin-2-yl)-1*H*-benzo[*d*]imidazole ligand (**18**) was carried out using the same three-step procedure as previously described in Section 2.2, for the synthesis of the 2,5-disubstituted tris-benzimidazole compounds (*vide supra*), using the relevant molar equivalents (Scheme 2.7).

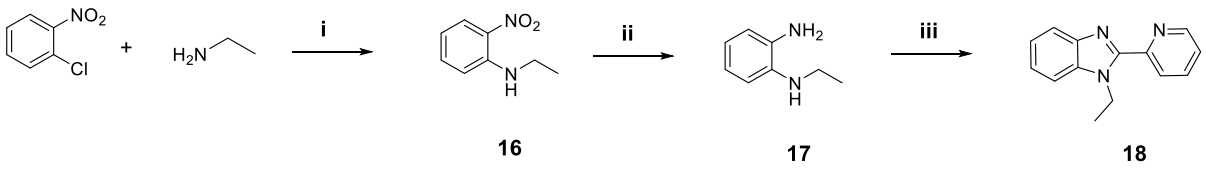

Scheme 2.7*: The synthesis of the synthons and the monomeric 2-pyridylbenzimidazole ligand (**18**). Reagents and conditions: i) DMF/ RT/ 24 h; ii) Zn/ NH_4Cl/ MeOH/ RT/ 1 h; iii) 2-Pyridinecarboxaldehyde / TFA/ EtOH/ $MgSO_4$/ RT/ 24 h.*

The synthesis of the nitroaniline precursor (**16**) involved a S_NAr reaction of 1-chloro-2-nitrobenzene with ethylamine. After 24 hours, the presence of a more polar product was observed on TLC. The nitroaniline **16** was isolated in a moderate yield of 37% as a bright yellow oil.

The nitroaniline (**16**), was successively reduced to the benzene-1,2-diamine (**17**). The benzene-1,2-diamine (**17**) was subsequently reacted with 2-pyridinecarboxaldehyde to yield the 2-pyridylbenzimidazole (**18**). The benzene-1,2-diamine precursor (**17**) and the benzimidazole ligand (**18**) were isolated in good yields of 83% and 42%, respectively.

2.3.2 Characterization

In the ^{1}H NMR spectrum of the nitroaniline (**16**) (Figure 2.8), resonances diagnostic of the formation of the desired products are observed. Firstly, in the aromatic region of the spectrum (δ_H 6.50 – 8.50 ppm), aromatic protons with a collective integration of four protons, assigned to the aromatic protons of the nitroaniline (**16**), are observed. The splitting pattern of these aromatic signals correlates to a 1,2-disubstituted aromatic, with two electronically different functionalities. Additionally, the two aliphatic signals at δ_H 3.34 ppm (H-h) and δ_H 1.37 ppm (H-i), integrating for two and three protons respectively, corresponding to the methylene and methyl protons of the ethyl functionality is indicative of the formation of the desired product.

As previously discussed, the comparison of the aromatic regions of the ^{1}H NMR of the benzene-1,2-diamine (**17**) (Figure 2.8) to that of the nitroaniline (**16**) reveals the successful reduction of the nitro- moiety to a primary amine functionality. Upon reduction of the nitro-group, the aromatic protons of the desired benzene-1,2-diamine (**17**) are observed to shift relatively upfield (from δ_H 6.50 – 8.50 ppm in **16**, to δ_H 6.60 – 6.90 ppm in **17**) and converge. This convergence of the aromatic protons of the benzene-1,2-diamine (**17**) is indicative of the similar electronic effects that the primary and secondary amine moieties exert on the aromatic ring. Additionally, a new broad signal is observed at δ_H 3.25 ppm (H-a), with an integration of two protons, corresponding to the protons of the primary amine functionality.

The successful cyclization of the benzene-1,2-diamine (**17**) to yield the desired 2-pyridylbenzimidazole (**18**) is evidenced by the presence of additional aromatic signals in the ^{1}H NMR spectrum of **18** relative to that of **17** (Figure 2.8). These additional aromatic protons collectively integrate for four protons and are assigned to the protons of the 2-pyridyl functionality on the benzimidazole core (H-i, H-j, H-k and H-l).

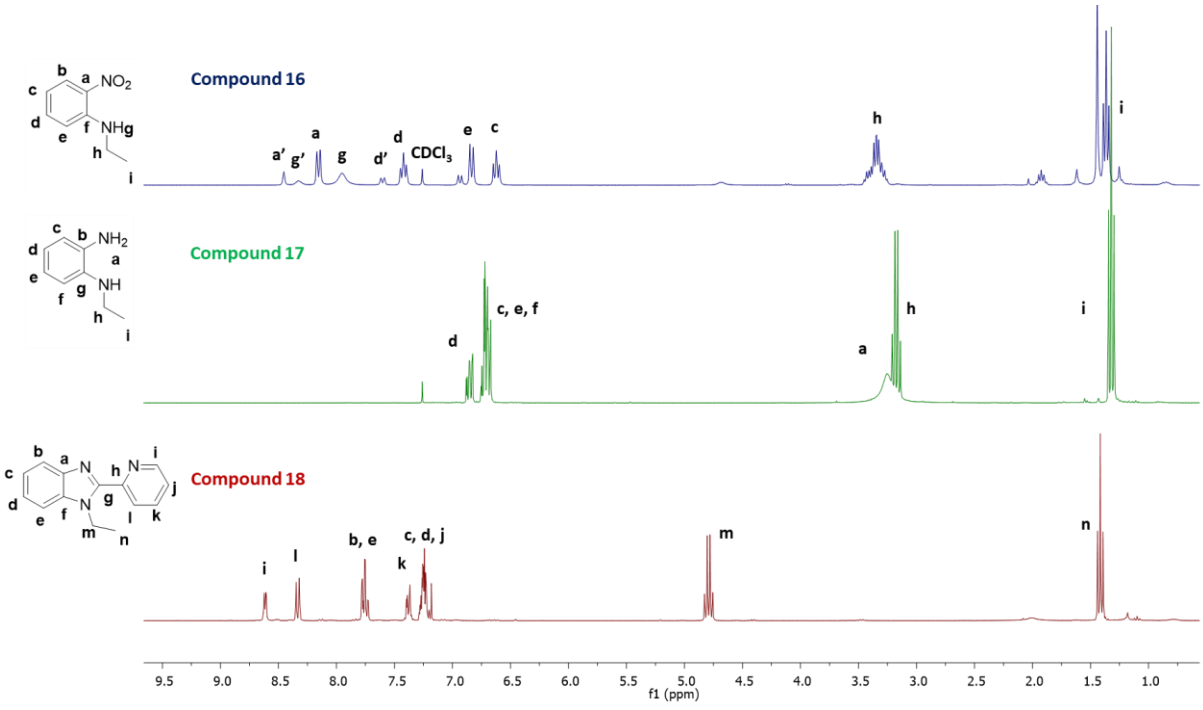

Figure 2.8: *The stacked ^{1}H NMR spectra of the nitroaniline (**16**) and benzene-1,2-diamine (**17**) precursors, and the monomeric 2-pyridylbenzimidazole ligand (**18**) in $CDCl_3$.*

The observed chemical shifts and signal multiplicities observed in the ^{1}H NMR spectra of the nitroaniline (**16**) precursor, the benzene-1,2-diamine (**17**) synthon and the monomeric 2-pyridylbenzimidazole ligand (**18**) are comparable to those reported in literature.[31–33]

2.4 Summary

A series of new 5-substituted 2-phenyl (**7** - **9**) and 2-pyridyl (**10** - **12**) tris-benzimidazole ligands were successfully synthesized. Additionally, a series of 5-substituted 2-ferrocenyl tris-benzimidazole trinuclear compounds (**13** – **15**) were synthesized. The synthesized compounds were characterized using an array of spectroscopic and analytic techniques such as ^{1}H, ^{13}C{^{1}H}, COSY, HSQC NMR spectroscopy, Infrared spectroscopy, HPLC and mass spectrometry. Single crystal XRD was used as a tool to confirm the molecular structure of compound **9** in the solid-state. The imine bond length was consistent with structurally similar to 2-phenyl benzimidazole ligands reported in literature.[29,30] Furthermore, the mononuclear 2-pyridylbenzimidazole (**18**), was synthesized. The ^{1}H NMR spectral data of this mononuclear 2-pyridyl ligand (**18**), and the precursors (**16** and **17**), all correlate to the ^{1}H NMR spectra reported in literature.[31–33]

The three-step procedure reported in this Chapter provides an efficient and facile procedure for the synthesis of the benzimidazole scaffold from relatively inexpensive starting materials. Additionally, the benzimidazole compounds reported in this Chapter may contribute towards the ever-growing field of the synthesis of potentially biological applications multimeric benzimidazoles. The synthesis of the 2-pyridylbenzimidazole (**18**), the monomeric counterpart of the 2-pyridyl tris-benzimidazole ligand **10**, may offer insight into the advantages that trimeric benzimidazoles have relative to monomeric benzimidazoles. These advantages may be highlighted by a comparison of the biological activity and mechanisms of action of the trimeric ligand **10** relative to that of the monomeric ligand **18**.

2.5 References

1 K. Singh, J. Okombo, C. Brunschwig, F. Ndubi, L. Barnard, C. Wilkinson, P. M. Njogu, M. Njoroge, L. Laing, M. Machado, M. Prudêncio, J. Reader, M. Botha, S. Nondaba, L. M. Birkholtz, S. Lauterbach, A. Churchyard, T. L. Coetzer, J. N. Burrows, C. Yeates, P. Denti, L. Wiesner, T. J. Egan, S. Wittlin and K. Chibale, *J. Med. Chem.*, 2017, **60**, 1432–

1448.

2 K. Sharma, A. Shrivastava, R. N. Mehra, G. S. Deora, M. M. Alam, M. S. Zaman and M. Akhter, *Arch. Pharm. (Weinheim).*, 2018, **351**, 1–13.

3 K. Shah, S. Chhabra, S. K. Shrivastava and P. Mishra, *Med. Chem. Res.*, 2013, **22**, 5077–5104.

4 P. Purushottamachar, R. Ramalingam and V. C. O. Njar, IntechOpen, 2019.

5 M. Gaba and C. Mohan, *Development of drugs based on imidazole and benzimidazole bioactive heterocycles: Recent advances and future directions*, Springer US, 2016, vol. 25.

6 D. C. Taylor-Robinson, N. Maayan, S. Donegan and P. Garner, *Cochrane Database Syst. Rev.*, 2017, 105–110.

7 B. D. Cheson, W. Brugger, G. Damaj, M. Dreyling, B. Kahl, E. Kimby, M. Ogura, E. Weidmann, C. M. Wendtner and P. L. Zinzani, *Leuk. Lymphoma*, 2016, **57**, 766–782.

8 R. D. Carvajal, S. Piperno-Neumann, E. Kapiteijn, P. B. Chapman, S. Frank, A. M. Joshua, J. M. Piulats, P. Wolter, V. Cocquyt, B. Chmielowski, T. R. J. Evans, L. Gastaud, G. Linette, C. Berking, J. Schachter, M. J. Rodrigues, A. N. Shoushtari, D. Clemett, D. Ghiorghiu, G. Mariani, S. Spratt, S. Lovick, P. Barker, E. Kilgour, Z. Lai, G. K. Schwartz and P. Nathan, *J. Clin. Oncol.*, 2018, **36**, 1232–1239.

9 V. C. O. Njar and A. M. H. Brodie, *J. Med. Chem.*, 2015, **58**, 2077–2087.

10 Y. H. Ji, D. Bur, W. Häsler, V. Runtz Schmitt, A. Dorn, C. Bailly, M. J. Waring, R. Hochstrasser and W. Leupin, *Bioorganic Med. Chem.*, 2001, **9**, 2905–2919.

11 C. Gnaccarini, S. Peter, U. Scheffer, S. Vonhoff, S. Klussmann and M. W. Göbel, *J. Am. Chem. Soc.*, 2006, **128**, 8063–8067.

12 N. Singh and P. Arya, *J. Appl. Chem.*, 2018, **7**, 52–58.

13 Z. E. Koc, H. Bingol, A. O. Saf, E. Torlak and A. Coskun, *J. Hazard. Mater.*, 2010, **183**,

251–255.

14 W. Huang and R. M. Scarborough, *Tetrahedron Lett.*, 1999, **40**, 2665–2668.

15 S. I. Alaqeel, *J. Saudi Chem. Soc.*, 2017, **21**, 229–237.

16 L. M. Dudd, E. Venardou, E. Garcia-Verdugo, P. Licence, A. J. Blake, C. Wilson and M. Poliakoff, *Green Chem.*, 2003, **5**, 187–192.

17 A. Mazurov, *Bioorganic Med. Chem. Lett.*, 2000, **10**, 67–70.

18 M. Haga, in *Comprehensive Coordination Chemistry II*, Elsevier Ltd., 2003, vol. 1, pp. 125–134.

19 S. Z. Taghavi, *E-Journal Chem.*, 2011, **8**, 101–106.

20 E. Moriarty, M. Carr, S. Bonham, M. P. Carty and F. Aldabbagh, *Eur. J. Med. Chem.*, 2010, **45**, 3762–3769.

21 Y. Keng, M. Ashraf, A. Chee, A. Nasrolahi, K. Parang and T. Soo, *Eur. J. Med. Chem.*, 2014, **83**, 448–454.

22 K. Bahrami, M. M. Khodaei and I. Kavianinia, *Synthesis (Stuttg).*, 2006, **4**, 547–550.

23 H. D. Kokare, J. N. Sangshetti and B. Shinde, *Synthesis (Stuttg).*, 2007, **18**, 2829–2834.

24 H. Xiangming, M. Huiqiang and W. Yulu, *Arkivoc*, 2007, 150–154.

25 R. G. Pearson and B. J. O. Edwards, *J. Am. Chem. Soc.*, 1962, **84**, 16–24.

26 B. J. Edwards, *J. Am. Chem. Soc.*, 1956, **78**, 1819–1820.

27 H. K. H. Jr and R. B. Bates, *Tetrahedron Lett.*, 2012, **53**, 1830–1832.

28 S. Lin and L. Yang, *Tetrahedron Lett.*, 2005, **46**, 4315–4319.

29 B. Arslan, C. Kazak, H. Karataş and S. Özden, *Acta Crystallogr. Sect. E Struct. Reports Online*, 2004, **60**, 1535–1537.

30 J. C. Zhou, Z. Y. Zhang, N. X. Li and C. M. Zhang, *Acta Crystallogr. Sect. E Struct. Reports Online*, 2009, **65**, 3019–3021.

31 N. Dalla Favera, L. Guénée, G. Bernardinelli and C. Piguet, *J. Chem. Soc. Dalton Trans.*, 2009, 7625–7638.

32 E. J. Hennessy, V. Oza, A. Adam, K. Byth, L. Castriotta, G. Grewal, G. A. Hamilton, V. M. Kamhi, P. Lewis, D. Li, P. Lyne, L. Öster, M. T. Rooney, J. C. Saeh, L. Sha, Q. Su, S. Wen, Y. Xue and B. Yang, *J. Med. Chem.*, 2015, **58**, 7057–7075.

33 L. Huang, K. Z. Wang, C. H. Huang, F. Y. Li and Y. Y. Huang, *J. Mater. Chem.*, 2001, **11**, 790–793.

Chapter 3

Synthesis and Characterization of neutral *C^N*-Ru(II) and cationic *N^N*-Ru(II) trimetallic complexes

3.1 Introduction

Metal-based complexes have been at the forefront of the rational design of cytotoxic agents in recent years. This was catalyzed by the fortuitous discovery of *cis*-dichloridodiammineplatinum(II), commonly known as cisplatin, by Rosenberg and co-workers in 1967.[1] Today, platinum-based drugs constitute as much as 70% of cancer chemotherapeutic regimens.[2] However, the dose-dependent side effects accompanied by the use of Pt(II)-based anticancer drugs has sparked the development of a new generation of metallodrugs based on alternative Platinum Group Metals (PGMs).[3] This is mainly aimed at developing PGM-based complexes that show improved selectivity while maintaining appreciable anticancer activity across a variety of malignancies, and unique mechanisms of action. From this category, ruthenium-based metallodrugs are by far the most successful, as they offer great potential as cytostatic and cytotoxic agents.[4] Ruthenium-based complexes have gained significant prominence as potential anticancer agents, as these metal complexes display diverse and non-conventional mechanisms of action.[5] Additionally, the ruthenium metal center offers the unique advantage of having Ru(II), Ru(III) and Ru(IV) oxidation states accessible under physiological conditions.[6] This distinctive feature presents a unique advantage in the rational design of metallodrugs, as the anticancer activity and mechanisms of action of most metal-based compounds are dependent on the oxidation state of the metal center.[7–11]

To date, the most successful ruthenium complexes are the New Anti-tumour Metastatic Inhibitor-A (NAMI-A) and IT-139 (Figure 3.1) which have entered clinical trials.[2,12] NAMI-A possesses anti-metastatic properties, reduces metastases mass and prevents the formation of secondary tumours. However, NAMI-A has minimal effects on primary tumour growth.[13] On the other hand, IT-139 is a cytotoxic agent that is effective against advanced solid tumours, showing promising activity against non-small lung cancer, neuroendocrine and sarcoma

tumours.[12,14] The success of ruthenium-based complexes and their alternate mechanisms of action suggests that these complexes may facilitate the discovery of new combination chemotherapy agents. This is due to several reports of half-sandwich ruthenium(II)-arene complexes (where the arene is either η^6-*p*-cymene or η^5-C_5H_5) having several intracellular targets, including but not limited to DNA interaction and binding,[15] and induction of apoptosis.[16,17]

Furthermore, ruthenium(II)-arene complexes have been reported to show potent inhibition of enzymes that are overexpressed in human cancers and play vital roles in the growth and progression of tumours, including the PARP-1,[18] the CDK1,[19] and cathepsin B enzymes.[20]

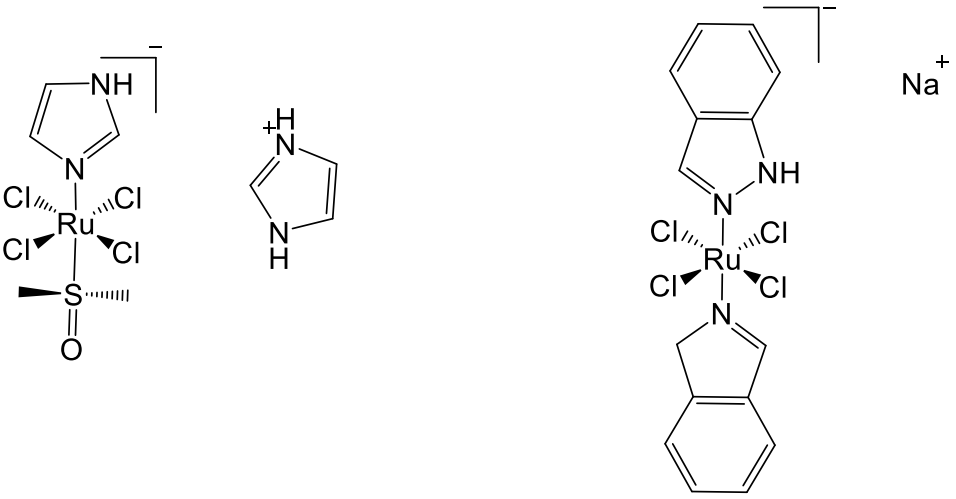

NAMI-A **IT-139**

Figure 3.1*: The structures of Ruthenium complexes, NAMI-A and IT-139, which are currently in clinical trials.*[15]

The incorporation of pharmacophores onto dendritic scaffolds and the combination of these dendritic ligands with PGMs, to form multinuclear organometallic complexes, is a prolific area of research which has been explored substantially as a strategy in anticancer drug design.[21–30] The interest in these multinuclear complexes is cultivated by the reported enhanced anticancer activity and selectivity observed for these multinuclear complexes, relative to their mononuclear counterparts.[26,28,31] To the best of our knowledge, no work has been reported on the synthesis of trinuclear benzimidazole-based complexes with ruthenium(II) nuclei at the periphery. This Chapter describes the synthesis and characterization of a series of benzimidazole-based ruthenium(II) organometallic compounds.

3.2 Synthesis of the neutral cyclometallated trimetallic *C^N*-Ruthenium(II)-*p*-cymene complexes (19 – 21)

3.2.1 Synthesis

The synthesis of the cyclometallated trimeric *C^N*-Ru(II)-*p*-cymene complexes (**19** – **21**) involved two reactions. Firstly, the preparation of the [RuCl(μ-Cl)(*p*-cymene)]$_2$ dimer was achieved following a literature procedure.[32] This was subsequently followed by cyclometallation of the 2-phenyl tris-benzimidazole ligands (**7** – **9**) to yield the trinuclear neutral complexes (**19** – **21**) *via* a sodium acetate assisted *C-H* activation reaction (Scheme 3.1). In this reaction, the appropriate 2-phenyl tris-benzimidazole ligand (**7** – **9**) was reacted with 1.5 molar equivalents of the [RuCl(μ-Cl)(*p*-cymene)]$_2$ dimer.

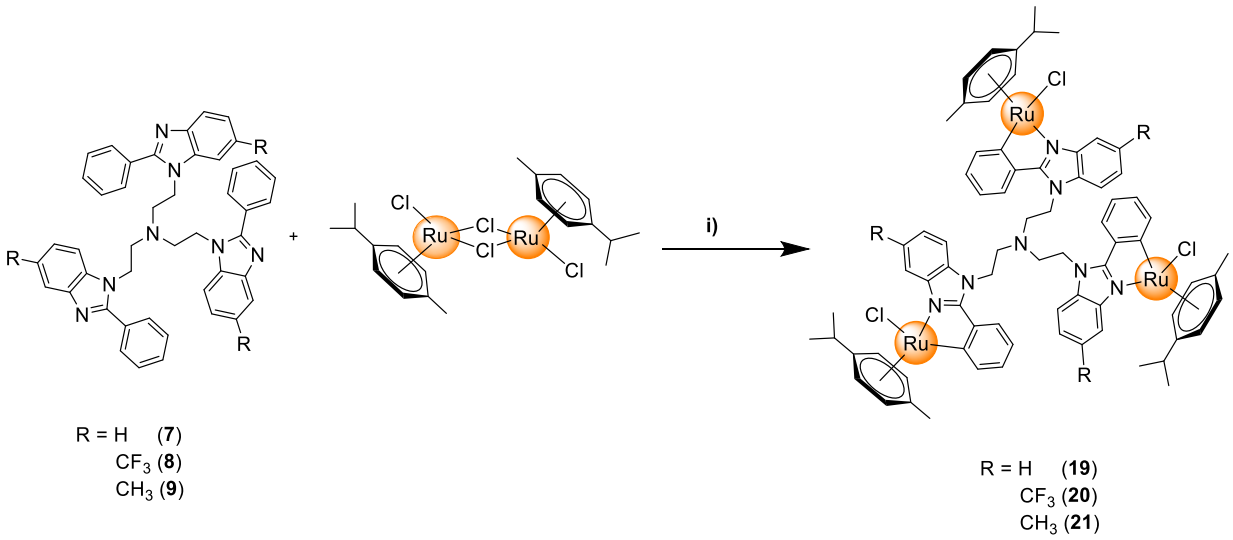

Scheme 3.1*: The general synthesis of the cyclometallated trimetallic Ru(II) complexes* ***(19 – 21)****. Reagents and conditions: i) MeCN or DCM: EtOH (1:1 v/v%)/ NaOAc/ RT/ 24 h.*

The application of cyclometallated complexes as biological agents has been an area of great interest in recent literature.[33–35] However, until recently, cyclometallation reactions typically required a strong base, [36] strong acid, [37] mercury reagent, [38] or borate salts[39,40] to provide the driving force in the activation of the C-H bond. However, an efficient and facile method of cyclometallation was discovered by Davies and co-workers.[41] This reported method entailed the sodium acetate-catalyzed cyclometallation of [MCp*Cl$_2$]$_2$ (where M is Rh or Ir) or [Ru(*p*-cymene)Cl$_2$]$_2$ with 2-substituted pyridines at room temperature.

Mechanistic insights of the reaction were briefly provided by Davies and co-workers, primarily through Density Functional Theory computational calculations, which shed light on the possible transition state.[42,43] More recently, Jones and co-workers undertook a more rigorous kinetic, mechanistic and computational study into the sodium acetate-promoted cyclometallation of phenyl imines and 2-phenyl pyridines with $[MCp^*Cl_2]_2$ (where M is Rh or Ir).[42] The proposed mechanism of the cyclometallation of 2-phenyl tris-benzimidazoles with the $[Ru(p\text{-cymene})Cl_2]_2$ dimer reported in this study (Scheme 3.2) is based on the mechanisms provided by Davies and co-workers[41] and Jones and co-workers.[42]

Although the role of sodium acetate in the cleavage of the $[RuCl(\mu\text{-}Cl)(p\text{-cymene})]_2$ dimer to form the intermediate **A** has not been clearly elucidated, in reported kinetic studies it was observed that the intermediates **A** and **B** are formed rapidly and are in a dynamic equilibrium.[42] From **A** and **B**, a vacant site is required for the formation of the transition state (**D**). As a result, **A** and **B** undergo dissociation of either the chloride or acetate anions, respectively, to form the key intermediate **C**. This is followed by the formation of the agostic transition state **D**, with the cleavage of the C-H bond being the rate-determining step in the formation of **D**. The proton from the cleavage of the C-H bond is transferred to acetate moiety to form intermediate **E**. The protonated acetate is subsequently substituted by an acetate ion to form the acetate intermediate **F**. The acetate coordinated **F** is rapidly converted to the corresponding cyclometallated complex by the dissociation of the κ^1-acetate by a chloride anion. This can be attributed to the stronger Ru-Cl bond compared to the Ru- κ^1-acetate interaction.

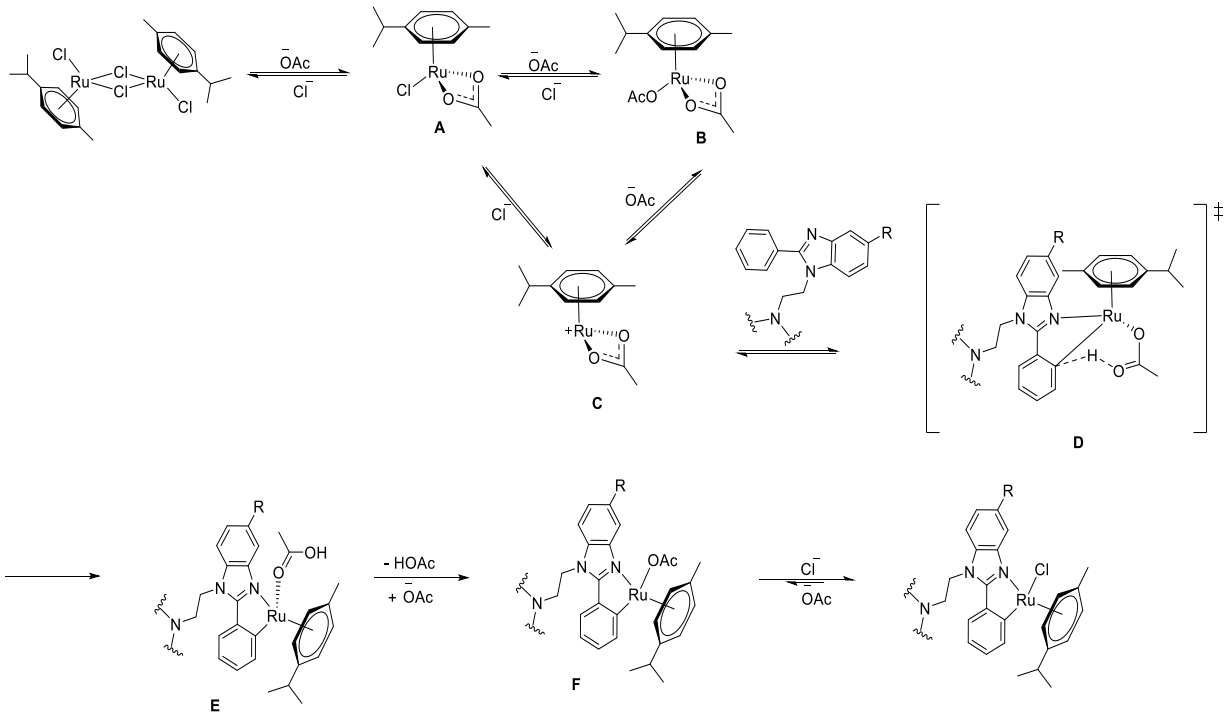

***Scheme 3.2**: The proposed mechanism of the C-H activation reaction yielding the cyclometallated trimetallic C^N-Ruthenium(II)-p-cymene complexes.*

The neutral trinuclear cyclometallated Ru(II) complexes (**19** – **21**) were isolated in excellent yields (84 – 88%) as either green (**19**) or dark yellow powders (**20** and **21**) that are air- and moisture-stable, and are soluble in dimethylsulfoxide, acetonitrile or acetone.

3.2.2 Characterization

The ^{1}H NMR spectra (Figure 3.2) of the cyclometallated complexes (**19** – **21**) correlates to the proposed structures of these complexes. In the obtained ^{1}H NMR spectra (Figure 3.2), the appearance of four (for **19**) or five (for **20** and **21**) signals between δ_H 5.00 and δ_H 6.00 ppm which collectively integrate for twelve protons, corresponding to the aromatic protons of the *p*-cymene ring (H-q, H-r, H-s and H-t), are the first indicator of cyclometallation. Additionally, the two multiplets observed in the range δ_H 0.51 – 1.00 ppm, integrating for eighteen protons, correspond to the methyl protons of the *iso*-propyl functionality of the *p*-cymene ancillary ligand (H-u and H-v for **19**, and H-v and H-x for **20** and **21**) and support the formation of the complex. These signals are observed as two multiplets due to the methyl groups of the *p*-cymene ring being in electronically distinct environments. This is attributed to the loss of

planar symmetry of the *p*-cymene ring, due to the chelation of the Ru(II) metal center to the 2-phenyl tris-benzimidazoles.

However, in the aromatic regions (in the range δ_H 6.50 – 8.50 ppm) of the ^{1}H NMR spectra of **20** and **21**, an intricate aromatic spectrum was observed for each of the complexes. As a result, additional analytical techniques were used to further attest to the integrity of the complexes **20** and **21**.

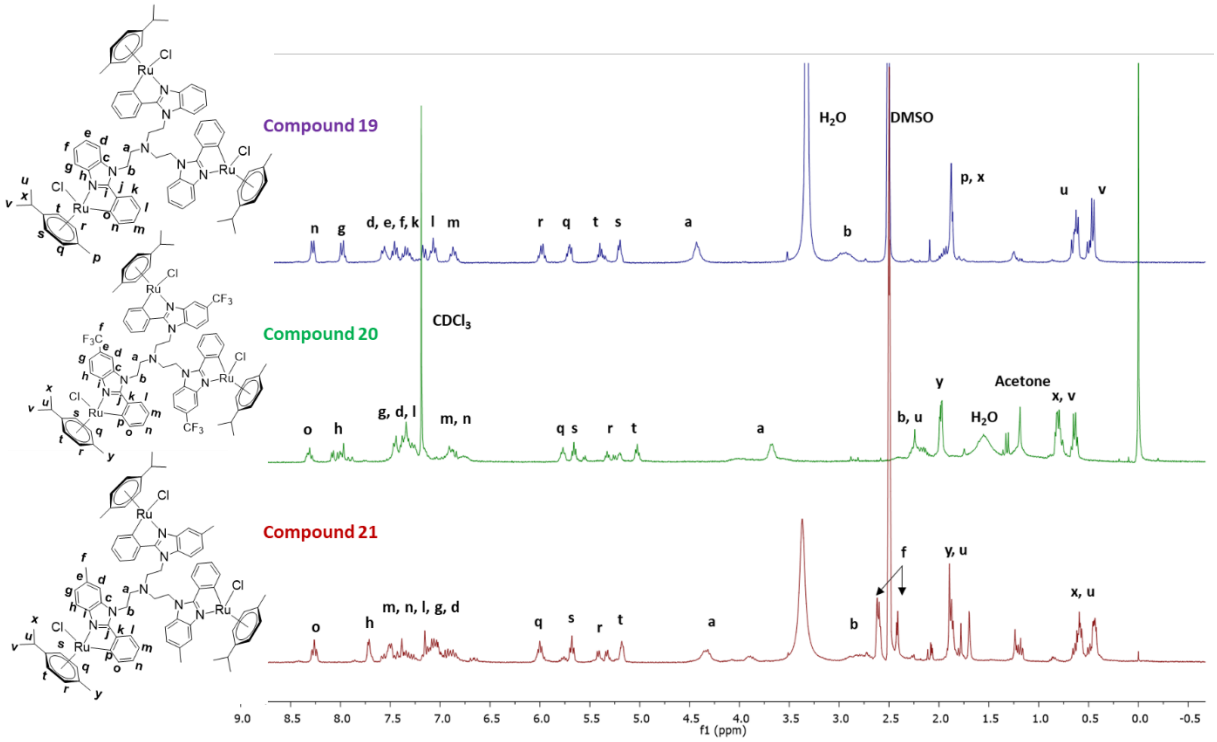

Figure 3.2: *The stacked ^{1}H NMR spectra of the trimeric cyclometallated C^N-Ru(II) complexes* ***19, 21,*** *and* ***20****, in DMSO (d_6) and $CDCl_3$, respectively.*

High-Resolution Electrospray Ionization Mass Spectrometry (HR ESI-MS) analysis of **21** revealed a molecular ion peak at *m/z* = 1494.3296 that corresponds to the $[M - Cl]^+$ ion and confirms the formation of the neutral complex **21** (Figure 3.3 a), and cyclometallation of all three benzimidazole cores. Additionally, upon analysis of the high-resolution mass spectrum of **20**, a molecular ion fragment at *m/z* = 1157.3227 that corresponds to $[M + Na^+ - C_{26}H_{25}ClF_3N_2Ru]^+$ was observed and this further substantiates metal complexation and synthesis of **20** (Figure 3.3 b).

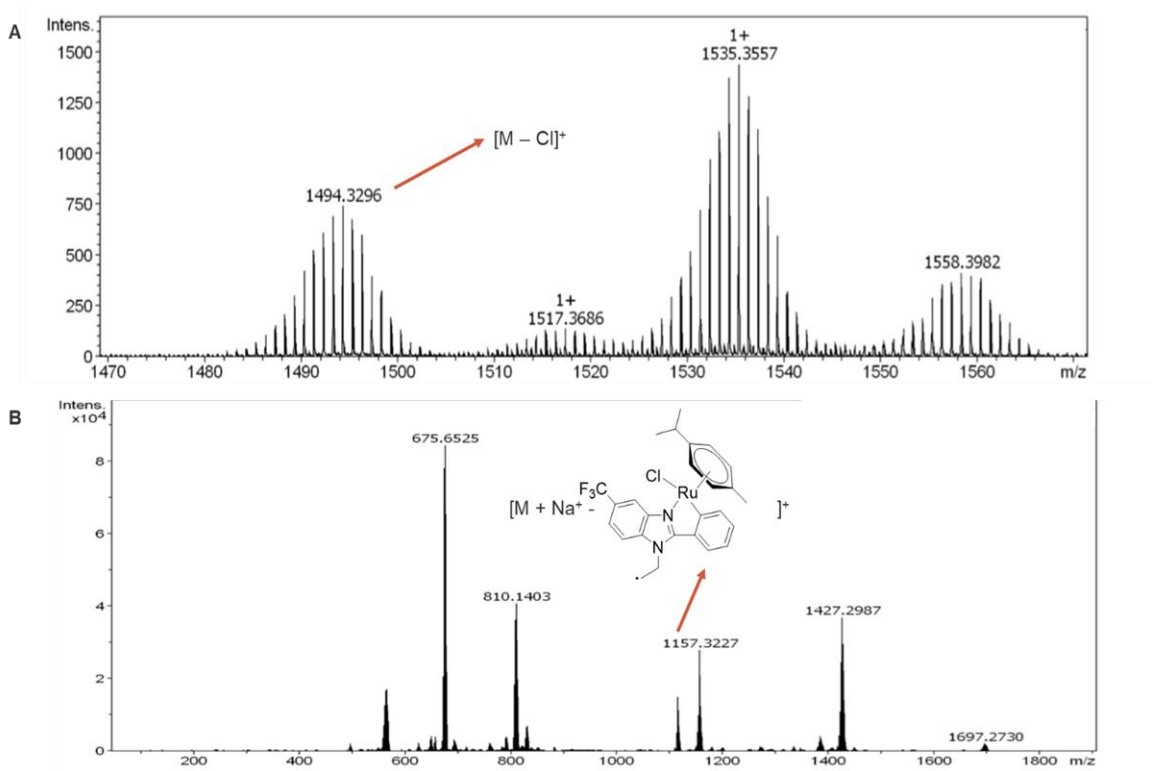

Figure 3.3: *The High-Resolution ESI Mass Spectra of* ***21*** *a) and* ***20*** *b) recorded in the positive-ion mode (+ve), with assigned characteristic fragments observed.*

In addition to the NMR and high-resolution mass spectrometry, IR spectroscopy was also useful in validating metal complexation. Generally, it was noted that the absorption band corresponding to the imine (C=N) functional group in the Ru(II) complexes (**19** – **21**) is observed at a lower wavenumber relative to the corresponding 2-phenyl tris-benzimidazole ligands (**7** – **9**), shifting from a range of 1625 – 1695 cm^{-1} in the ligands to 1578 – 1581 cm^{-1} in the corresponding complexes (Figure 3.4, which is representative of the generally observed trend).

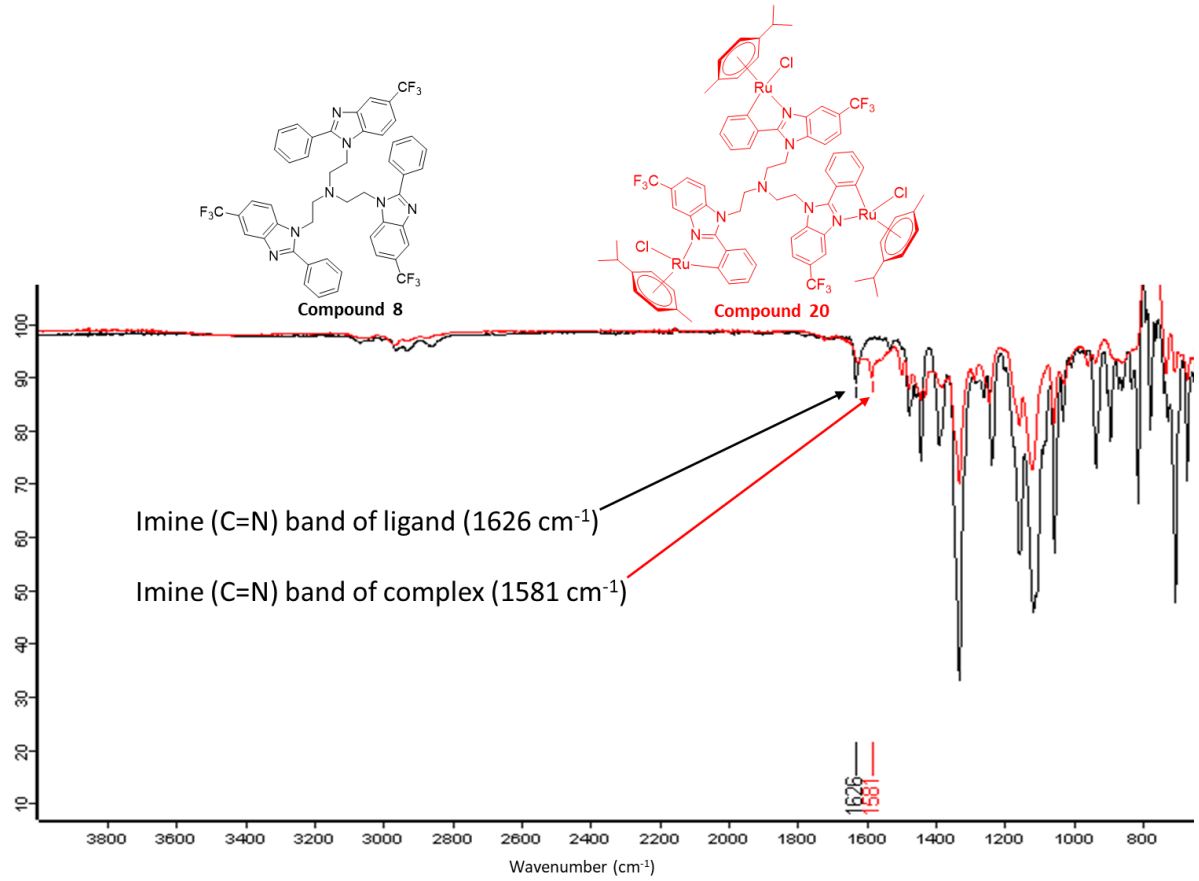

Figure 3.4: *The stacked Infrared spectra of the 5-trifluoromethyl substituted 2-phenyl tris-benzimidazole ligand (**8**) and its corresponding cyclometallated complex (**20**).*

This observed lowering in wavenumber of the absorption band correlating to the imine moiety in the cyclometallated complexes (**19** – **21**), relative to their respective ligands (**7** – **9**), confirms successful coordination of the Ru(II) metal center to the imine nitrogen. The resultant lowering of the wavenumber is attributed to π-backbonding between the imine nitrogen atom and the Ru(II) metal center (Scheme 3.3). This is a synergistic phenomenon in which there is a sigma donation of electron density from the imine nitrogen atom to a vacant bonding orbital of the Ru(II) center. Concurrently, there is back-donation of electron density from the filled *d*-orbitals of the Ru(II) center to the unoccupied π*-antibonding orbitals of the imine. This results in the strengthening of the Ru(II)-N bond, which is accompanied by the synergistic decrease in the bond order of the imine C=N bond, yielding the consequential lowering of the wavenumber of the C=N bond in the cyclometallated complexes.

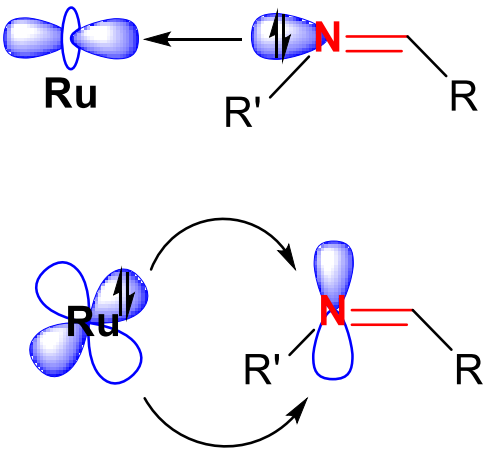

Scheme 3.3: *A schematic representation of π-backbonding interactions in the cyclometallated benzimidazole complexes. With the C=N: ⟶ Ru σ-donation (top) and the Ru ⟶ N=C back-donation (bottom).*

Additionally, to attest to the purity of the cyclometallated complexes **20** and **21**, these complexes were analyzed using CHN elemental analysis. The entrapment of solvent molecules was anticipated, as the arms of the tris-core tend to fold back on one another.[44] This may be the cause of the inclusion of three water molecules with each molecule of either complex **20** or **21**. The presence of water molecules correlates with the peaks observed in both the ^{1}H NMR spectra of **20** and **21** (Figure 3.2, *vide supra*) which correspond to water (the broad signal at δ_H 1.56 ppm in the ^{1}H NMR spectra of **20**, and the signal at δ_H 3.33 ppm in the ^{1}H NMR spectra of **21**).

3.3 Synthesis of the cationic trimetallic *N^N*-Ruthenium(II)-*p*-cymene complexes (22 – 24)

3.3.1 Synthesis

The synthesis of the cationic *N^N*-Ruthenium(II)-*p*-cymene complexes was achieved by two steps: i) firstly, the bridge splitting reaction of the [RuCl(μ-Cl)(*p*-cymene)]$_2$ dimer with the appropriate 2-pyridyl tris-benzimidazole ligand (**10** – **12**) in a mixture of DCM: EtOH (1: 1 *v/v%*) at room temperature. This was followed by, ii) a salt metathesis reaction using ammonium hexafluorophosphate to yield the appropriate complex as a hexafluorophosphate salt (Scheme 3.4).

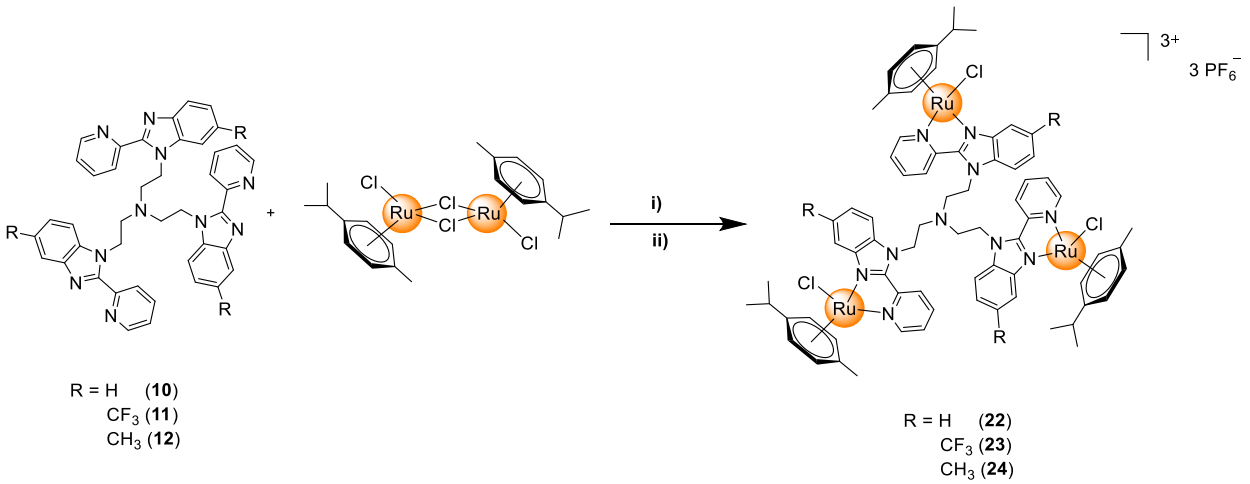

***Scheme 3.4**: The general synthetic route of the cationic N^N-Ruthenium(II)-p-cymene complexes (**22** – **24**). Reagents and conditions: i) EtOH: DCM (1:1 v/v%)/ RT/ 24 h; ii)) EtOH: DCM (1:1 v/v%)/ NH_4PF_6/ RT/ 1 h.*

After 24 hours, TLC analysis revealed that the limiting reagent (the 2-pyridyl tris-benzimidazole ligands **10** – **12**) had completely reacted. This suggested that the reaction had reached completion, and thereafter the crude reaction product was reacted with NH_4PF_6 in DCM: EtOH (1: 1 *v/v%*). The cationic complexes were isolated in moderate to good between 51% and 75%, as yellow hexafluorophosphate salts that are air- and moisture-stable, and are soluble in dimethylsulfoxide, dichloromethane or acetone.

3.3.2 Characterization

Analysis and comparison of the ^{1}H NMR spectra of the cationic Ru(II) complexes **22** – **24** (Figure 3.5) to that of the corresponding 2-pyridyl tris-benzimidazole ligands (**10** – **12**, in Figure 2.5, *vide supra*) reveals resonances characteristic of successful complex formation. Firstly, the signal corresponding to the proton bonded to the carbon adjacent to the pyridyl nitrogen (H-n for **10** and **22**, H-o for **11**, **12**, **23** and **24**) was observed at a significantly higher chemical shift in the ruthenium(II) complexes **22** – **24** (from δ_H 8.25 – 8.50 ppm in the ligands, to δ_H ~9.6 ppm in the metal complexes). This is due to the bonding of the pyridyl nitrogen to the ruthenium metal center resulting in π-backbonding, which consequentially results in the reduction of electron density on the carbon adjacent to the pyridyl nitrogen. Additionally, three (for **22**) or four (for **23** and **24**) signals were observed in the range δ_H 6.00 – 6.50 ppm which collectively integrate for twelve protons, corresponding to the aromatic protons of the *p*-cymene ring (H-p, H-q, H-r and H-s for **22**, or H-q, H-r, H-s and H-t for **23** and **24**).

These resonances confirm the bidentate coordination of the ruthenium(II) center to both the imine and the pyridyl nitrogen atoms, as these signals are indicative of the stereogenicity introduced by the chelation of the Ru(II) metal center to the imine and the 2-pyridyl nitrogen atoms.

On comparing the $^{13}C\{^{1}H\}$-NMR spectra of complexes (**22** – **24**) to that of the corresponding 2-pyridyl ligands (**10** – **12**), it was generally noted that the signal corresponding to the carbon adjacent to the pyridyl nitrogen in the complexes was observed at a significantly higher chemical shift relative to that of the corresponding ligand (from δ_C 148.52 – 149.37 ppm in the ligands, to δ_C 157.89 – 158.85 ppm in the metal complexes). This is consistent with the same trend which was observed in the ^{1}H NMR spectra, and further corroborates the bonding of the pyridyl nitrogen to the ruthenium metal center, which results in the reduction of electron density on the pyridyl carbon through π-backbonding.

The $^{31}P\{^{1}H\}$-NMR spectra of the cationic complexes (**22** – **24**) revealed a high field septet at δ_P ~-114 ppm. This signal correlates to the phosphorus atom of the PF_6 counter-ions, which couples to the six fluorine atoms with $^{1}J_{P\text{-}F}$ = 711 Hz. This further attesting to the successful counter-ion exchange and confirms the presence of one phosphorus salt.

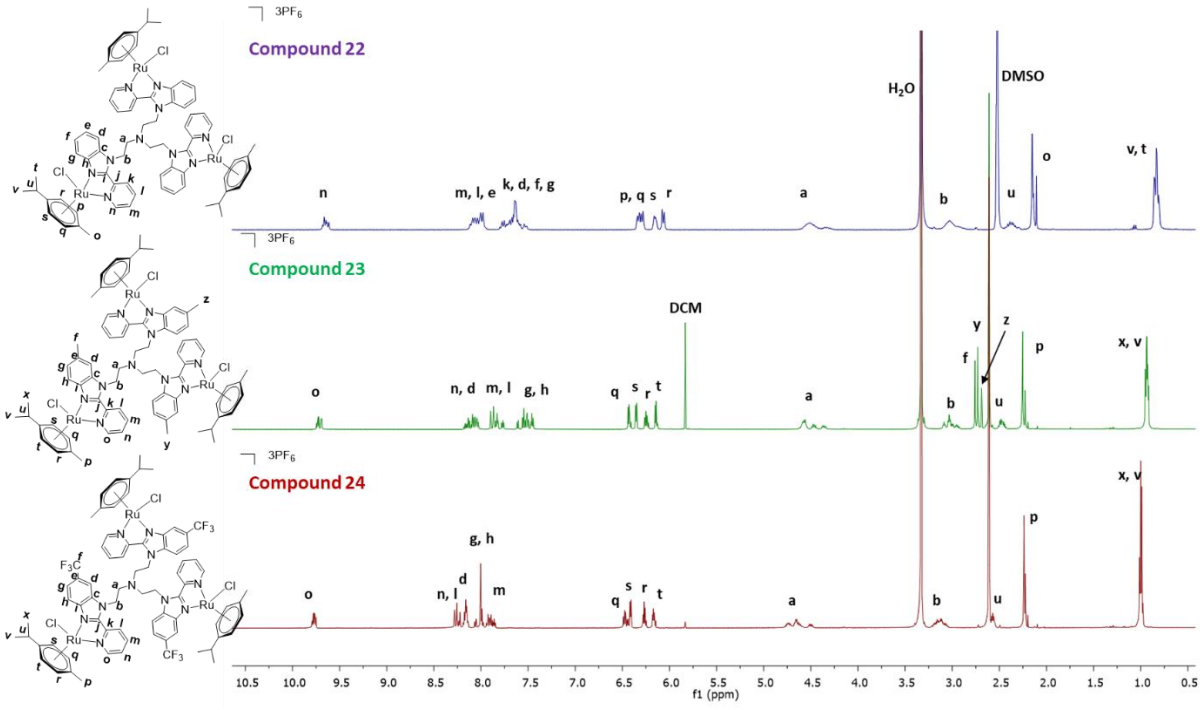

Figure 3.5: *The stacked ^{1}H NMR spectra of the cationic N^N-Ruthenium(II)-p-cymene complexes (**22** – **24**) in DMSO (d_6).*

In addition to the ^{1}H NMR and $^{13}C\{^{1}H\}$-NMR spectral analyses, the Ru(II) complexes (**22** – **24**) were analyzed using IR spectroscopy, and the results obtained are summarised in Table 3.1. Generally, the IR spectra revealed absorption bands corresponding to the imine (C=N) moiety of the benzimidazole cores and the pyridyl C=N bond at lower wavenumbers in the complexes (**22** – **24**), relative to their respective 2-pyridyl tris-benzimidazole ligands (**10** – **12**). The observed lowering of the absorption bands corresponding to the abovementioned C=N bonds can be explained by the π-backbonding interactions of the Ru(II) metal center and the nitrogen atoms of the imine and pyridyl functionalities (Scheme 3.3, *vide supra*). The observed lowering of both the imine C=N and pyridyl C=N stretching frequencies in the cationic complexes (**22** – **24**), relative to their respective 2-pyridyl ligands (**10** – **12**), confirms the chelation of the Ru(II) centers to both the imine and pyridyl nitrogen atoms.

Table 3.1*: The wavenumber (cm^{-1}) of the C=N bonds of the cationic ruthenium(II) complexes **22** – **24** and their corresponding ligands **10** – **12**.*

Compound	5-substituent	Wavenumber (cm^{-1})	
		$(C=N)_{Imine}$	$(C=N)_{Pyridyl}$
10	H	1733	1586
22 (Ru)		1599	1481
11	CH_3	1726	1590
23 (Ru)		1674	1464
12	CF_3	1620	1587
24 (Ru)		1574	1490

The correlation of the analytical data and the proposed structures leads to the conclusion that the desired complexes have been successfully synthesized.

3.4 Synthesis of the cationic mononuclear *N^N*-Ruthenium(II)-*p*-cymene complex (25)

3.4.1 Synthesis

The synthesis of the cationic mononuclear complex (**25**) was achieved using the same two-step procedure as reported in Section 3.3.1 (*vide supra*), for the synthesis of the trimetallic cationic *N^N*-Ru(II) complexes (**22** – **24**), using the appropriate molar equivalents (Scheme 3.5).

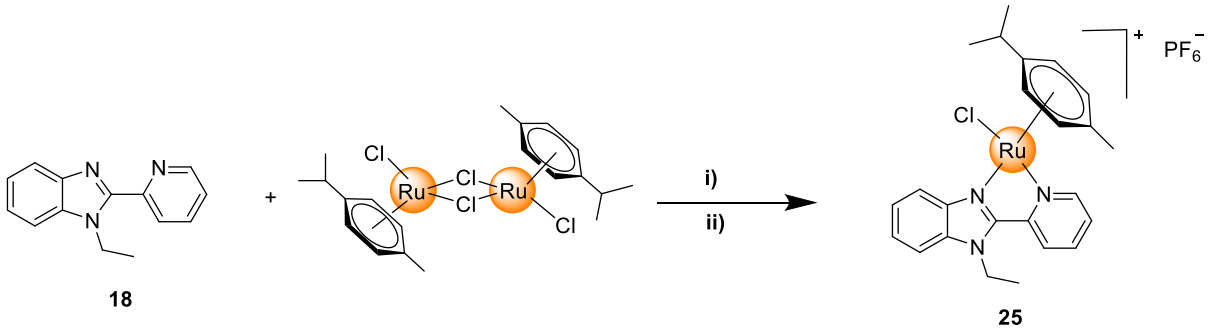

***Scheme 3.5**: Synthesis of the cationic N^N-Ru(II)-p-cymene complex (**25**). Reagents and conditions: i) EtOH: DCM (1:1 v/v%)/ RT/ 24 h; ii)) EtOH: DCM (1:1 v/v%)/ NH_4PF_6/ RT/ 1 h.*

After 24 hours, TLC analysis revealed that the 2-pyridylbenzimidazole ligand (**18**) had completely reacted. This suggested that the reaction had reached completion, and thereafter the crude reaction product was reacted with NH_4PF_6 in DCM: EtOH (1: 1 *v/v%*). The cationic complex (**25**) was isolated in a good yield of 81%, as a yellow hexafluorophosphate salt that is air- and moisture-stable and is soluble in dimethylsulfoxide, dichloromethane or acetone.

3.4.2 Characterization

Upon comparison of the ^{1}H NMR spectra of the cationic complex (**25**) to that of the 2-pyridylbenzimidazole ligand (**18**), numerous resonances that are diagnostic of complex formation are present (Figure 3.6). The first indicator of successful complex formation is the splitting of the signal corresponding to the methylene protons of the ethyl functionality from a distinct quartet (at δ_H 4.85 ppm), in the ligand (**18**), to an intricate multiplet, in the complex **25** (at δ_H 4.90 ppm). This splitting is due to the introduction of stereogenicity by the Ru(II) center, resulting in the diastereotopicity of these methylene protons.

Additionally, three signals between δ_H 6.00 and δ_H 6.50 ppm, collectively integrating for four protons, correlate with the aromatic protons of the *p*-cymene auxiliary ligand.

The $^{13}C\{^1H\}$-NMR spectrum of the mononuclear complex (**25**) revealed a signal corresponding to the carbon adjacent to the pyridyl nitrogen (C-i) at δ_C 157.91 ppm. This observed chemical shift is comparable to that of the carbon signal corresponding to the carbon adjacent to the pyridyl nitrogen (C-o, at δ_C 157.98 ppm) in the $^{13}C\{^1H\}$-NMR spectrum of the trinuclear cationic complex (**22**), and support successful complex formation. Additionally, the signals corresponding to the methyl carbons on the *iso*-propyl functionality of the *p*-cymene ancillary ligand are observed at δ_C 22.13 (C-r) and δ_C 22.10 (C-p) in the spectrum of the mononuclear complex (**25**). These signals are comparable to those observed for the same *iso*-propyl functionality of the *p*-cymene auxiliary ligand (C-t and C-v, at δ_C 22.25 ppm and 22.13 ppm, respectively) in the trinuclear cationic complex (**22**). These signals corroborate the successful synthesis of the mononuclear cationic complex (**25**).

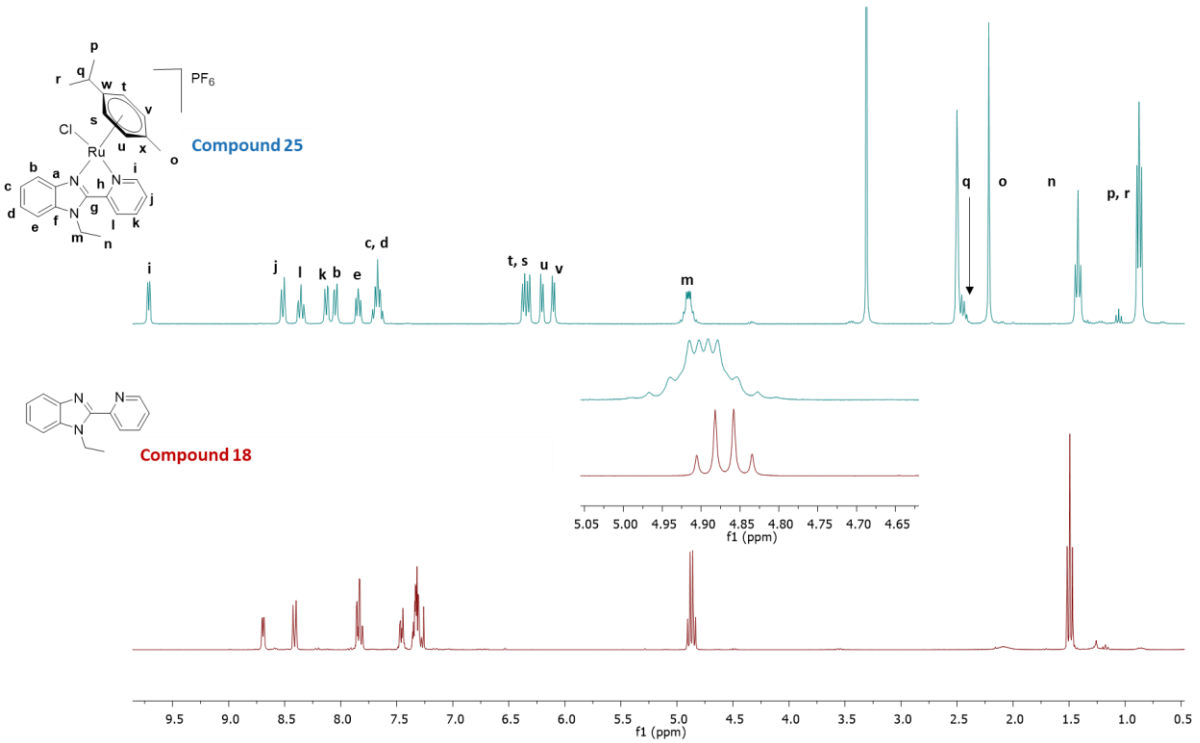

Figure 3.6: *The stacked ^1H NMR spectra of the mononuclear cationic N^N-Ruthenium(II)-p-cymene complex (**25**) in DMSO (d_6) and the 2-pyridylbenzimidazole ligand (**18**) in $CDCl_3$.*

Further complementing spectroscopic and analytical data, was the ESI mass spectrometry data for the mononuclear cationic complex (**25**), which showed a molecular ion base peak at *m/z* = 494.0948 that corresponds to the $[M\text{-}PF_6]^+$ ion, further supporting successful complex synthesis.

3.5 Summary

A series of neutral cyclometallated *C^N*-Ru(II)-*p*-cymene (**19** – **21**) and cationic *N^N*-Ru(II)-*p*-cymene (**22** – **24**) trinuclear complexes were successfully synthesized. The complexes were afforded in moderate to excellent yields (51 – 88%). Additionally, the mononuclear cationic *N^N*-Ru(II)-*p*-cymene complex (**25**) was synthesized and isolated in an excellent yield (81%). All the complexes were fully characterized using a range of spectroscopic and analytic techniques including NMR (^{1}H, ^{13}C{^{1}H}, ^{31}P{^{1}H}, HSQC and COSY) spectroscopy, IR spectroscopy, elemental analysis and mass spectrometry (electrospray ionization), which all attest to the integrity of the complexes. The attained analytical and spectroscopic data correlate well with the proposed structures (**19** – **25**).

The small library of novel ruthenium(II) complexes reported in this Chapter may contribute to the ever-growing field of the biological applications of multinuclear organometallic complexes. These complexes will be evaluated for their anticancer activity against an array of malignant cells and mechanistic studies will be conducted on the most promising complexes from this series. Additionally, the synthesis of the mononuclear counterpart of the trinuclear cationic complex **22** may highlight the merit in the investigation of multinuclear complexes relative to their mononuclear counterparts. The anticancer evaluation of the trinuclear complex **22** and its mononuclear counterpart **25** may highlight the unique advantage that multinuclear complexes have of exploiting the Enhanced Permeability and Retention (EPR) effect, thus potentially resulting in superior anticancer activity and selectivity.

3.6 References

1 B. Rosenberg, L. Vancamp, J. E. Trosko and M. V. H., *Nature*, 1969, **222**, 385–386.

2 C. S. Allardyce and P. J. Dyson, *Dalton Trans.*, 2016, **45**, 3201–3209.

3 J. Reedijk, *Eur. J. Inorg. Chem.*, 2009, 1303–1312.

4 W. Han and P. J. Dyson, *Eur. J. Inorg. Chem.*, 2006, 4003–4018.

5 E. Alessio, *Eur. J. Inorg. Chem.*, 2017, 1549–1560.

6 C. S. Allardyce and P. J. Dyson, in *Platin. Met. Rev.,* John Matthey, 2001, vol. 45, pp.

62–69.

7 P. J. Dyson and G. Sava, *Dalton Trans.*, 2006, 1929–1933.

8 C. S. Allardyce, A. Dorcier, C. Scolaro and P. J. Dyson, *Appl. Organomet. Chem. Appl.*, 2005, **19**, 1–10.

9 I. Kostova, *Curr. Med. Chem.*, 2006, **13**, 1085–1107.

10 M. Galanski, V. B. Arion, M. A. Jakupec and B. K. Keppler, *Curr. Pharm. Des.*, 2003, **9**, 2078–2089.

11 P. Zhang and P. J. Sadler, *J. Organomet. Chem.*, 2017, **839**, 5–14.

12 G. K. Gransbury, P. Kappen, C. J. Glover, J. N. Hughes, A. Levina, P. A. Lay, I. F. Musgrave and H. H. Harris, *Metallomics*, 2016, **8**, 762–773.

13 A. Levina, A. Mitra and P. A. Lay, *Metallomics*, 2009, **1**, 458.

14 D. S. Thompson, G. J. Weiss, S. F. Jones, H. A. Burris, R. K. Ramanathan, J. R. Infante, J. C. Bendell, A. Ogden and D. D. Von Hoff, *J. Clin. Oncol.*, 2012, **30**, 3033–3033.

15 R. Carter, A. Westhorpe, M. J. Romero, A. Habtemariam, C. R. Gallevo, Y. Bark and N. Menezes, *Nat. Publ. Gr.*, 2016, 1–12.

16 P. R. Florindo, D. M. Pereira, P. M. Borralho, M. P. Rodrigues, M. F. M. Piedade and A. C. Fernandes, *J. Med. Chem.*, 2015, **58**, 4339–4347.

17 N. Mohan, S. Muthumari and R. Ramesh, *J. Organomet. Chem.*, 2016, **807**, 45–51.

18 Z. Wang, H. Qian, S. Yiu, J. Sun and G. Zhu, *J. Inorg. Biochem.*, 2014, **131**, 47–55.

19 N. Martínez-Alonso, N. Busto, F. A. Jalón, B. R. Manzano, J. M. Leal, A. M. Rodríguez, G. B. and G. Espino, *Inorg. Chem.*, 2014, **53**, 11274–11288.

20 M. Maroto-Díaz, B. T. Elie, P. Gómez-Sal, J. Pérez-Serrano, R. Gómez, M. Contel and J. de la Mata, *Dalton Trans.*, 2016, **45**, 7049–7066.

21 P. Chellan, K. M. Land, A. Shokar, A. Au, S. H. An, D. Taylor, P. J. Smith, T. Riedel, P. J. Dyson, K. Chibale and G. S. Smith, *Dalton Trans.*, 2014, **43**, 513–526.

22 B. C. E. Makhubela, M. Meyer and G. S. Smith, *J. Organomet. Chem.*, 2014, **772**–**773**, 229–241.

23 A. R. Burgoyne, C. H. Kaschula, M. I. Parker and G. S. Smith, *J. Organomet. Chem.*, 2017, **846**, 100–104.

24 I. Cassells, T. Stringer, A. T. Hutton, S. Prince and G. S. Smith, *JBIC J. Biol. Inorg. Chem.*, 2018, **23**, 763–774.

25 A. R. Burgoyne, C. H. Kaschula, M. I. Parker and G. S. Smith, *Eur. J. Inorg. Chem*, 2016, 1267–1273.

26 A. Eskandari, A. Kundu, S. Ghosh and K. Suntharalingam, *Angew. Chem. Int. Ed.*, 2019, **58**, 12059–12064.

27 N. Baartzes, C. Szabo, M. Cenariu, F. Imre-Lucaci, S. Aurel, E. Fischer-Fodor and G. S. Smith, *Inorg. Chem. Commun.*, 2018, **98**, 75–79.

28 D. Giffard, E. Fischer-Fodor, C. Vlad, P. Achimas-Cadariu and G. S. Smith, *Eur. J. Med. Chem.*, 2018, **157**, 773–781.

29 G. Gasser, I. Ott and N. Metzler-Nolte, *J. Med. Chem.*, 2011, **54**, 3–25.

30 A. P. Basto, N. Anghel, R. Rubbiani, M. J, S. D, F. Gianni, G. Suss-Fink, V. Balmer, G. Gasser, J. Furrer and A. Hemphill, *Metallomics*, 2019, **11**, 462–474.

31 A. Lapasam, E. Pinder, R. M. Phillips, W. Kaminsky and M. Rao, *J. Organomet. Chem.*, 2019, **899**, 120887.

32 M. A. Bennett and A. K. Smith, *Dalton Trans.*, 1974, 233.

33 H. Huang, P. Zhang, H. Chen, L. Ji and H. Chao, *Chem. Eur. J.*, 2015, **21**, 715–725.

34 Y. Li, Q. Wu, G. Yu, L. Li, X. Zhao, X. Huang and W. Mei, *Eur. J. Med. Chem.*, 2019, **164**,

282–291.

35 L. Zeng, Y. Chen, H. Huang, J. Wang, D. Zhao, L. Ji and H. Chao, *Chem. Eur. J.*, 2015, **21**, 15308–15319.

36 S. Fernandez, M. Pfeffer, V. Ritleng and C. Sirlin, *Organometallics*, 1999, **18**, 2390–2394.

37 R. J. Foot and B. T. Heaton, *J. Chem. Soc. Dalton Trans.*, 1979, 295–298.

38 R. K. Rath, S. G. Valavi, K. Geetha and A. R. Chakravarty, *J. Organomet. Chem.*, 2000, **596**, 232–236.

39 G. C. Martin and J. M. Boncella, *Organometallics*, 1989, **8**, 2968–2970.

40 J. Pérez, V. Riera, A. Rodríguez and D. Miguel, *Organometallics*, 2002, **21**, 5437–5438.

41 Y. Boutadla, O. Al-Duaij, D. L. Davies, G. A. Griffith and K. Singh, *Organometallics*, 2009, **28**, 433–440.

42 L. Li, W. W. Brennessel and W. D. Jones, *Organometallics*, 2009, **28**, 3492–3500.

43 D. L. Davies, O. Al-Duaij, J. Fawcett, M. Giardiello, S. T. Hilton and D. R. Russell, *J. Chem. Soc. Dalton Trans.*, 2003, **3**, 4132–4138.

44 J. F. G. A. Jansen, E. M. M. D. B. Den Berg and E. W. Meijer, *Science*, 1994, **266**, 1226–1229.

Chapter 4

In Vitro Biological Evaluation of Trinuclear Ruthenium(II)-*p*-cymene complexes of 2,5-Disubstituted Benzimidazole-Based Trimeric Ligands

4.1 Introduction

Classical platinum(II)-based metallodrugs with the *cis*-[$PtX_2(amine)_2$] general chemotype (where X = leaving group; amine = neutral or carrier group) have been in clinical use for the treatment of cancer for over thirty years, with the most commonly known example being cisplatin.[1] However, these platinum anticancer agents lack specificity for cancer cells and target all rapidly dividing cells including those in the hair follicles, bone marrow and the gastrointestinal tract.[2] This lack of selectivity often leads to the development of severe adverse side effects including hair loss, vomiting and neurotoxicity.[3] Additionally, the prevalence of resistance towards clinically used platinum drugs displayed by various cancers is a growing concern, as platinum drugs constitute the majority of current combination chemotherapy regimens.[4,5] Overcoming the aforementioned challenges has thus been of great interest to cancer researchers.

One approach that can be used to reduce the side effects caused by platinum-based metallodrugs is to replace the platinum metal center with an alternative Platinum-Group Metal (PGM). Motivated by the promising results of the ruthenium drug candidates, NAMI-A, IT-139 and TLD-1433, ruthenium-based organometallic complexes have been of great interest.[6] Indeed, numerous ruthenium(II)-arene complexes which show promising anticancer activity have been developed.[7–9] For example, RM179 (Figure 4.1 a) which was developed by the Sadler group in 2001, is one of the first ruthenium(II)-arene complexes to be investigated for anticancer activity.[10] This ruthenium complex was reported to be a potent inhibitor of MDA-MB-231 and MCF-7 breast cancer cell metastasis *in vitro*, through its ability to inhibit the matrix metalloprotease-2 (MMP-2) enzyme.[2] Furthermore, the complex was also observed to reduce murine mammary carcinoma (MCa) tumours *in vivo*. RAPTA-C (Figure 4.1 b), was the second notable ruthenium(II)-arene complex developed by the Dyson group.

RAPTA-C exhibits selectivity towards the TS/A mouse mammary adenocarcinoma cell line as opposed to non-tumorigenic mammary epithelial cells (HBL-100).[11] Additionally, it was noted that RAPTA-C shows activity similar to that of NAMI-A in the reduction of the growth of lung metastases in mice bearing the MCa tumours. Despite the promising strides in the development of organometallic complexes with enhanced selectivity, the threat of either intrinsic or developed resistance of cancer cells to chemotherapeutic agents remains a major hurdle in rational anticancer metallodrug design.

A strategy that may be used to overcome intrinsic or developed resistance of cancer cells to clinically used metal-based anticancer agents is to develop multinuclear organometallic complexes with novel mechanisms of action. This concept was used in the development of BBR3464 (Figure 4.1 c), a complex comprised of three *trans*-configured platinum moieties linked by diaminoalkanes. The BBR3464 trinuclear complex has been reported to show a higher degree of DNA interstrand crosslinking compared to cisplatin.[12] Furthermore, it was reported to show enhanced activity two to three times the magnitude of that noted for cisplatin in the cisplatin-resistant A2780cisR, 41McisR and the CH1cisR human ovarian cancer cell lines.[13] Despite the limited success of BBR3464 in Phase II clinical trials for the treatment of patients with small-cell lung carcinoma, gastric and gastroesophageal cancers,[14–16] the trinuclear complex provides additional credibility for the concept that multinuclearity may improve the potency of potential anticancer drugs.

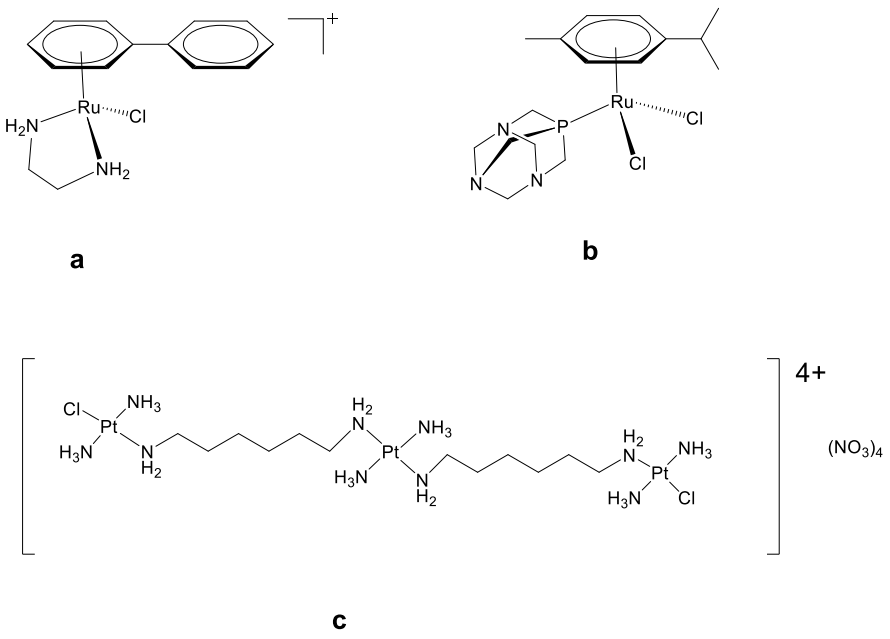

***Figure 4.1**: The structures of the ruthenium(II)-arene complexes **RM175** a) and **RAPTA-C** b), and the trans-platinum(II)-based complex **BBR3464** c).*

The enhanced potency of multinuclear systems, relative to their mononuclear analogues, may be attributed to the Enhanced Permeability and Retention (EPR) effect.[17,18] The EPR effect refers to the preferential accumulation of multinuclear complexes in solid tumours, over normal tissues, due to tumours having porous vasculature. Once inside the tumour cells, the multinuclear complexes are retained at a high concentration due to poor lymphatic drainage of tumours. This results in enhanced cytotoxicity specifically towards tumour cells and thus minimize side effects.[19]

The development of trinuclear complexes has been mainly focused on the platinum metal center. Analogous trinuclear ruthenium complexes have been less studied for their anticancer properties with only a handful of examples in the literature.[20–24] This chapter therefore explores the *in vitro* anticancer activity of the 2,5-disubstituted tris-benzimidazole compounds (**7** – **15**) and their respective triruthenium(II) complexes (**19** – **24**) that were synthesized in this study. Furthermore, the interaction of the most active trinuclear ruthenium(II) complex with Guanosine 5'-monophosphate disodium (5'-GMP) was also investigated as a possible mechanism of action.

4.2 *In vitro* single dose pre-screen

To identify compounds with potential anticancer activity, the 2,5-disubstituted tris-benzimidazole compounds (**7** – **15**) and their corresponding ruthenium(II) complexes (**19** – **24**) synthesized in this study were pre-screened for their *in vitro* cytotoxicity against the MCF-7 and MDA-MB-231 breast cancer cell lines and the 501 melanoma skin carcinoma cell line. The compounds were firstly tested for their cytotoxicity at 10 µM using the MTT (3-(4,5-dimethylthiazol-2-yl)-2,5 diphenyltetrazolium bromide) assay.[26] This concentration was selected based on the approach by the National Cancer Institute (NCI, USA) which conducts a pre-screen of putative anticancer drug candidates at 10 µM.[25] MTT is a yellow tetrazolium salt that gets reduced to purple water-insoluble formazan crystals (3-(4,5-dimethylthiazol-2-yl)-2,5-diphenylformazan) by dehydrogenase enzymes in viable cells, using NADH and NADPH as co-substrates (Scheme 4.1).[27] After solubilization of the formazan crystals, the number of viable cells can be quantified colorimetrically by measuring the absorbance at 600 nm. In all the biological assays, cisplatin was used as a positive control. Due to the compounds showing mild to no activity at 10 µM, their cytotoxicity was subsequently tested at 20 µM.

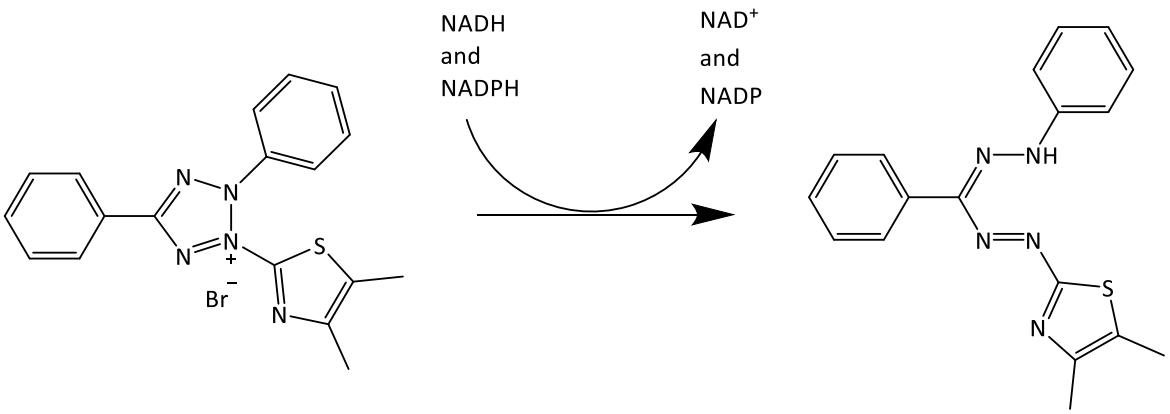

MTT **Formazan**

Scheme 4.1 *: Conversion of MTT (3-(4,5-dimethylthiazol-2-yl)-2,5 diphenyltetrazolium bromide) to formazan (3-(4,5-dimethylthiazol-2-yl)-2,5-diphenylformazan).*[27]

4.2.1 In vitro cytotoxicity of the 2,5-disubstituted trimeric ligands (7 – 12) and their trinuclear Ru(II) complexes (19 – 24) in the MCF-7 breast cancer cell line

The data obtained for the *in vitro* anticancer evaluation of the 2-phenyl tris-benzimidazole ligands (**7** – **9**) and their corresponding cyclometallated complexes (**19** – **21**) against the MCF-7 breast cancer cell line is summarized in Figure 4.2. At 10 µM, all the tested compounds from this series showed mild to no activity, as they were only able to reduce cancer cell viability by 3% to 19%. Upon doubling the concentration to 20 µM, the 2-phenyl tris-benzimidazole ligands (**7** – **9**) and their respective complexes (**19** – **21**) reduced MCF-7 cell viability by 14% to 22%. There was therefore only a slight increase in their activity at 20 µM.

The most active compound from this series was the 5-unsubstituted ligand **7** which inhibits MCF-7 cell viability by 19% and 22% at 10 and 20 µM, respectively. Additionally, with the exception of ligand **7** and its corresponding cyclometallated complex **19**, there was a significant enhancement of the anticancer activity of the 2-phenyl tris-benzimidazole ligands (**8** and **9**) upon complexation with the ruthenium(II) metal centers to yield the corresponding complexes (**20** and **21**, respectively). For example, when comparing the activity of ligand **8** and its corresponding cyclometallated complex (**20**), the complex (**20**) shows 4% and 16% greater inhibition of cancer cell viability at 10 and 20 µM, respectively.

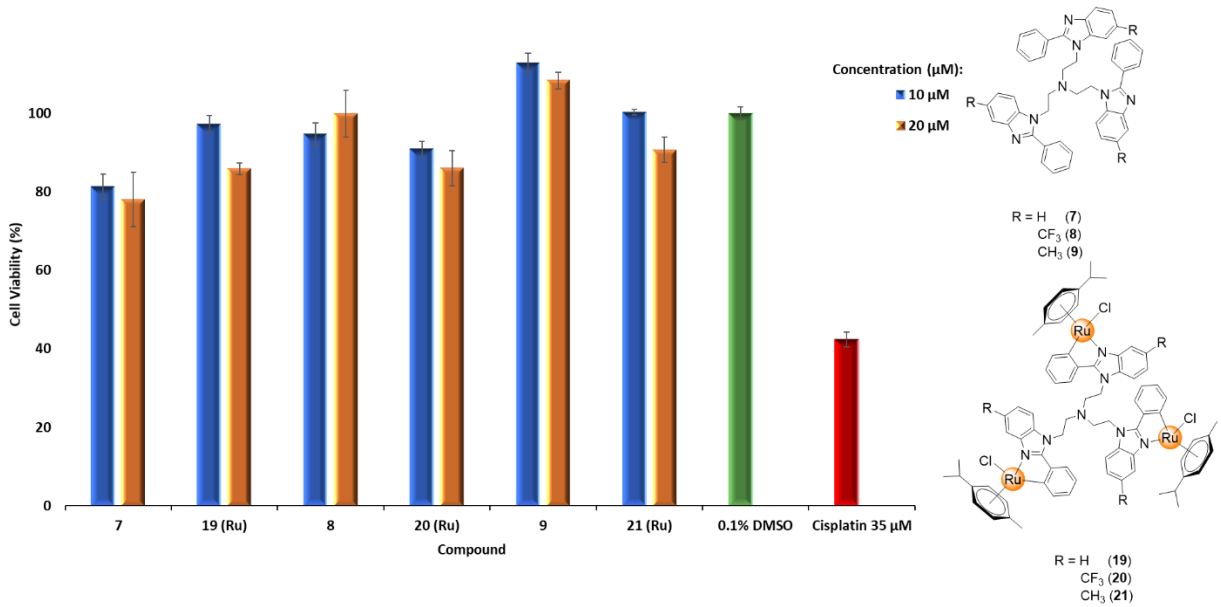

***Figure 4.2**: The percentage cell viability as measured by MTT assays in MCF-7 breast cancer cells exposed to either vehicle (0.1% DMSO) or the 2-phenyl ligands (**7** - **9**) and their corresponding neutral C^N-Ru(II) complexes (**19** - **21**) at 10 and 20 µM concentrations for 48 hours. 35 µM cisplatin (the IC_{50} of cisplatin in MCF-7 cells treated for 48 hours[28]) was included as a positive control.*

The 2-pyridyl tris-benzimidazole ligands (**10** – **12**) and their corresponding cationic complexes (**22** – **24**) showed appreciable cytotoxic activity in the MCF-7 breast cancer cell line (Figure 4.3). Indeed, at 10 µM they reduced MCF-7 cancer cell viability by 5% to 31% and this was improved by 12% to 57% at 20 µM. The most active compound from this series is the 5-unsubstituted ligand **10** which inhibits MCF-7 breast cancer cell viability to 69% at 10 µM and to 43% at 20 µM. Importantly, ligand **10** at 20 µM has comparable cytotoxicity to cisplatin at 35 µM which suggests that ligand **10** may be more cytotoxic to MCF-7 cells at equivalent concentrations of cisplatin. Furthermore, with the exception of the trimeric ligand **10** and its corresponding cationic complex **22**, at 10 µM the ruthenium(II) complexes (**23** and **24**) show enhanced activity relative to their corresponding 2-pyridyl tris-benzimidazole ligands (**11** and **12**, respectively). For example, the cationic ruthenium(II) complex **23** was observed to show 15% greater inhibition of cancer cell viability relative to its corresponding 5-methyl substituted 2-pyridyl ligand (**12**). With the exception of ligand **11** and its corresponding complex **23**, which both reduced MCF-7 cell viability to 73%, the same trend was observed at 20 µM for the other compounds tested. This general trend observed highlights the synergistic effects of the ruthenium(II) metal centers and the organic ligand in eliciting anticancer activity.

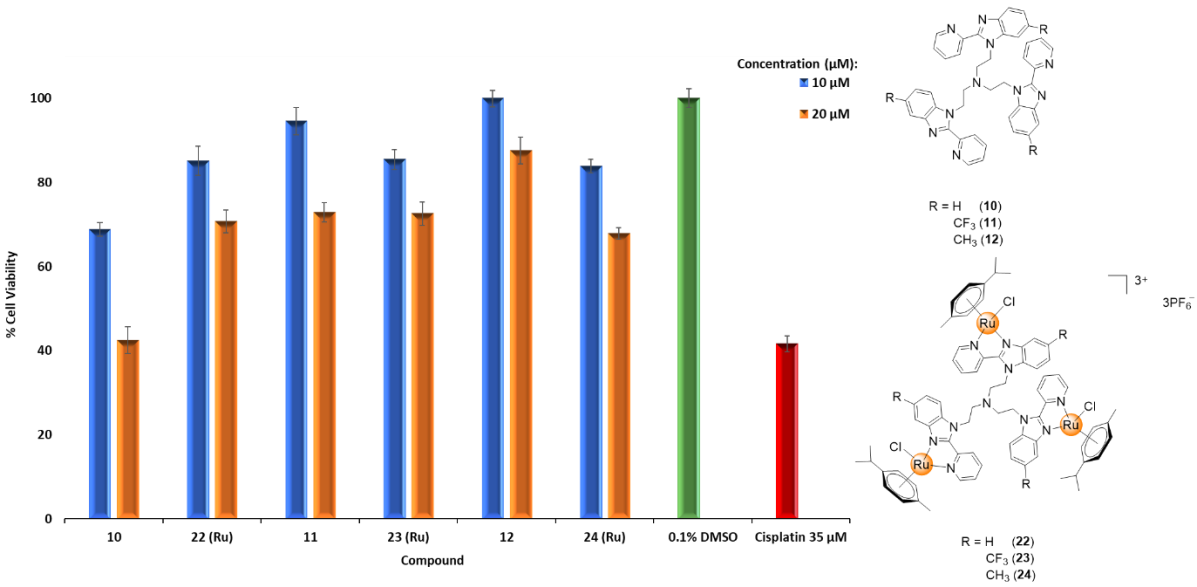

***Figure 4.3**: The percentage cell viability as measured by MTT assays in MCF-7 breast cancer cells exposed to either vehicle (0.1% DMSO) or the 2-pyridyl trimeric ligands (**10** – **12**) and corresponding trinuclear N^N-Ru(II) cationic complexes (**22** - **24**) at 10 and 20 μM concentrations for 48 hours. 35 μM cisplatin (the IC_{50} of cisplatin in MCF-7 cells treated for 48 hours[28]) was included as a positive control.*

A comparison of the *in vitro* anticancer activity obtained for the 2-phenyl tris-benzimidazole ligands (**7** - **9**) and their corresponding neutral *C^N*-Ru(II) complexes (**19** – **21**) shown in Figure 4.2, to that of the 2-pyridyl tris-benzimidazole ligands (**10** – **12**) and their respective cationic *N^N*-Ru(II) complexes (**22** – **24**) as shown in Figure 4.3, reveals a number of trends. Firstly, at 10 and 20 μM, the 5-unsubstituted trimeric ligands (**7** and **10**) show greater activity than the corresponding ruthenium(II) complexes (**19** and **22**, respectively). Additionally, the 2-pyridyl tris-benzimidazole ligands (**10** – **12**) show activity superior to that of their respective 2-phenyl tris-benzimidazole ligands (**7** – **9**). This is exemplified by the 5-unsubstituted 2-pyridyl ligand (**10**) showing 12% and 35% greater MCF-7 cell inhibition, at 10 and 20 μM respectively, compared to the 5-unsubstituted 2-phenyl ligand (**7**).

Furthermore, the cationic trimetallic complexes (**22** – **24**) show enhanced cytotoxicity relative to their respective neutral cyclometallated complexes (**19** – **21**). This is evidenced by the cationic complex **22** showing 12% to 15% greater inhibition of MCF-7 cancer cell viability, relative to the neutral complex **19**, at both 10 and 20 μM. A similar trend was previously reported, in which cationic organometallic complexes showed significantly enhanced anticancer activity relative to their neutral counterparts.[29–32] This may be attributed to greater

intracellular accumulation of the cationic compounds relative to their neutral conjugates, as it has been noted that the ability of cationic complexes to cross the cellular membrane may be equal and even superior to that of neutral complexes.[33–35]

4.2.2 In vitro pre-screen of the anticancer activity of 2-ferrocenyl tris-benzimidazole compounds (13 – 15) in the MCF-7 breast cancer cell line

The use of the ferrocenyl moiety as a non-planar bioisostere for aryl and heteroaryl rings was first introduced in the 1970s.[36] However, the medicinal applications of these compounds have only been fully appreciated in the last two decades. This resulted from the independent discoveries that ferroquine and ferrocifens showed enhanced antimalarial and anticancer activity, respectively, relative to their organic counterparts.[37] The aqueous stability and favorable electrochemical properties have made the ferrocenyl functionality an ideal candidate for biological applications and conjugation to biomolecules.[38] This prompted the evaluation of the anticancer activity in the MCF-7 breast cancer cell line of 10 and 20 µM 2-ferrocenyl tris-benzimidazoles (**13** – **15**) which were synthesized in this study.

The biological data obtained from the *in vitro* pre-screening of the 2-ferrocenyl tris-benzimidazole compounds (**13** – **15**) are summarized in Figure 4.4. Interestingly, all the 2-ferrocenyl compounds (**13** – **15**) screened did not show any appreciable reduction in MCF-7 cancer cell viability at both concentrations tested. This was unexpected as ferrocenyl-conjugated molecules are known to promote the production of Reactive Oxygen Species (ROS) *via* Fenton-type processes, which generally trigger cell death. An example of compounds that are known to use this mechanism of action to elicit anticancer effects is the ferrocifen family of complexes.[37,39,40]

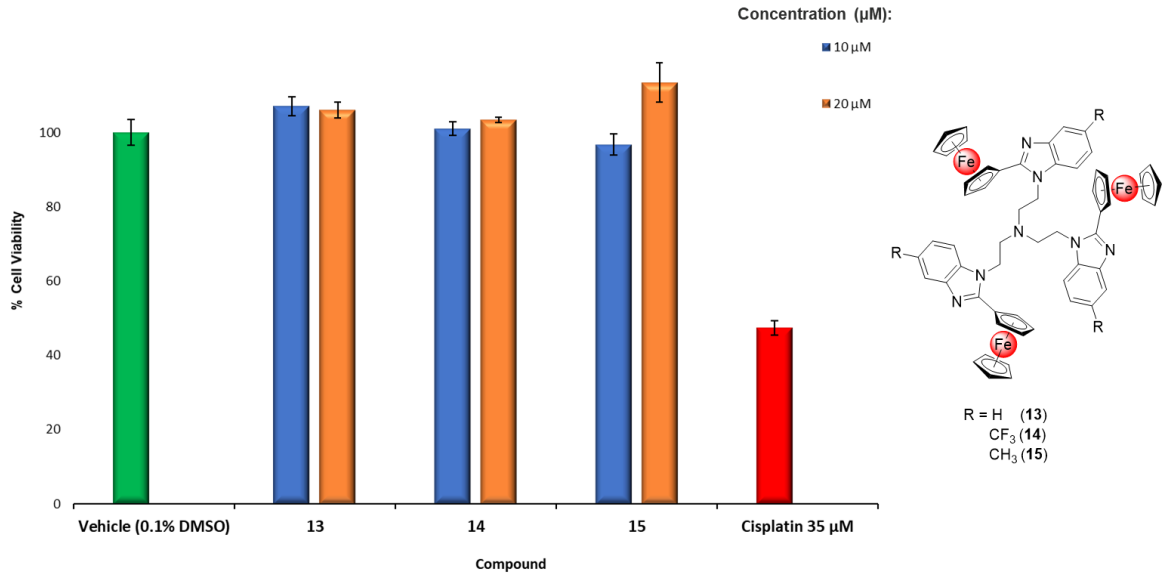

***Figure 4.4**: The percentage cell viability as measured by MTT assays in MCF-7 breast cancer cells exposed to either vehicle (0.1% DMSO) or the 2-ferrocenyl compounds (**13** – **15**) at 10 and 20 µM concentrations for 48 hours. 35 µM cisplatin (the IC_{50} of cisplatin in MCF-7 cells treated for 48 hours[28]) was included as a positive control.*

Upon closer inspection, precipitation was observed in the medium of cells treated after 3 to 5 hours with 10 and 20 µM compounds **13** – **15** (red arrows in Figure 4.5 a, b and c). This may explain the inactivity of the 2-ferrocenyl compounds (**13** – **15**) in the MTT assays. Because the tested compounds were initially dissolved in DMSO, this observation prompted the change to another Generally Regarded as Safe (GRAS) solvent, Ethanol.

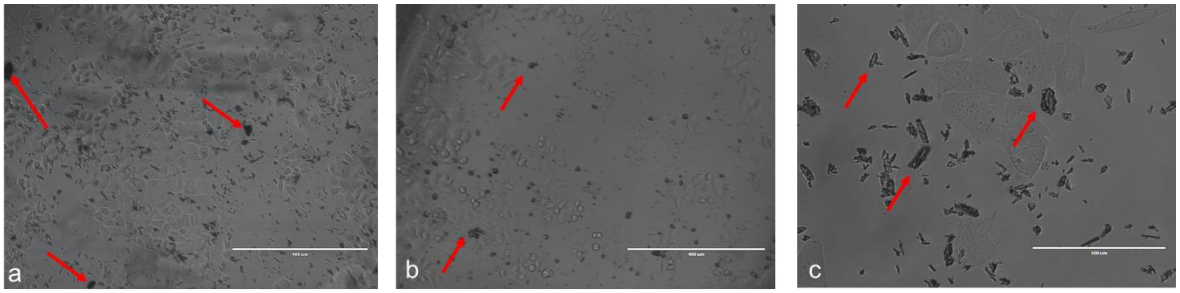

***Figure 4.5**: Microscopic images of the MCF-7 breast cancer cells in culture after treatment with the 2-ferrocenyl compounds **13** (a), **14** (b) and **15** (c), showing extensive precipitation of these compounds 3 – 5 hours after treatment (red arrows).*

However, this change in solvent did not prevent the precipitation of the 2-ferrocenyl compounds (**13** – **15**). Indeed, microscopic inspection of the cells treated for 3 – 5 hours with 20 µM of the 2-ferrocenyl tris-benzimidazoles (**13** – **15**) dissolved in Ethanol (Figure 4.6 a, b and c) revealed more extensive precipitation than when DMSO was used as the solvent (Figure 4.5 a, b and c, *vide supra*).

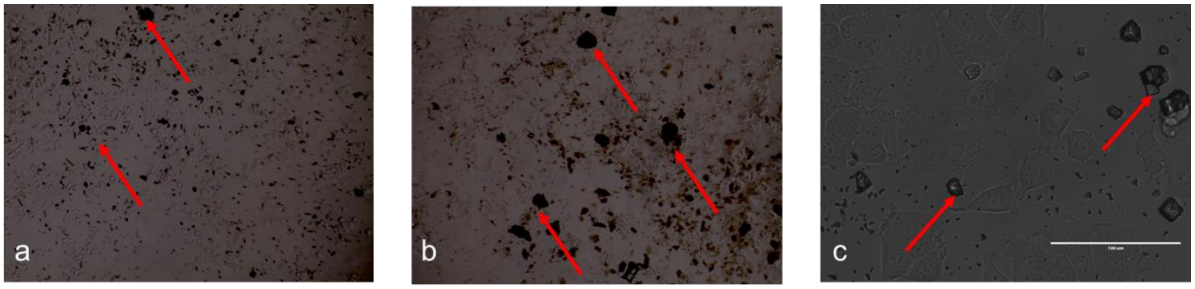

***Figure 4.6**: Microscopic images of the MCF-7 breast cancer cells in culture after treatment for 3 – 5 hours with the 2-ferrocenyl compounds **13** (a), **14** (b) and **15** (c) dissolved in Ethanol. Extensive precipitation is shown with red arrows.*

The observed precipitation of the 2-ferrocenyl tris-benzimidazoles (**13** – **15**) out of growth media, correlated with them not exhibiting any cytotoxic effects in MCF-7 breast cancer cells (Figure 4.7).

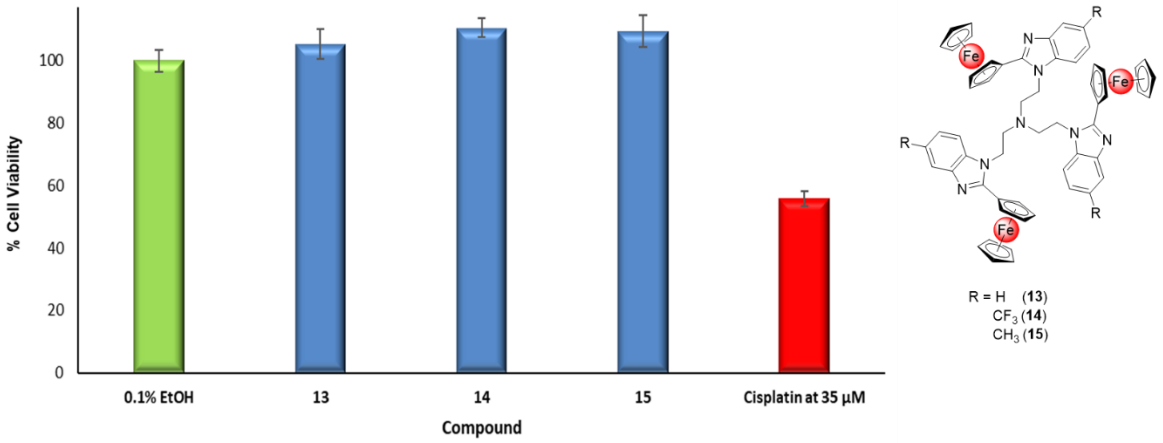

***Figure 4.7**: The percentage cell viability as measured by MTT assays in MCF-7 breast cancer cells exposed to either vehicle (0.1% EtOH) or the 2-ferrocenyl compounds (**13** – **15**) at 20 µM for 48 hours. 35 µM cisplatin (the IC_{50} of cisplatin in MCF-7 cells treated for 48 hours[28]) was included as a positive control.*

4.2.3 In vitro pre-screen of the cytotoxicity of the 2-pyridyl trimeric ligands (10 – 12) and the cationic complexes (22 – 24) against the MDA-MB-231 cell line

Due to the promising cytotoxic activity observed for the 2-pyridyl tris-benzimidazole ligands (**10** – **12**) and their corresponding trinuclear cationic complexes (**22** - **24**) in the MCF-7 breast cancer cell line, they were evaluated for their cytotoxic activity in the MDA-MB-231 breast cancer cell line. The MDA-MB-231 cell line is a triple-negative (oestrogen, progesterone and human epidermal growth factor 2 receptor-negative) and highly invasive breast cancer cell subtype[41,42] which is notoriously hard to treat.[43]

The data obtained from the *in vitro* pre-screening of the 2-pyridyl ligands (**10** – **12**) and their corresponding cationic complexes (**22** – **24**) against the MDA-MB-231 cell line at 20 µM are summarized in Figure 4.8. When these results are compared with those obtained for the MCF-7 breast cancer cell line at 20 µM (Figure 4.3 *vide supra*), the 2-pyridyl tris-benzimidazole ligands (**10** – **12**) and their corresponding trinuclear cationic complexes (**22** - **24**) were significantly less active. Indeed, these compounds inhibited MCF-7 cell viability by 11% to 23% more than in the MDA-MB-231 breast cancer cells. An exception was the 5-methyl substituted cationic complex (**24**) which was 5% more potent in the MDA-MB-231 cell line than in the MCF-7 cell line.

When the activity of the 2-pyridyl tris-benzimidazole ligands (**10** – **12**) was compared to that of their corresponding trimetallic cationic complexes (**22** – **24**) in the MDA-MB-231 cell line, similar trends were observed as in the MCF-7 breast cancer cell line. Firstly, the activity of the 5-unsubstituted 2-pyridyl ligand (**10**) is superior to that of the corresponding ruthenium(II) complex (**22**). Additionally, the general enhanced activity of the cationic complexes (**23** and **24**) relative to their respective ligands (**11** and **12**, respectively) is also observed.

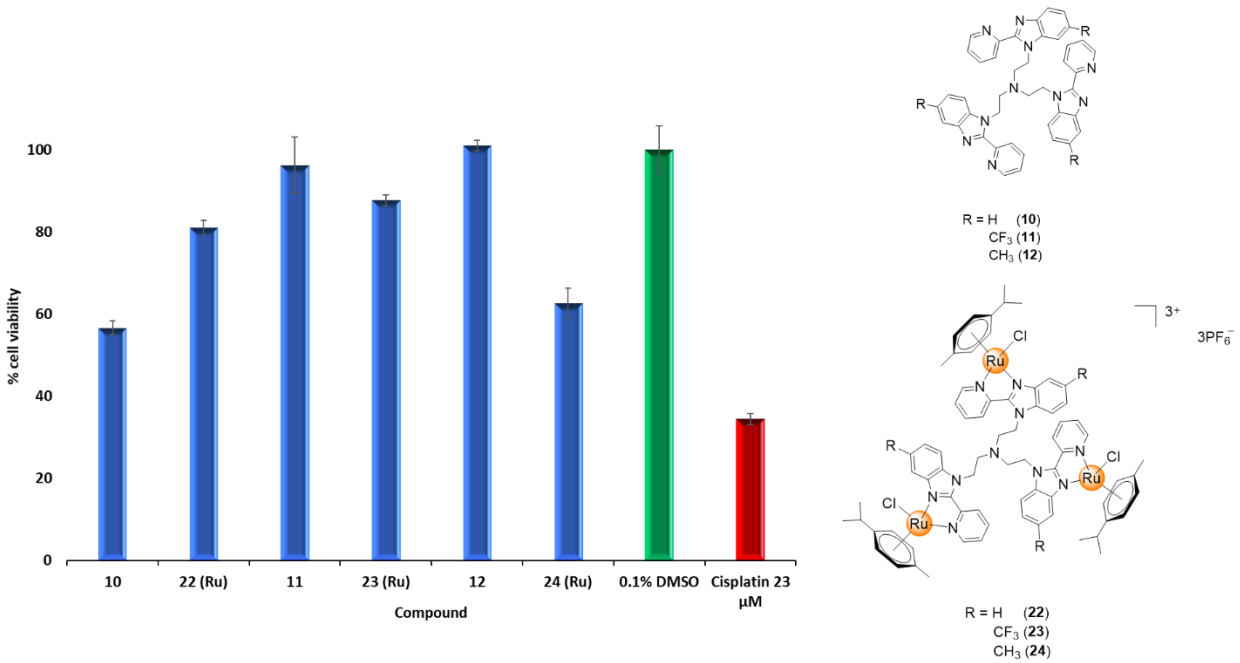

***Figure 4.8**: The percentage cell viability as measured by MTT assays in MDA-MB-231 breast cancer cells exposed to either vehicle (0.1% DMSO) or the 2-pyridyl ligands (**10** – **12**) and their corresponding trinuclear N^N-Ru(II) chelated complexes (**22** - **24**) at 20 µM for 48 hours. 23 µM cisplatin (the IC_{50} of cisplatin in MDA-MB-231 cells treated for 48 hours[44]) was included as the positive control.*

Owing to their promising activity in the pre-screens in the MCF-7 and the MDA-MB-231 breast cancer cell lines, the promising 2-pyridyl ligands (**10** and **11**), and their respective cationic trimetallic complexes (**22** and **23**), were selected for further multidose screening. The multidose experiments were aimed at determining the IC_{50} values of the selected compounds against the MCF-7 and MDA-MB-231 breast cancer cell lines and are discussed in Section 4.3, *vide infra*.

4.2.4 In vitro cytotoxic evaluation of the 2-pyridyl trimeric ligands (10 - 11) and the cationic Ru(II) complexes (22 – 23) in the 501 melanoma cells

The threat of malignant melanoma continues to loom over the global population, as the incidence of this aggressive cancer is increasing rapidly more than any other solid tumour.[45] This is exacerbated by the limited success of current chemotherapeutic strategies in the treatment of malignant melanomas, and the ability of melanoma cells to metastasize rapidly to other organs.[46,47] To this end, the promising 2-pyridyl tris-benzimidazole ligands (**10** and **11**) and their corresponding cationic ruthenium(II) complexes (**22** and **23**, respectively) were

pre-screened for their *in vitro* anticancer activity against the metastatic 501 melanoma (501mel) cell line at 10 and 20 µM (Figure 4.9).

Generally, at 10 µM the 2-pyridyl ligands (**10** and **11**) and their respective trinuclear cationic complexes (**22** and **23**) were observed to show mild to no activity. However, except for the 5-trifluoromethyl substituted ligand (**11**), all the compounds tested show slightly enhanced activity at 20 µM. An example of this is the ruthenium(II) complex **22** which at 20 µM inhibited 501mel cell viability by 19% more relative to at 10 µM. Additionally, in general the cationic complexes (**22** and **23**) were more cytotoxic compared to their respective 2-pyridyl ligands (**10** and **11**). This suggests that incorporation of the ruthenium(II) metal centers onto the trimeric 2-pyridylbenzimidazole scaffold results in the enhancement of anticancer activity due to the synergism of the organic scaffold and the metal centers.

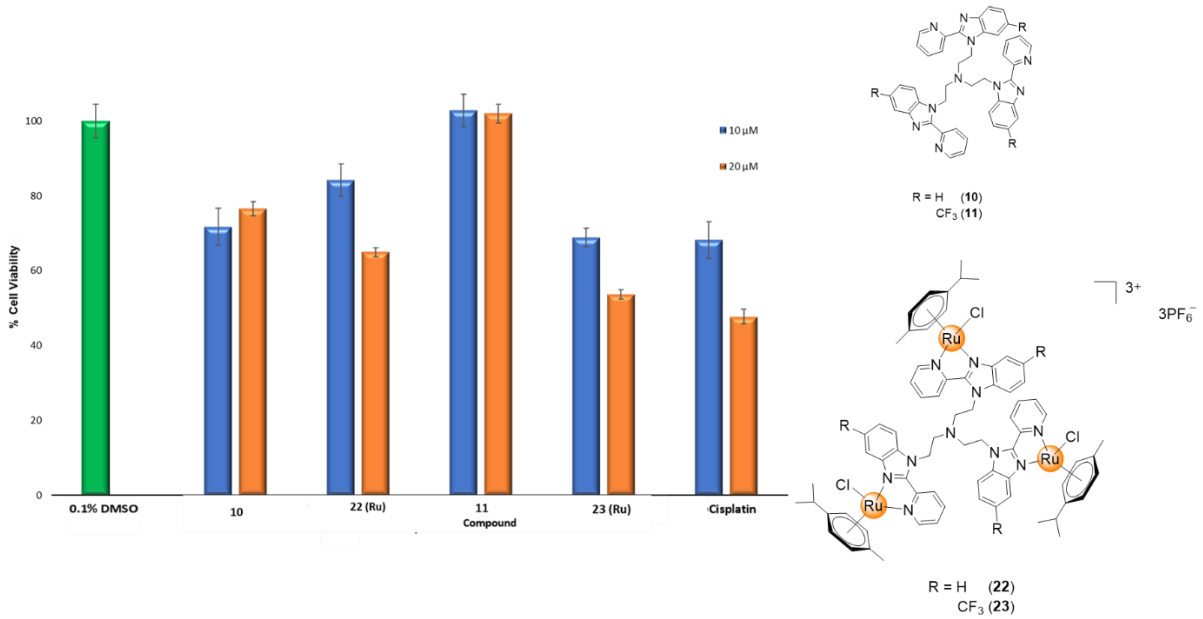

Figure 4.9*: The percentage cell viability as measured by MTT assays in 501 melanoma cells exposed to either vehicle (0.1% DMSO) or the 2-pyridyl ligands (**10** and **11**) and their respective N^N-Ru(II) chelated complexes (**22** and **23**) at 10 and 20 µM concentrations for 48 hours. Cisplatin (at 10 and 20 µM) was included as the positive control.*

Interestingly, at 10 and 20 µM, the 5-trifluoromethyl cationic complex (**23**) and cisplatin showed comparable activity. However, the rest of the compounds tested showed significantly less potent cytotoxic activity relative to cisplatin at both the concentrations tested. As a result, the 5-trifluoromethyl complex (**23**) and its corresponding trimeric ligand (**11**), were selected

for multidose experiments to determine the IC_{50} values of these compounds in the 501 melanoma cell line (Section 4.3.2, *vide infra*).

4.3 *In vitro* multidose screening

The IC_{50} values of the selected 2-pyridyl ligands (**10** and **11**) and their corresponding cationic complexes (**22** and **23**, respectively) were next determined in the MCF-7 and MDA-MB-231 breast cancer cell lines, and the 501 melanoma cell line. In these experiments, the cancer cells were treated with the test compounds (**10**, **11**, **22** and **23**) at concentrations ranging from 5 to 35 µM, and cisplatin was included as a positive control. These multidose experiments were performed in quadruplicate on two different occasions and the dose-response data and IC_{50} values obtained from the experiments are discussed in Sections 4.3.1 – 4.3.3, *vide infra*.

4.3.1 IC_{50} concentrations obtained in MCF-7 breast cancer cells

When the compounds were tested in MCF-7 breast cancer cells, the 5-unsubstituted 2-pyridyl ligand (**10**) was the most active compound, with an IC_{50} of 28.65 µM, which was closely followed by its 5-unsubstituted cationic complex (**22**), which had an IC_{50} of 33.87 µM (Figure 4.10). These findings are consistent with the data from the pre-screen (Figure 4.3, *vide supra*). It is also worth noting that ligand **10** and complex **22** show cytotoxic activity superior to that of cisplatin (IC_{50} = 35 µM for cisplatin).

The IC_{50} value of the 5-trifluoromethyl substituted 2-pyridyl trimeric ligand (**11**) could not be determined because none of the concentrations tested inhibited MCF-7 cell viability (Figure 4.10). However, the 5-trifluoromethyl substituted cationic complex (**23**) had an IC_{50} of 35.06 µM which is comparable to the IC_{50} for cisplatin in MCF-7 cells. As previously observed in the pre-screen, enhanced activity against the MCF-7 cell line is observed for the 5-trifluoromethyl substituted cationic complex (**23**) relative to its respective trimeric ligand (**11**).

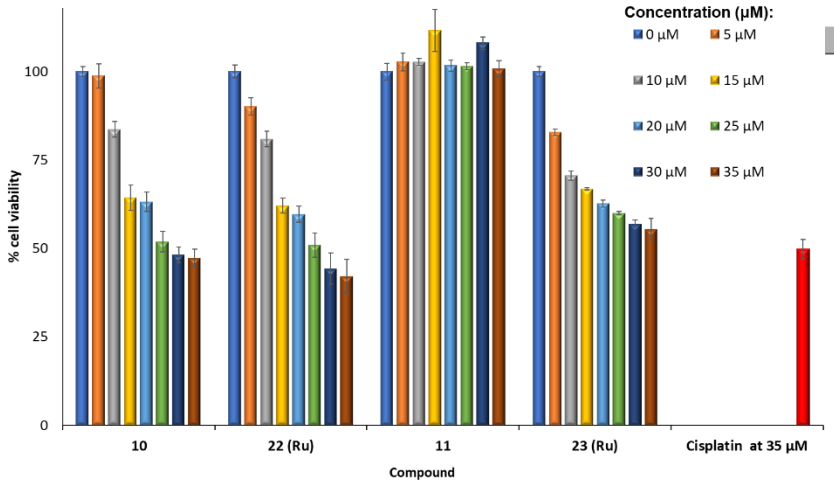

Compound	IC_{50} (µM) ± SD
10	28.65 ± 1.08
22 (Ru)	33.87 ± 1.16
11	N/A*
23 (Ru)	35.06 ± 1.07
Cisplatin	35 [28]

* N/A Not active at tested concentrations

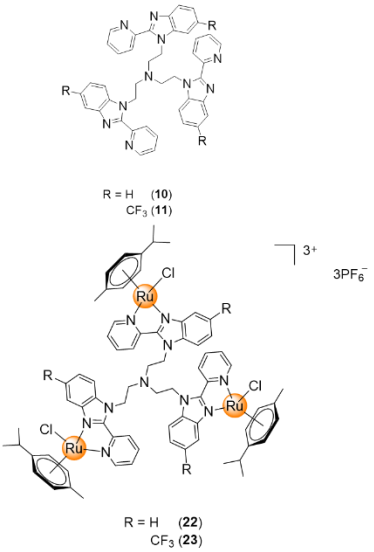

***Figure 4.10**: Percentage cell viability as measured by MTT assays in MCF-7 breast cancer cells treated for 48 hours with increasing concentrations of the 2-pyridyl trimeric ligands (**10** and **11**) and the respective trinuclear N^N-Ru(II) chelated complexes (**22** and **23**) or cisplatin at 35 µM[28]. Cells treated with 0.1% DMSO were included as a vehicle control. The table shows the concentration of each tested compound required to kill 50% of the cancer cells (IC_{50}) which was calculated from sigmoidal plots with GraphPad Prism V5.01.*

As previously discussed, the monomeric 5-unsubstituted 2-pyridylbenzimidazole ligand (**18**) and its corresponding mononuclear cationic ruthenium(II) complex (**25**), were synthesized to compare their anticancer activity to that of their trimeric counterparts **10** and **22**, respectively. Multidose screening experiments were thus performed for ligand (**18**) and complex (**25**) but their IC_{50} values could not be determined because none of the concentrations tested were able to inhibit MCF-7 cell viability to 50% (Figure 4.11). However, a comparison of the cytotoxic activity of the monomeric ligand (**18**) (Figure 4.11) to that of its respective trimeric counterpart (**10**) (Figure 4.10, *vide supra*) at 35 µM in MCF-7 cells reveals that the trimeric ligand (**10**) is approximately twice as potent as the monomeric ligand (**18**).

In addition, at 35 µM concentrations, the trinuclear complex (**22**) (Figure 4.10, *vide supra*) is also approximately twice as active as its mononuclear conjugate (**25**) (Figure 4.11).

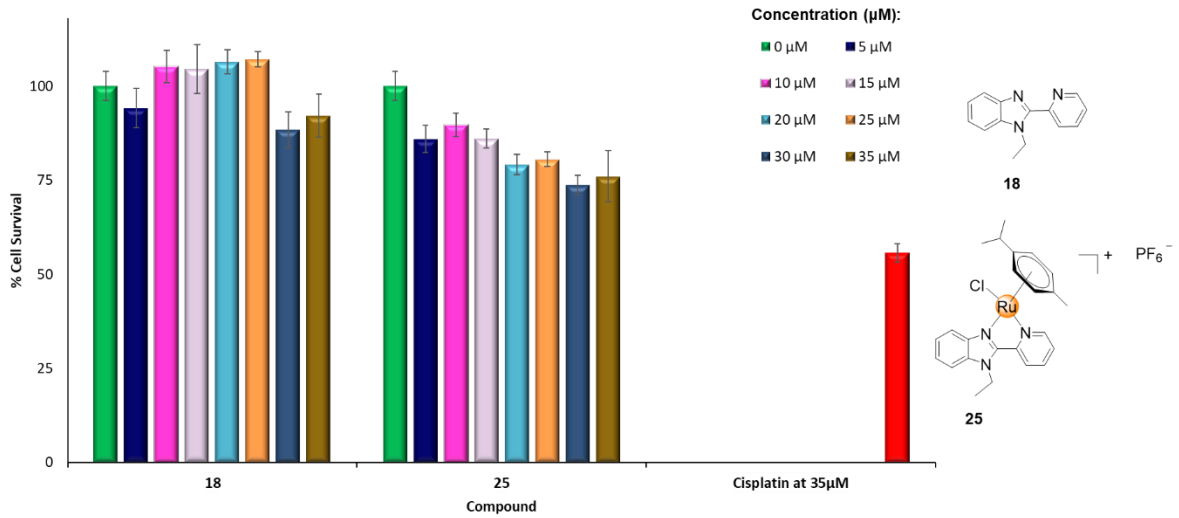

***Figure 4.11**: Percentage cell viability as measured by MTT assays in MCF-7 breast cancer cells exposed for 48 hours to increasing concentrations of the monomeric 2-pyridylbenzimidazole ligand (**18**) and the respective mononuclear N^N-Ru(II) chelated complex (**25**) or cisplatin at 35 µM[28]. Cells treated with 0.1% DMSO were included as a vehicle control.*

The observations that the trimeric ligand (**10**) and the trinuclear complex (**22**) have a two-fold increased potency compared to their respective monomeric counterparts are consistent with reports in the literature and highlight the merit for further investigating multimeric systems as potential anticancer agents.[48–50]

4.3.2 IC_{50} concentrations obtained in MDA-MB-231 TNBC cells

When tested against the more aggressive MDA-MB-231 TNBC cell line, only the 5-unsubstituted trimeric 2-pyridyl ligand (**10**) showed mild cytotoxic activity, with an IC_{50} of 33.53 µM (Figure 4.12). The ligand **10** was however less potent than cisplatin (IC_{50} = 23 µM). The IC_{50} values of all the other compounds tested (the 5-trifluoromethyl ligand **11**, and the cationic complexes **22** and **23**) could not be determined because none of the concentrations tested inhibited MDA-MB-231 cell viability to 50% (Figure 4.12).

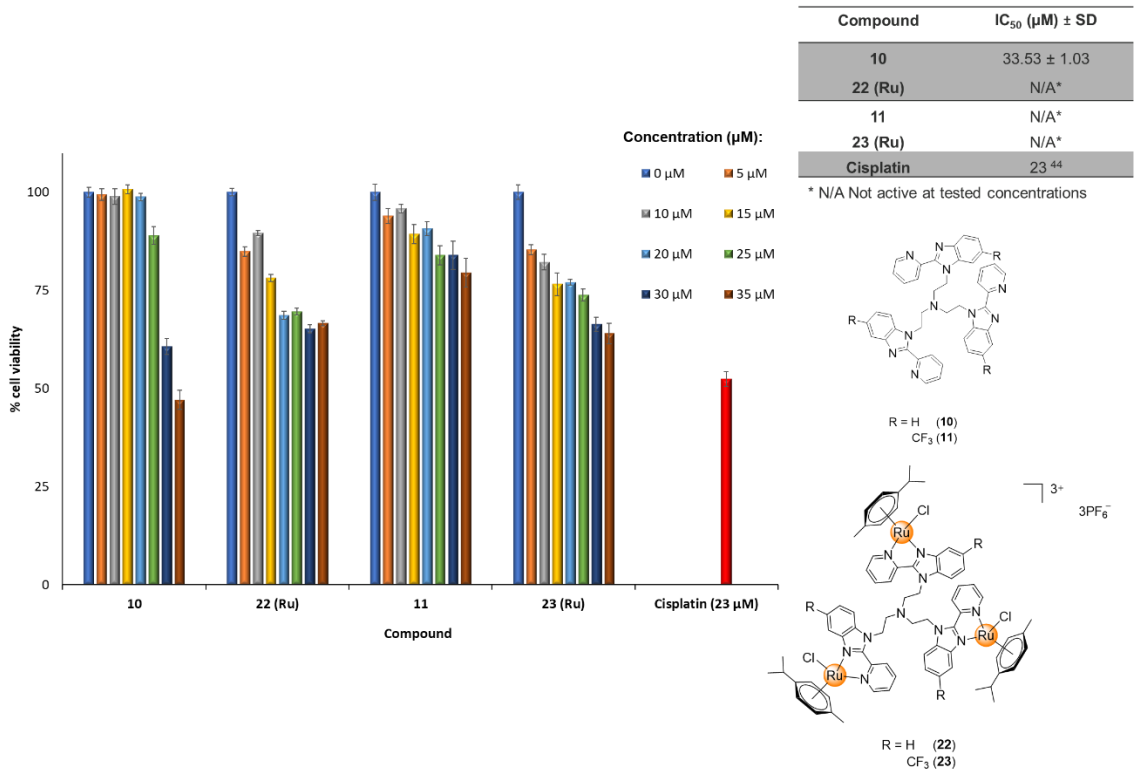

Compound	IC_{50} (μM) ± SD
10	33.53 ± 1.03
22 (Ru)	N/A*
11	N/A*
23 (Ru)	N/A*
Cisplatin	23 [44]

* N/A Not active at tested concentrations

***Figure 4.12**: Percentage cell viability as measured by MTT assays in MDA-MB-231 breast cancer cells treated for 48 hours with increasing concentrations of the 2-pyridyl ligands (**10** and **11**) and corresponding trinuclear N^N-Ru(II) chelated complexes (**22** and **23**) or cisplatin at 23 μM[44]. Cells treated with 0.1% DMSO were included as a vehicle control. The table illustrates the concentration of the tested compounds required to reduce cell viability to 50% (IC_{50}) which was calculated from sigmoidal curves with GraphPad Prism V5.01.*

It is worth noting that the MDA-MB-231 TNBC cell line is known to be resistant to an array of anticancer chemotherapeutic agents.[51] Therefore, the activity of the trimeric ligand (**10**) in the MDA-MB-231 cell line, albeit moderate, presents a promising scaffold for the rational design of anticancer agents to target this notoriously drug resistant triple-negative breast cancer sub-type.

4.3.3 Cytotoxic evaluation of the 5-trifluoromethyl 2-pyridyl ligand (11) and complex (23) against the 501mel cell line

The anticancer data obtained for the 5-trifluoromethyl substituted ligand (**11**) and its corresponding trinuclear cationic ruthenium(II) complex (**23**) in the 501mel cell line is summarized in Figure 4.13. The results show that none of the concentrations tested for the 5-trifluoromethyl ligand (**11**) were able to inhibit 501mel cell viability (Figure 4.13). Consequently, the IC_{50} for ligand **11** in these cells could not be determined. However, the cationic complex (**23**) showed significant, albeit moderate, cytotoxic activity in 501mel cells with an IC_{50} of 34.67 µM. When the 501mel cells were treated with cisplatin an IC_{50} of 21 µM was obtained and thus cisplatin exhibits increased potency relative to complex **23**.

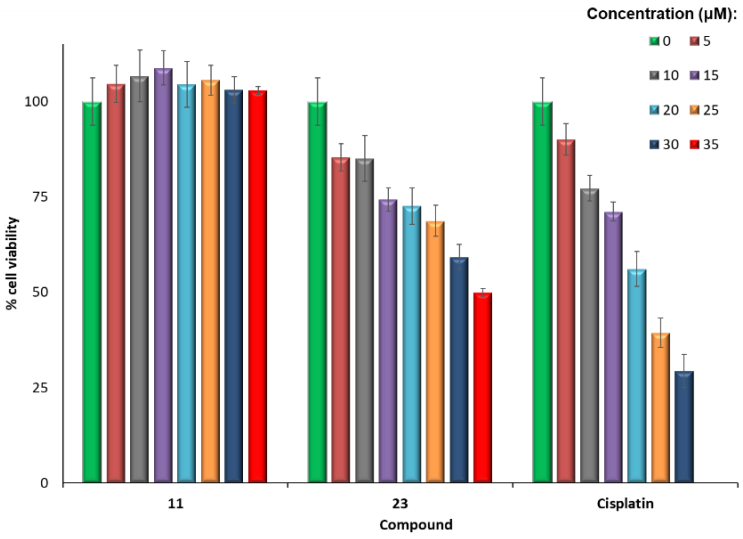

Compound	IC_{50} (µM) ± SD
11	N/A*
23 (Ru)	34.67 ± 1.13
Cisplatin	21.00 ± 1.05

* N/A Not active at tested concentrations

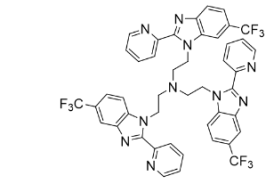

11

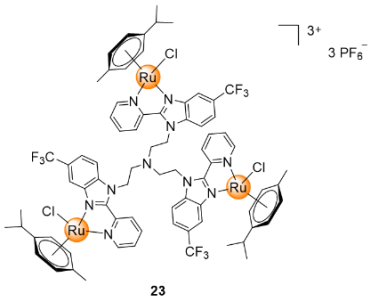

23

***Figure 4.13**: The percentage of 501mel cell viability as measured by MTT assays after 48 hour treatment with varying concentrations of the 2-pyridyl 5-trifluoromethyl ligand (**11**), the respective N^N-Ru(II) chelated complex (**23**) and cisplatin. Vehicle (0.1% DMSO) treated cells were included as a vehicle control. The table shows the concentration of each of the tested compounds required to reduce cell viability to 50% (IC_{50}) which was calculated from sigmoidal plots with GraphPad Prism V5.01.*

The relatively moderate activity of the 5-trifluoromethyl cationic ruthenium(II) complex (**23**) in 501mel cancer cells suggests that complex **23** may present a novel scaffold for the development of organometallic agents that target malignant melanomas.

4.4 *In vitro* cytotoxicity studies

One of the main challenges with current chemotherapeutic drugs is their non-specificity which is often accompanied by numerous undesirable side-effects. A pertinent example is cisplatin, and its second and third-generation derivatives, carboplatin and oxaliplatin.[2] Thus, understanding the selectivity of potential anticancer agents for cancer cells is imperative for drug development. The selected 2-pyridyl trimeric ligands (**10** and **11**) and their corresponding trinuclear cationic ruthenium(II) complexes (**22** and **23**, respectively) were therefore investigated for their cytotoxicity against the non-tumorigenic MCF-12A breast epithelial cell line. Briefly, the cells were treated with the test compounds at concentrations varying from 5 to 35 µM for 48 hours and cell viability was assessed using the colorimetric MTT assay.

From the results obtained it is evident that IC_{50} values could not be experimentally determined for the compounds tested (the ligands **10** and **11**, and their respective complexes **22** and **23**) which suggested that they were more selective for breast cancer cells relative to cisplatin (Figure 4.14). Therefore, IC_{50} values for the compounds tested were predicted by the GraphPad Prism V5.01 software and a comparison with cisplatin show that cisplatin was more cytotoxic to the normal MCF-12A cells (Table 4.1).

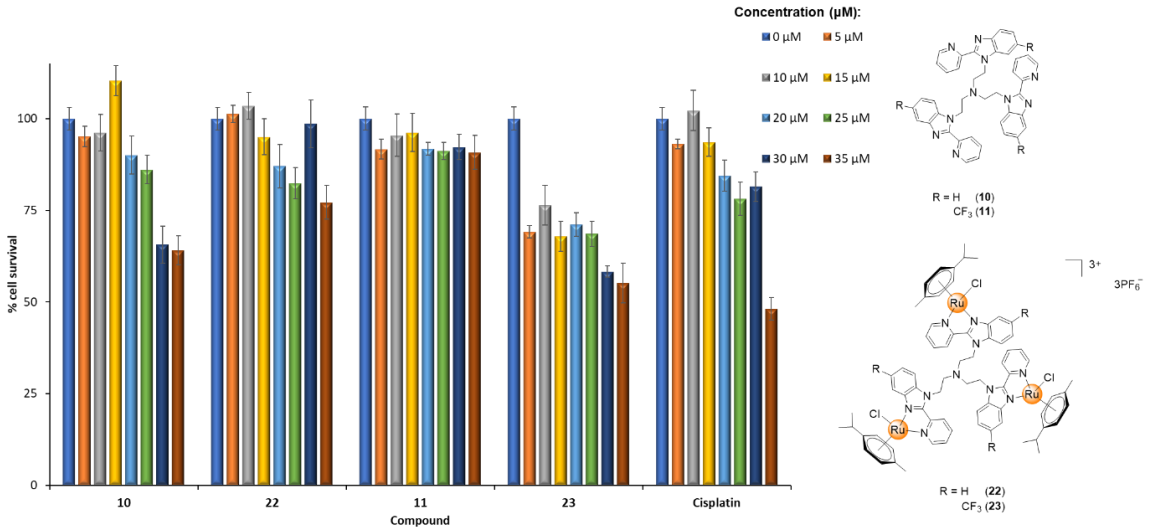

***Figure 4.14**: Percentage non-tumorigenic MCF-12A breast epithelial cell viability as measured by MTT assays following 48 hour treatment with varying concentrations of either the 2-pyridyl ligands (**10** and **11**) or the respective N^N-Ru(II) chelated complexes (**22** and **23**) or cisplatin. Vehicle (0.1% DMSO) treated cells were included as a vehicle control.*

Compared to cisplatin, the 5-unsubstituted 2-pyridyl tris-benzimidazole ligand (**10**) and its respective cationic complex (**22**) showed less cytotoxicity towards the non-tumorigenic MCF-12A breast epithelial cell line (IC_{50} = 38.72 µM and 82.42 µM for **10** and **22**, respectively, and IC_{50} = 36.32 µM for cisplatin). Importantly, the 5-trifluoromethyl substituted ligand (**11**) showed no significant reduction in MCF-12A cell viability at any of the concentrations tested and its corresponding cationic complex (**23**) was three-fold less cytotoxic towards MCF-12A cells relative to cisplatin (IC_{50} = 122.20 µM for **23** and IC_{50} = 36.32 µM for cisplatin).

The selectivity indices (S.I.) of the compounds tested (**10**, **11**, **22** and **23**) were calculated by dividing their IC_{50} in the non-tumorigenic MCF-12A breast epithelial cell line by their IC_{50} in each of the breast cancer cell lines and are summarized in Table 4.1. The S.I. is a useful indicator of the selectivity of an anticancer drug for cancer cells and the larger the S.I. value the more selectively cytotoxic a compound is towards cancer cells as opposed to the non-tumorigenic cells.

The S.I. values obtained for the 5-unsubstituted 2-pyridyl tris-benzimidazole ligand (**10**) and its respective cationic complex (**22**) in MCF-7 cells were 1.35 and 2.43, respectively, which were significantly higher than the S.I. value of 1.04 obtained for cisplatin. Thus, compounds **10** and **22** showed greater cytotoxicity and selectivity towards the MCF-7 breast cancer cells (Section 4.3.1, *vide supra*) than cisplatin. While the 5-trifluoromethyl triruthenium(II) complex **23** and cisplatin showed comparable cytotoxic activity in MCF-7 cells (Section 4.3.1, *vide supra*), complex **23** was more selective for MCF-7 breast cancer cells relative to cisplatin (S.I. = 3.49 for **23** and S.I. = 1.04 for cisplatin).

***Table 4.1**: The IC_{50} concentrations and the selectivity indices of the selected trimeric 2-pyridyl ligands (**10** and **11**) and their corresponding trinuclear cationic complexes (**22** and **23**, respectively), and the mononuclear conjugate of the most active ligand and complex.*

Compound	R-group	IC_{50} (µM) ± SD				Selectivity Indices[a, b]	
		MCF-7	MDA-MB-231	501mel	MCF-12A		
10	H	28.65 ± 1.08	33.53 ± 1.03	-	38.72 ± 1.10 ǂ	1.35[a]	1.15[b]
22 (Ru)	H	33.87 ± 1.16	N/A*	-	82.42 ± 2.29 ǂ	2.43[a]	-[b]
11	CF_3	N/A*	N/A*	N/A*	N/A*	-[a]	-[b]
23 (Ru)	CF_3	35.06 ± 1.07	N/A*	34.67 ± 1.13	122.20 ± 2.62 ǂ	3.49[a]	-[b]
18	H	N/A*	-	-	-	-	-
25 (Ru)	H	N/A*	-	-	-	-	-
Cisplatin	-	35[28]	23[44]	21.00 ± 1.05	36.32 ± 1.09	1.04[a]	1.58[b]

* N/A Not active at tested concentrations

ǂ Predicted by GraphPad Prism V5.01

[a] (IC_{50} MCF-12A/ IC_{50} MCF-7)

[b] (IC_{50} MCF-12A/ IC_{50} MDA-MB-231)

The larger S.I. values obtained for the trinuclear ruthenium(II) complexes (**22** and **23**), relative to cisplatin, suggests that these compounds may present a potent class of organometallic complexes with either enhanced or comparable activity respectively to cisplatin with minimal side effects.

4.5 Solution stability and mechanistic insights

The determination of the stability of compounds in solution, aqueous media and blood plasma is important in the identification of viable drug leads.[52] The aforementioned stability studies are usually conducted in the presence of DMSO, which is arguably one of the most widely used organic solvents in the *in vitro* biological screening of compounds. However, reports of the platinum(II)-based metallodrugs cisplatin, carboplatin and oxaliplatin reacting with DMSO have prompted the question of stability of metal complexes in DMSO.[53,54] The reaction of platinum(II) metallodrugs with DMSO is attributed to the affinity of the Pt(II) center to the nucleophilic sulfur donor atom of the DMSO molecule.[55] Additionally, the

reported significant lowering of the cytotoxicity of these platinum(II)-based drugs, upon being dissolved in DMSO, in various cell lines has stimulated interest in investigating the effects of DMSO coordination to the cytotoxic activity of organometallic complexes.[53] With this in mind, the stability of the triruthenium(II) complexes (**22** - **24**) was monitored using Ultraviolet-Visible (UV/ Vis) spectroscopy at 37 °C over 48 hours. Owing to reports of ruthenium(II) complexes undergoing rapid chloride/ aqua ligand exchanges forming aquated complexes which may form adducts with DNA,[56,57] the potential interaction of the most active complex (**22**) with guanosine 5'-monophosphate disodium salt hydrate (5'-GMP) was monitored by ^{1}H NMR spectroscopy.

4.5.1 Solvent stability

The stability of the trimetallic cationic ruthenium(II) complexes (**22** – **24**) was investigated using UV/ Vis spectroscopy at 37 °C to simulate the chemical environment prior to cell viability studies. In the obtained UV/ Vis spectra of the cationic complexes **22** – **24** (Figure 4.15 a - c), no significant changes are noted after 24 and 48 hours of incubating the compounds at 37 °C.

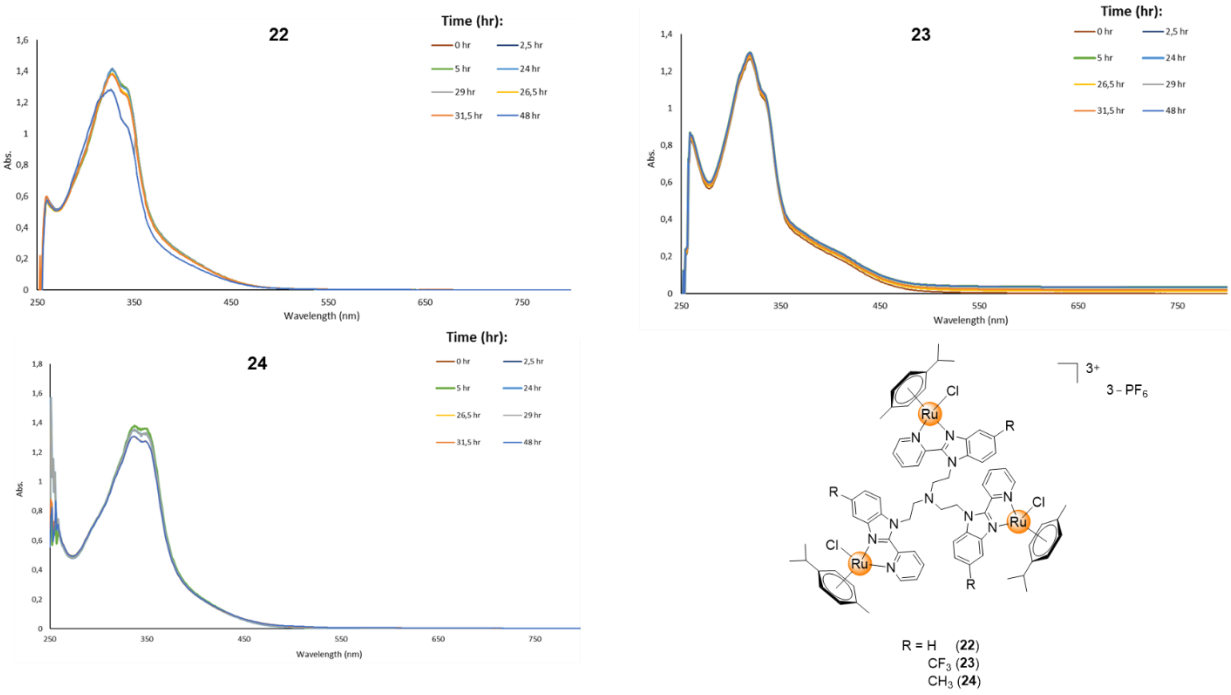

***Figure 4.15**: The UV/ Vis spectra of the trimetallic N^N-Ru(II) chelated complexes **22** (a), **23** (b) and **24** (c) over 48 hours, recorded at 37 °C.*

The results obtained in this study suggest that these ruthenium(II) complexes do not undergo solvation and further suggest that the complexes by themselves are eliciting cytotoxic effects. Additionally, the compounds remaining intact in DMSO suggest that they do not interact with DMSO, which may influence their cytotoxic activity.

4.5.2 Mechanistic insight: 5'-GMP binding

DNA is regarded as a potential target for metal complexes in the treatment of cancer, as metal complexes have been reported to form various interactions with DNA. The most widely known example of a complex that forms these metal complex-DNA interaction phenomenon is cisplatin, which has been reported to interact in a covalent manner with purine nucleotides in DNA (adenine and guanine).[58] As a result, the interaction of the most active ruthenium(II) complex (**22**) synthesized in this study was studied for its interactions with Guanosine 5'-monophosphate disodium (5'-GMP) by ^{1}H NMR spectroscopy in a 1:1 *v/v%* mixture of H_2O and DMSO (d_6) incubated at 37 °C over 24 hours. 5'-GMP is a simplistic model used to study possible nucleotide interactions.

Free 5'-GMP was studied at 37 °C in the same conditions over 24 hours and no significant changes were observed in the ^{1}H NMR spectra over 24 hours. Ruthenium complexes have been reported to bind to single-stranded DNA *via* the N-7 nitrogen of the guanosine nucleotide.[24,59] In the model used, this binding to the N-7 nitrogen atom of the 5'-GMP will be reflected by the downfield shift of the signal corresponding to H-8 from δ_H 8.0 ppm in the ^{1}H NMR spectrum of free 5'-GMP to a higher chemical shift in the ruthenium-5'-GMP adduct. This shift may be attributed to the π-backbonding of the N-7 nitrogen atom to the ruthenium(II) metal center, resulting in reduced electron density on the H-8 proton, thus causing the signal to be observed at a higher chemical shift.

Inspection of the obtained initial ^{1}H NMR spectrum of the 5'-GMP and complex **22** mixture (Figure 4.16 c) reveals resonances that correspond to signals noted for the free 5'-GMP (Figure 4.16 a) and the complex **22** (Figure 4.16 b) in an approximately 1:1 ratio. After incubation of the mixture at 37 °C for 24 hours, the obtained ^{1}H NMR spectrum (Figure 4.16 d) signals corresponding to free 5'-GMP and broadened signals corresponding to the complex **22** are observed. Additionally, it is worth noting that there was no significant shift of the H-8

signal from δ_H 8.0 ppm, thus suggesting that the ruthenium(II) metal centers of complex **22** do not interact with the N-7 nitrogen atom of 5'-GMP after 24 hours of incubation.

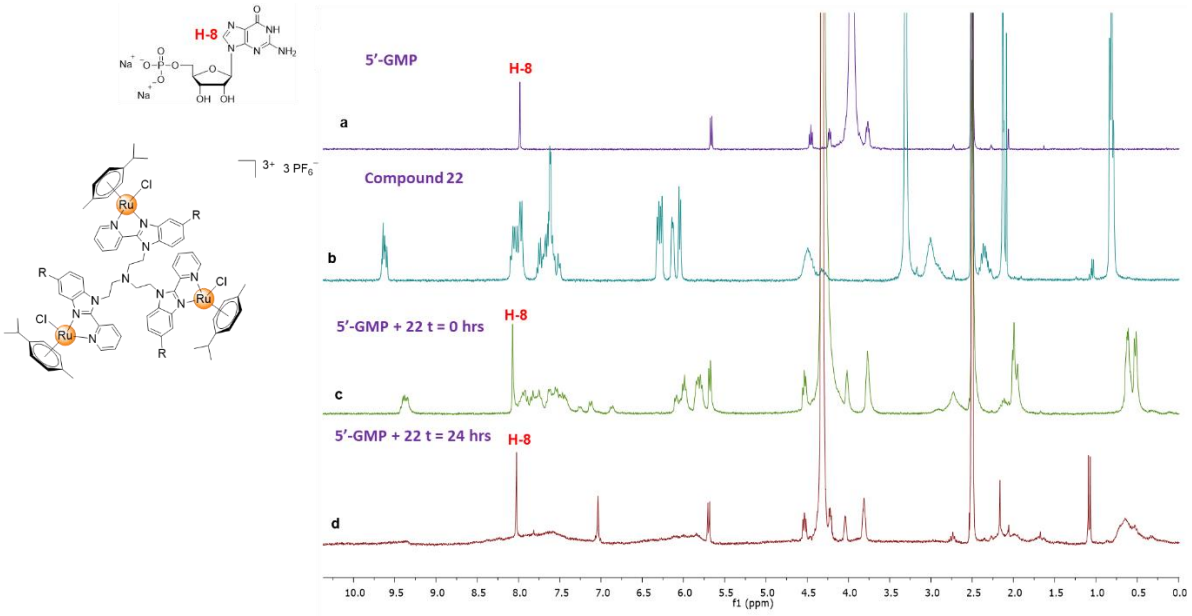

***Figure 4.16**: The stacked ^{1}H NMR spectra of 5'-GMP (a), the cationic complex **22** (b) and the mixture of **22** and 5'-GMP before incubation (c) and after incubation at 37 °C for 24 hours (d) in a mixture of H_2O: DMSO (d_6) 1:1 v/v%.*

The results obtained from this binding study suggests that DNA may not be the primary target of the complex **22**, thus suggesting that complex **22** may elicit anticancer activity *via* an alternative mechanism of action.

4.6 Summary

The cytotoxicity of the 2,5-disubstituted tris-benzimidazole ligands (**7** – **12**) and their respective cyclometallated (**19** – **21**) and cationic (**22** – **24**) triruthenium(II) complexes was investigated in pre-screen experiments against the MCF-7 breast cancer cell line at 10 and 20 µM. The 2-pyridyl ligands (**10** – **12**) showed significantly enhanced anticancer activity relative to their respective 2-phenyl counterparts (**7** – **9**) at both tested concentrations on the MCF-7 breast cancer cell line. The same trend was observed upon the comparison of the cytotoxic activity of the cationic trimetallic complexes (**22** – **24**) to that of the respective neutral cyclometallated complexes (**19** – **21**). The 2-ferrocenyl tris-benzimidazole compounds (**13** – **15**) were also pre-screened against the MCF-7 breast cancer cell line at 10 and 20 µM.

However, all the 2-ferrocenyl compounds (**13** – **15**) were not observed to significantly reduce MCF-7 cell viability. This observed inactivity was attributed to the precipitation of the 2-ferrocenyl compounds (**13** – **15**) in growth media.

The promising activity noted for the 2-pyridyl ligands (**10** – **12**) and their respective trimetallic cationic complexes (**22** – **24**) against the MCF-7 cancer cell line prompted further cytotoxic evaluation of these compounds against the MDA-MB-231 breast cancer and the 501mel cell lines. In the MCF-7 cell line, the 5-unsubstituted ligand (**10**) and the corresponding complex (**22**), were observed to show enhanced cytotoxicity relative to cisplatin, and the 5-trifluoromethyl complex (**23**) showed activity comparable to cisplatin (IC_{50} = 28.65 µM, 33.87 µM and 35.06 µM for **10**, **22** and **23**, respectively). Against the MDA-MB-231 breast cancer cell line, only the ligand **10** showed mild activity (IC_{50} = 33.53 µM). Cytotoxic data obtained for the ligand (**11**) and its respective complex (**23**), against the 501mel cell line, revealed that the complex **23** showed mild activity which is less potent relative to cisplatin. When screened against the non-tumorigenic MCF-12A breast epithelial cell line, the 2-pyridyl ligands (**11** and **12**) and their corresponding complexes (**22** and **23**) were noted to be less cytotoxic relative to cisplatin on the non-tumorigenic MCF-12A cell line.

The most active complex (**22**) was investigated for nucleotide binding as a possible mechanism of action. This was achieved by studying the interaction of **22** with 5'-GMP using ^{1}H NMR spectroscopy. The complex **22** was not observed to interact with 5'-GMP to form an adduct. Thus, suggesting that **22** elicits anticancer activity *via* an alternate mechanism, that is yet to be investigated. The possibility of the complex **22** having an alternate mechanism of action may be a contributing factor towards the enhanced selectivity, relative to cisplatin.

4.7 References

1 A. K. Gorle, A. J. Ammit, L. Wallace, F. R. Keene and J. G. Collins, *New J. Chem.*, 2014, **38**, 4049–4059.

2 J. P. C. Coverdale, T. Laroiya-McCarron and I. Romero-Canelón, *Inorganics*, 2019, **7**, 1–15.

3 A. M. Florea and D. Büsselberg, *Cancers (Basel).*, 2011, **3**, 1351–1371.

4 D. W. Shen, L. M. Pouliot, M. D. Hall and M. M. Gottesman, *Pharmacol. Rev.*, 2012, **64**, 706–721.

5 Z. Ai, Y. Lu, S. Qiu and Z. Fan, *Cancer Lett.*, 2016, **373**, 36–44.

6 L. Zeng, P. Gupta, Y. Chen, E. Wang, L. Ji, H. Chao and Z. S. Chen, *Chem. Soc. Rev.*, 2017, **46**, 5771–5804.

7 A. A. Nazarov, C. G. Hartinger and P. J. Dyson, *J. Organomet. Chem.*, 2014, **751**, 251–260.

8 R. Fernández, M. Melchart, A. Habtemariam, S. Parsons and P. J. Sadler, *Chem. Eur. J.*, 2004, **10**, 5173–5179.

9 S. Thota, D. A. Rodrigues, D. C. Crans and E. J. Barreiro, *J. Med. Chem.*, 2018, **61**, 5805–5821.

10 W. Han and P. J. Dyson, *Eur. J. Inorg. Chem.*, 2006, 4003–4018.

11 S. Chatterjee, S. Kundu, A. Bhattacharyya, C. G. Hartinger and P. J. Dyson, *J. Biol. Inorg. Chem.*, 2008, **13**, 1149–1155.

12 J. Kašpárková, O. Nováková, O. Vrána, N. Farrell and V. Brabec, *Biochemistry*, 1999, **38**, 10997–11005.

13 C. Manzotti, G. Pratesi, E. Menta, R. Di Domenico, E. Cavalletti, H. H. Fiebig, L. R. Kelland, N. Farrell, D. Polizzi, R. Supino, G. Pezzoni and F. Zunino, *Clin. Cancer Res.*,

2000, **6**, 2626–2634.

14 C. X. Zhang and S. J. Lippard, *Curr. Opin. Chem. Biol.*, 2003, **7**, 481–489.

15 D. I. Jodrell, T. R. J. Evans, W. Steward, D. Cameron, J. Prendiville, C. Aschele, C. Noberasco, M. Lind, J. Carmichael, N. Dobbs, G. Camboni, B. Gatti and F. De Braud, *Eur. J. Cancer*, 2004, **40**, 1872–1877.

16 T. A. Hensing, N. H. Hanna, H. H. Gillenwater, M. Gabriella Camboni, C. Allievi and M. A. Socinski, *Anticancer. Drugs*, 2006, **17**, 697–704.

17 H. Maeda, G. Y. Bharate and J. Daruwalla, *Eur. J. Pharm. Biopharm.*, 2009, **71**, 409–419.

18 D. F. Baban and L. W. Seymour, *Adv. Drug Deliv. Rev.*, 1998, **34**, 109–119.

19 A. K. Iyer, G. Khaled, J. Fang and H. Maeda, *Drug Discov. Today*, 2006, **11**, 812–818.

20 P. Chellan, K. M. Land, A. Shokar, A. Au, S. H. An, D. Taylor, P. J. Smith, T. Riedel, P. J. Dyson, K. Chibale and G. S. Smith, *Dalton Trans.*, 2014, **43**, 513–526.

21 B. C. E. Makhubela, M. Meyer and G. S. Smith, *J. Organomet. Chem.*, 2014, **772**–**773**, 229–241.

22 A. R. Burgoyne, C. H. Kaschula, M. I. Parker and G. S. Smith, *J. Organomet. Chem.*, 2017, **846**, 100–104.

23 I. Cassells, T. Stringer, A. T. Hutton, S. Prince and G. S. Smith, *J. Biol. Inorg. Chem.*, 2018, **23**, 763–774.

24 A. R. Burgoyne, C. H. Kaschula, M. I. Parker and G. S. Smith, *Eur. J. Inorg. Chem*, 2016, 1267–1273.

25 M. A. Rudek, C. A. Chau, W. Figg and M. H. L, Eds., *Handbook of Anticancer Pharmacokinetics and Pharmacodynamics*, Humana Press, Totowa, 2nd edn., 2014.

26 T. Mosmann, *J. Immunol. Methods*, 1983, **65**, 55–63.

27 D. F. Gilbert, in *Cell Viability Assays Methods and Protocols*, eds. D. F. Gilbert and O. Friedrich, Humana Press, New York, 2017, pp. 1–19.

28 Y. Mizumura, Y. Matsumura, T. Hamaguchi, N. Nishiyama, K. Kataoka, T. Kawaguchi, W. J. M. Hrushesky, F. Moriyasu and T. Kakizoe, *Japanese J. Cancer Res.*, 2001, **92**, 328–336.

29 G. Gupta, A. Garci, B. S. Murray, P. J. Dyson, G. Fabre, P. Trouillas, F. Giannini, J. Furrer and B. Therrien, *Dalton Trans.*, 2013, **42**, 15457–15463.

30 A. Ibao, M. Gras, B. Therrien, G. Süss-Fink, O. Zava and P. J. Dyson, *Eur. J. Inorg. Chem.*, 2012, **2**, 1531–1535.

31 P. Govender, F. Edafe, B. C. E. Makhubela, P. J. Dyson, B. Therrien and G. S. Smith, *Inorg. Chim. Acta*, 2014, **409**, 112–120.

32 M. M. Subarkhan, R. N. Prabhu, R. R. Kumar and R. Ramesh, *RSC Adv.*, 2016, **6**, 25082–25093.

33 Z. Ma, J. R. Choudhury, M. W. Wright, C. S. Day, G. Saluta, G. L. Kucera and U. Bierbach, *J. Med. Chem.*, 2008, **51**, 7574–7580.

34 A. V Klein and T. W. Hambley, *Chem. Rev.*, 2009, **109**, 4911–4920.

35 J. Mattsson, O. Zava, A. K. Renfrew, Y. Sei, K. Yamaguchi, J. Dyson and B. Therrien, *Dalton Trans.*, 2010, **39**, 8248–8255.

36 A. Singh, I. Lumb and V. Kumar, *Dalton Trans.*, 2019, **48**, 2840–2860.

37 G. Gasser and N. Metzler-Nolte, *Curr. Opin. Chem. Biol.*, 2012, **16**, 84–91.

38 D. R. Van Staveren and N. Metzler-Nolte, *Chem. Rev.*, 2004, **104**, 5931–5985.

39 G. Jaouen, A. Vessieres and S. Top, *Chem. Soc. Rev.*, 2015, **44**, 8802–8817.

40 W. A. Wlassoff, C. D. Albright, M. S. Sivashinski, A. Ivanova, J. G. Appelbaum and R. I. Salganik, *J. Pharm. Pharmacol.*, 2007, 1549–1553.

41 D. L. Holliday and V. Speirs, *Breast Cancer Res.*, 2011, **13**, 215–222.

42 J. Welsh, in *Animal Models for Studying Prevention and Treatment of Breast Cancer*, ed. M. P. Conn, Academic Press, 2013, pp. 997–1018.

43 L. K. Diaz, V. L. Cryns, W. F. Symmans and N. Sneige, *Adv. Anat. Pathol.*, 2007, **14**, 419–430.

44 A. Zaim, M. Pauzi, S. K. Yeap, N. Abu, K. L. Lim, A. R. Omar, S. A. Aziz, A. Leow, T. Chow, T. Subramani and S. G. Tan, *Chin. Med.*, 2016, 1–11.

45 W. Li and D. W. Melton, *Oncogene*, 2012, **31**, 2412–2422.

46 S. Aliwaini, A. J. Swarts, A. Blanckenberg, S. Mapolie and S. Prince, *Biochem. Pharmacol.*, 2013, **86**, 1650–1663.

47 C. Wellbrock and A. Hurlstone, *Biochem. Pharmacol.*, 2010, **80**, 561–567.

48 A. Eskandari, A. Kundu, S. Ghosh and K. Suntharalingam, *Angew. Chem. Int. Ed.*, 2019, **58**, 12059–12064.

49 D. Giffard, E. Fischer-Fodor, C. Vlad, P. Achimas-Cadariu and G. S. Smith, *Eur. J. Med. Chem.*, 2018, **157**, 773–781.

50 A. Lapasam, E. Pinder, R. M. Phillips, W. Kaminsky and M. Rao, *J. Organomet. Chem.*, 2019, **899**, 120887.

51 J. Chen, L. Lu, Y. Feng, H. Wang, L. Dai, Y. Li and P. Zhang, *Cancer Lett.*, 2011, **300**, 48–56.

52 A. Hussain, M. F. Alajmi, T. Rehman, S. Amir and R. A. Khan, *Sci. Rep.*, 2019, 1–17.

53 M. D. Hall, K. A. Telma, K. Chang, T. D. Lee, J. P. Madigan, J. R. Lloyd, I. S. Goldlust, J. D. Hoeschele and M. M. Gottesman, *Cancer Res.*, 2014, 3913–3923.

54 Y. W. Yi and I. Bae, *DNA Repair (Amst).*, 2011, **10**, 1084–1085.

55 N. Summa, W. Schiessl, R. Puchta and N. V. E. Hommes, *Inorg. Chem.*, 2006, **45**, 2499–

2510.

56 F. Aman, M. Hanif, W. A. Siddiqui, A. Ashraf, L. K. Filak, T. So, S. M. F. Jamieson and C. G. Hartinger, *Organometallics*, 2014, **33**, 5546–5553.

57 W. Vanderlinden, P. J. Kolbeck, W. Frederickx, S. F. Konrad, T. Nicolaus, C. Lampe and A. S. Urban, *Chem. Commun.*, 2019, **55**, 8764–8767.

58 A. C. Komor and J. K. Barton, *Chem. Commun.*, 2014, **49**, 3617–3630.

59 C. Scolaro, A. B. Chaplin, C. G. Hartinger, A. Bergamo, M. Cocchietto, B. K. Keppler and P. J. Dyson, *Dalton Trans.*, 2007, **2**, 5065–5072.

Chapter 5

Conclusions and Future Outlook

5.1 Overall summary and conclusions

A series of trimeric 2,5-disubstituted benzimidazole ligands (**7** – **12**) and their respective 2-ferrocenyl bioisosteres (**13** – **15**) were synthesized in this study. The respective trimetallic ruthenium(II)-*p*-cymene complexes (**19** – **24**) were successfully synthesized. All the synthesized compounds were characterized using various spectroscopic and analytical techniques including one (^{1}H, ^{13}C{^{1}H}, ^{19}F{^{1}H}, ^{31}P{^{1}H}) and two (HSQC, COSY, HMBC) dimensional NMR spectroscopy, mass spectrometry (electrospray ionization) and FT-IR spectroscopy. Additionally, the molecular structure of the 5-trifluoromethyl 2-phenyl tris-benzimidazole ligand (**10**) in the solid-state was confirmed *via* single crystal X-ray diffraction. To the best of our knowledge, most of the target compounds and synthons reported in this study are new.

The trimeric 2,5-disubstituted benzimidazole-based compounds (**9** – **15**) were prepared *via* a three-step procedure from commercially available reagents. Characterization data obtained validates the synthesis of the desired compounds (**9** – **15**). The 2,5-disubstituted ligands (**9** - **12**) were reacted with the [RuCl(μ-Cl)(*p*-cymene)]$_2$ dimer in either a *C-H* activation reaction or a bridge-splitting reaction to afford the respective trinuclear neutral *C^N*-Ru(II) complexes (**19** - **21**) and the cationic *N^N*-Ru(II) complexes (**22** – **24**). The isolated complexes were novel and were fully characterized. The obtained characterization data correlates to the proposed structures of the novel ruthenium(II) complexes (**19** – **24**).

The 2,5-disubstituted tris-benzimidazole ligands (**7** – **12**) and their respective cyclometallated (**19** – **21**) and cationic (**22** – **24**) trimetallic ruthenium(II) complexes synthesized were pre-screened for their anticancer activity at fixed concentrations of 10 and 20 µM against the MCF-7 breast cancer cell line. The pre-screen studies revealed that the 2-pyridyl ligands (**9** – **12**) and the corresponding cationic complexes (**22** – **24**) showed superior activity relative to their 2-phenyl (**7** – **9**) and cyclometallated (**19** – **21**) counterparts. This prompted the study

of the 2-pyridyl ligands (**9** – **12**) and their corresponding cationic complexes (**22** – **24**) in the MDA-MB-231 TNBC and the 501mel cancer cell lines at either 10 or 20 µM. In the MDA-MB-231 breast cancer cell line, the 5-unsubstituted ligand (**10**) was the most active, inhibiting cancer cell viability by 43% at 20 µM. In the 501mel cell line, the 5-trifluoromethyl substituted cationic complex showed activity comparable to that of cisplatin at 10 and 20 µM.

In the MCF-7 cell line, the 5-unsubstituted ligand (**10**) and the corresponding complex (**22**), showed cytotoxicity more potent than that of cisplatin (IC_{50} < 35 µM for **10** and **22,** respectively). In addition, the 5-trifluoromethyl complex (**23**) showed activity comparable to cisplatin (and $IC_{50} \approx 35$ µM for **23**). Against the MDA-MB-231 breast cancer cell line, the ligand **11** and both the cationic complexes **22** and **23**, were all inactive at the concentrations tested. Cytotoxic data obtained for the ligand (**11**) and its respective complex (**23**), in the 501mel cell line, revealed that the complex **23** showed mild activity which is less potent relative to cisplatin. The 2-pyridyl ligands (**11** and **12**) and their corresponding complexes (**22** and **23**) were screened in non-tumorigenic MCF-12A breast epithelial cells to gain insight on the selectivity of these compounds. All the compounds tested were noted to be less cytotoxic relative to cisplatin in the non-tumorigenic MCF-12A cell line and more selective for MCF-7 breast cancer cells relative to cisplatin (1.35 < S.I. < 2.43 for **11**, **12**, **23** and **24**, and S.I. = 1.04 for cisplatin).

The possible interaction of **22** with a purine nucleotide was studied as a possible mode of action. The complex **22** was not observed to interact with 5'-GMP to form an adduct. Thus, suggesting that **22** possibly does not interact with DNA and elicits anticancer activity *via* an alternate mechanism, that is yet to be investigated. The possibility of the complex **22** having an alternate mechanism of action may be a contributing factor towards the enhanced selectivity, relative to cisplatin.

5.2 Future outlook

Based on the results obtained in this study, the synthesized series of trimeric benzimidazole-based compounds show promising anticancer activity. Further mechanistic studies and structural modifications could be made to fine-tune the activity of the compounds and gain further insight into the mechanism(s) of action in which these compounds elicit anticancer activity.

5.2.1 Mechanistic studies

The cationic complex **20** was the most active ruthenium(II) complex from the series. However, preliminary mechanistic studies revealed that the complex does not interact with the guanosine nucleotide, suggesting that the complex does not target DNA. Therefore, the interaction of the complex **20** with Calf Thymus DNA could be studied *via* UV/ Vis spectroscopy to fully ascertain that **20** does not interact with DNA. Further electrochemical characterization of the complex may assist in characterizing the redox activity of the complex and this may be supplemented with the DCFDA ROS detection assay to determine whether the complex may generate ROS intracellularly. In addition, Western Blot studies may be conducted to investigate the potential protein targets that the complex may interact with. Furthermore, exploring the mechanism of cell death by flow cytometry and measuring the level of expression of pro- and anti-apoptotic molecular markers, assessing for autophagy and investigating the role of the compounds in DNA damage, could be done to understand the mechanisms in which the complex exerts anticancer effects. Evaluation of the anticancer activity of the promising complexes in this study against additional cell lines (for example A2780, WHC01 and HeLa) may give additional information about the biological profile of the complexes.

5.2.2 Structural alterations to enhance biological activity

The biological evaluation of the 2-ferrocenyl tris-benzimidazole compounds revealed that these compounds precipitate out of aqueous growth media. Thus, the aqueous solubility of these ferrocenyl bioisosteres may be improved by oxidation of the iron centers and isolation of the corresponding ferrocenium salts (Figure 5.1). These ferrocenium salts could then be investigated for their anticancer activity, as the improved aqueous solubility of the ferrocenium salt may result in improved biological activity compared to the ferrocenyl compounds.[1,2] Additionally, the variation of the counter ion of ferrocenium salts has been reported to have an effect on the anticancer activity of ferrocenium compounds.[3] Therefore, an investigation of the effects of the counterion on the anticancer activity of the proposed trimeric ferrocenium salts may be a promising avenue to explore. Additionally, the introduction of a sulfonate group to the 5-positions of the benzimidazole rings to improve solubility may be an interesting avenue to explore.

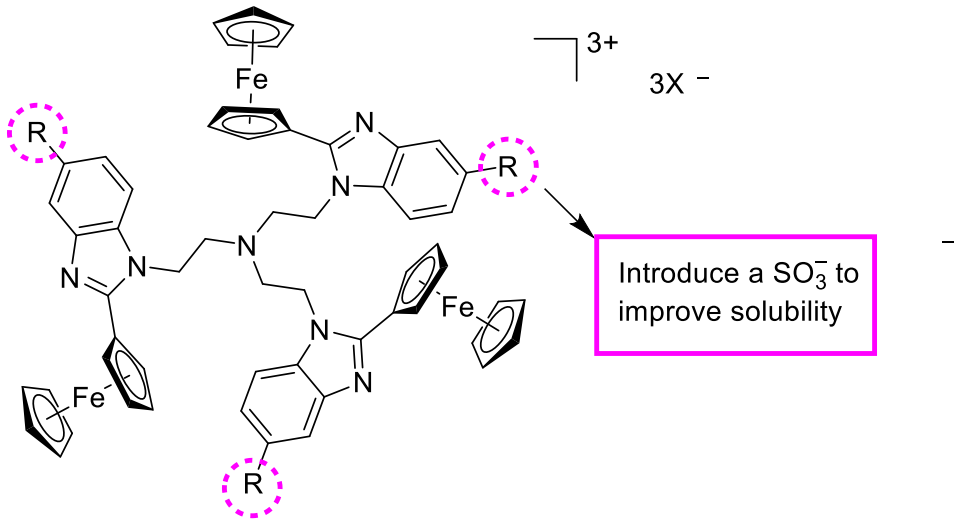

R = H, CH_3, CF_3

X^- = BF_4^-, PF_6^-

***Figure 5.1**: The proposed general structure of the ferrocenium salts.*

The project has demonstrated a great scope in the development of trinuclear ruthenium-arene complexes as biological agents. However, various modifications could be made to the

trinuclear complexes synthesized in this study to improve the cytotoxic activity and selectivity of these complexes.

Firstly, the 1,3,5-triazine core could be incorporated into the trimeric organic ligand. The 1,3,5-triazine core has been extensively studied due to its vast biological activity,[4] thus making the core an interesting anchor for the development of new trimeric complexes. The introduction of a water-soluble ligand (for example the PTA ligand) may increase the overall aqueous solubility of the complexes and thus, may enhance the anticancer activity of the complexes. In addition, replacing the chloride ligand with the iodido ligand may significantly increase the selectivity and anticancer activity of the compounds.[5] Therefore, investigating the effect of the halogen ligand on the cytotoxicity and selectivity of the complexes may yield interesting results. One most obvious alteration to the trinuclear ruthenium(II) moieties is varying the size of the arene ring. Thus, introducing the biphenyl and tetrahydroanthracene rings, which have been shown to enhance cytotoxicity relative to ruthenium complexes bearing the *p*-cymene functionality.[6] A proposed general structure that incorporates the suggested changes to the complexes is shown in Figure 5.2. Exploring the synthesis, the anticancer evaluation and gaining mechanistic insights of such complexes could provide a fruitful extension of this study for future research.

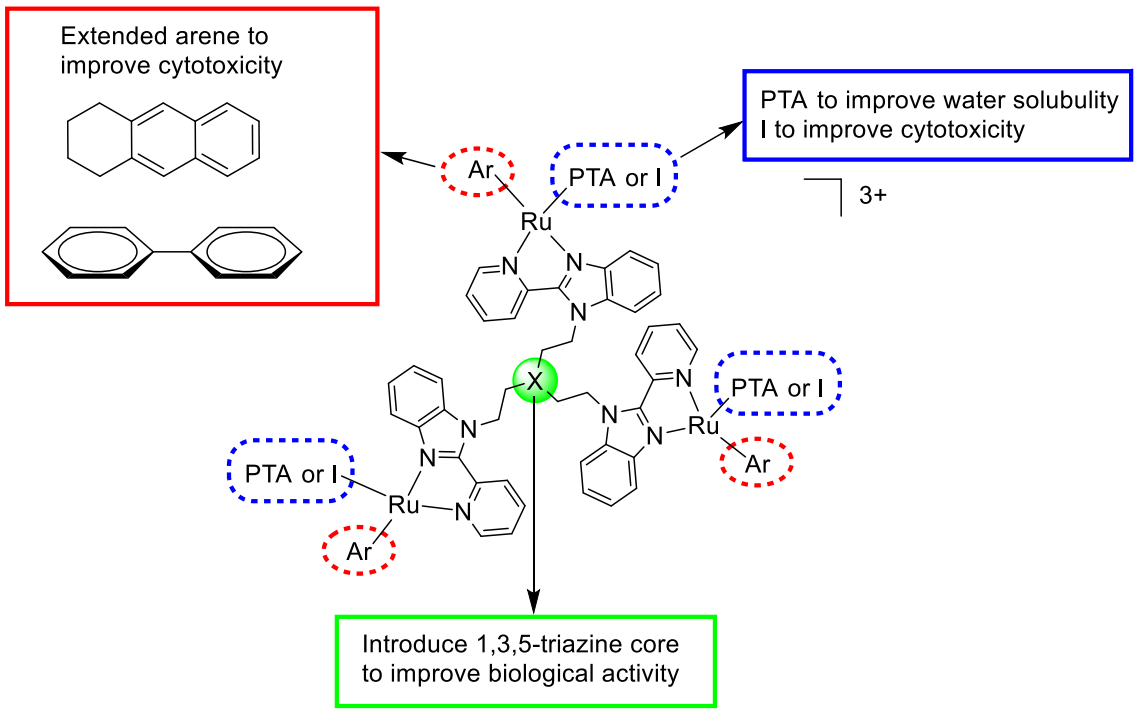

***Figure 5.2**: The proposed general structure for the alteration of the most active complex.*

5.3 References

1 P. Kopf-Maier, H. Kopf and E. W. Neuse, *Angew. Chem. Int. Ed.*, 1984, **23**, 456–457.

2 H. Tamura and M. Miwa, *Chem. Lett.*, 1997, **26**, 1177–1178.

3 G. Gasser, I. Ott and N. Metzler-Nolte, *J. Med. Chem.*, 2011, **54**, 3–25.

4 A. Carbone, A. Montalbano, S. Cascioferro, B. Parrino, V. Span, P. Barraja, P. Diana and G. Cirrincione, *Eur. J. Med. Chem.*, 2017, **142**, 523–549.

5 A. M. Pizarro, A. Habtemariam, I. Romero-canelo and P. J. Sadler, *Metallomics*, 2012, **44**, 1271–1279.

6 Y. K. Yan, M. Melchart, A. Habtemariam and P. J. Sadler, *Chem. Commun.*, 2005, 4764–4776.

Chapter 6

Experimental

6.1 General details

All reactions were carried out under an inert argon atmosphere unless stated otherwise. All reagents were purchased from commercial sources (Sigma-Aldrich or Combi-blocks) and used without further purification. The heat to reactions conducted above room temperature was supplied by a hot plate and silicone oil. All aqueous solutions were prepared using deionized water. The $[Ru(p\text{-cymene})Cl_2]_2$ dimeric precursor was prepared following a literature method.[1] Reactions were monitored by TLC using aluminium-backed Merck silica-gel F254 plates, and compounds were visualized under UV-lamp. All column chromatography was carried out using Fulka Silica Gel 60, 40 – 63 microns.

Nuclear Magnetic Resonance spectra were recorded on either a Bruker Top-spin GmbH 400 plus spectrometer (^{1}H: 399.95 MHz; ^{13}C{^{1}H}: 100.65 MHz; ^{31}P{^{1}H}: 162.01 MHz; ^{19}F{^{1}H}: 376.58 MHz) or a Varian Mercury 300 spectrometer (^{1}H: 300.08 MHz; ^{13}C{^{1}H}: 75.46 MHz; ^{31}P{^{1}H}: 121.47 MHz), with a Brucker Biospin GmbH casing and sample injector at 30 °C. Chemical shifts were reported using tetramethylsilane (TMS) as the internal standard. Chemical shifts and *J*-coupling values were reported in ppm and Hz, respectively. Infrared (IR) spectroscopy was conducted on a Perkin-Elmer Spectrum 100 FT-IR spectrometer using Attenuated Total Reflectance (ATR) in the solid-state, with bond vibrations measured in reciprocal centimetres (cm^{-1}). Mass Spectrometry (MS) determinations were carried out using Electron Impact (EI) on a JEOL GCmatell instrument or Electrospray Ionisation (ESI) on a Waters API Quattro Micro triple quadrupole mass spectrometer with data recorded using the positive mode. A Büchi Melting Point Apparatus B-540 machine was used to obtain the uncorrected melting points of each compound. The purity of the ligands was determined using an analytical Agilent HPLC 1260 with an Agilent infinity diode array detector (DAD) 1260 UV/ Vis detector which was set to wavelengths ranging from 210 – 640 nm. Two solvent mixtures were used to elute the

compounds, Solvent A (10 mM NH_4OAc/ H_2O) and Solvent B (10 mM NH_4OAc/ MeOH), at a flow rate of 0.9 mL/min. The set gradients were as follows: 90% Solvent A from 0 – 1 min, 90 – 5% Solvent A from 1 – 3 min and 5% Solvent B between 3 and 5 min. Determination of C/ H/ N was done using a 2400 CHN Elemental Analyzer by Perkin Elmer.

6.2 The general procedure for the synthesis of the tris-nitrobenzenes (1 – 3)

Tris(2-aminoethyl)amine (1 eq.) was dissolved in DMF (5 mL) at room temperature. Thereafter, the appropriate nitrobenzene (3 eq.) was added to the reaction vessel and the reaction was allowed to stir at room temperature for 24 hours, reaction progress was monitored by TLC analysis. Upon completion, the reaction mixture was diluted with a saturated brine solution (30 mL) and then extracted with two aliquots of ethyl acetate (2 x 30 mL). The organic extracts were collected and dried over anhydrous sodium sulfate, and excess solvent was reduced *in vacuo*. The resultant crude was purified using column chromatography to afford the desired tris-nitrobenzene product.

*6.2.1 The synthesis of N^1-(2-nitrophenyl)-N^2,N^2-bis(2-((2nitrophenyl)amino)ethyl)ethane-1,2-diamine[2] (**1**)*

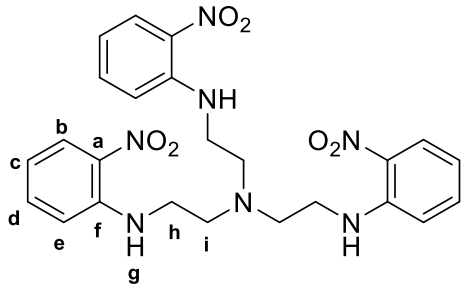

Tris(2-aminoethyl)amine (0.500 mL, 3.34 mmol) was reacted with 1-fluoro-2-nitrobenzene (1.06 mL, 10.1 mmol) at room temperature for 24 hours. The desired compound (**1**) was isolated as a bright yellow solid (1.11 g, 2.18 mmol). **R_f (4:6 EtOAc: Pet. Ether):** 0.50. **Yield:** 48.3%. **^{1}H NMR (300 MHz, DMSO) δ (ppm)**: 8.21 (t, *J* = 5.1 Hz, 3H, H-g), 8.00 (dd, *J* = 8.6, 1.6 Hz, 3H, H-b), 7.46 (ddd, *J* = 8.5, 7.0, 1.4 Hz, 3H, H-d), 6.98 (d, *J* = 8.0 Hz, 3H, H-e), 6.64 (ddd, *J* = 8.3, 6.9, 1.1 Hz, 3H, H-c), 3.45 (q, *J* = 6.1 Hz, 6H, H-h), 2.90 (t, *J* = 6.3 Hz, 6H, H-i). **^{13}C{^{1}H}-NMR (101 MHz, DMSO)** δ (ppm): 145.50 (C-f), 136.87 (C-b), 131.53 (C-a), 126.64 (C-d), 115.55 (C-c), 114.85 (C-e), 52.93 (C-h), 41.19 (C-i). **MP** (°C): 103.8 – 105.3.

*6.2.2 Synthesis of N^1-(2-nitro-4-(trifluoromethyl)phenyl)-N^2,N^2-bis(2-((2-nitro-4-(trifluoromethyl)phenyl)amino)ethyl)ethane-1,2-diamine (**2**)*

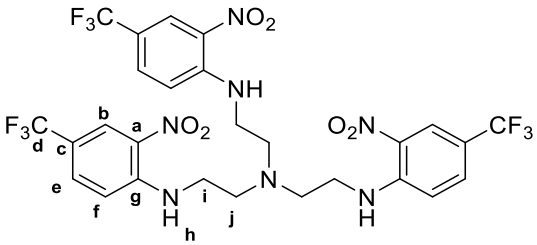

Tris(2-aminoethyl)amine (0.500 mL, 3.34 mmol) and 4-chloro-3-nitrobenzotrifluoride (1.49 mL, 10.0 mmol) were dissolved in DMF and allowed to stir at room temperature for 24 hours. The pure compound (**2**) was isolated as a bright yellow solid (0.841 g, 1.18 mmol). **R_f (2:1 Pet. Ether: EtOAc):** 0.56. **Yield:** 35.3%. **^{1}H NMR (300 MHz, DMSO) δ (ppm)**: 8.45 (t, *J* = 5.0 Hz, 3H, H-h), 8.15 (d, *J* = s1.6 Hz, 3H, H-b), 7.66 (dd, *J* = 9.1, 2.1 Hz, 3H, H-e), 7.15 (d, *J* = 9.1 Hz, 3H, H-f), 3.49 (dd, *J* = 11.0, 5.5 Hz, 6H, H-i), 2.92 (t, *J* = 5.9 Hz, 6H, H-j). **^{13}C{^{1}H}-NMR (101 MHz, DMSO) δ (ppm):** 146.49 (C-g), 131.53 (C-f), 129.96 (C-a), 124.97 (C-d), 123.68 (C-b), 115.60 (C-e), 114.70 (C-d), 52.17 (C-j), 40.80 (C-i). **MP** (°C): 170.6 – 172.1.

*6.2.3 The synthesis of N^1-(4-methyl-2-nitrophenyl)-N^2,N^2-bis(2-((4-methyl-2-nitrophenyl)amino)ethyl)ethane-1,2-diamine (**3**)*

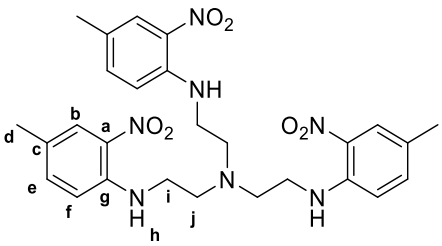

Tris(2-aminoethyl)amine (0.500 mL, 3.34 mmol) and 4-fluoro-2-nitrotoluene (1.55 g, 10.0 mmol) were dissolved in DMF and allowed to stir at room temperature for 24 hours. The pure compound (**3**) was isolated as a dark orange solid (0.887 g, 1.62 mmol). **R_f (4:1 Pet. Ether: EtOAc):** 0.51. **Yield:** 39.2%.**^{1}H NMR (300 MHz, DMSO) δ (ppm)**: 8.08 (t, *J* = 5.0 Hz, 3H, H-h), 7.79 (d, *J* = 1.0 Hz, 3H, H-b), 7.29 (dd, *J* = 8.8, 1.9 Hz, 3H, H-e), 6.89 (d, *J* = 8.8 Hz, 3H, H-f), 3.41 (dd, *J* = 11.5, 5.9 Hz, 6H, H-i), 2.87 (t, *J* = 6.2 Hz, 6H, H-j), 2.20 (s, 9H, H-d). **^{13}C{^{1}H}-NMR (101 MHz, DMSO) δ (ppm)**: 143.33 (C-a), 137.76 (C-e), 130.53 (C-g),

125.07 (C-b), 124.02 (C-c), 114.39 (C-f), 52.47 (C-j), 40.70 (C-i), 19.36 (C-d). **MP** (°C): 125.6 - 127.3.

6.3 The synthesis of the tris-1,2-benzenediamines (4 – 6)

The appropriate tris-nitrobenzene (1 eq.) was dissolved in dry methanol (10 mL) and allowed to stir for 5 minutes. Ammonium chloride (30 eq.) and zinc (60 eq.) were added to the reaction vessel. The reaction mixture was then stirred vigorously at room temperature for 1 hour. After 1 hour, TLC analysis showed the complete conversion of the starting materials to a new product. The reaction mixture was filtered through Celite® and rinsed with copious methanol. The filtrate was subsequently collected, and the excess solvent was reduced by rotary evaporation. The resultant residue was redissolved in ethyl acetate (30 mL) and washed with two aliquots of a saturated sodium bicarbonate solution (2 x 30 mL), a 1M solution of sodium hydroxide (30 mL) and deionized water (30 mL). The organic extracts were collected, dried over anhydrous sodium sulfate and excess solvent was reduced under reduced pressure. The resultant crude was purified using column chromatography (100% ethyl acetate).

*6.3.1 Synthesis of N^1-(2-(bis(2-((2-aminophenyl)amino)ethyl)amino)ethyl)benzene-1,2-diamine^2 (**4**)*

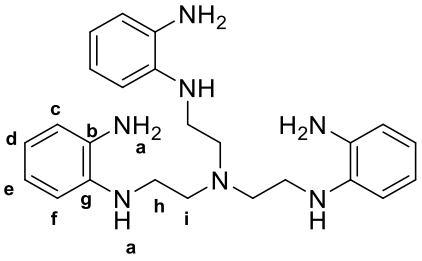

N^1-(2-nitrophenyl)-N^2,N^2-bis(2-((2nitrophenyl)amino)ethyl)ethane-1,2-diamine (0.810 g, 1.59 mmol) was reacted with ammonium chloride (2.52 g, 47.0 mmol) and zinc powder (6.16 g, 94.2 mmol) at room temperature for 24 hours. The desired product (**4**) was isolated as a dark brown solid (0.778 g, 1.86 mmol). **R_f (EtOAc):** 0.45. **Yield**: 97.0%. **^{1}H NMR (300 MHz, DMSO) δ (ppm)**: 6.57 (dd, $^3J_{HH}$ = 7.2 Hz, $^4J_{HH}$ = 1.5 Hz, 3H, H-d), 6.53 – 6.38 (m, 9H, H-c, H-e and H-f), 4.38 (s, 9H, H-a), 3.13 (dd, $^3J_{HH}$ = 4.7 Hz, $^4J_{HH}$ =11.8 Hz, 6H, H-h), 2.79 (t, $^3J_{HH}$ = 6.6 Hz, 6H, H-i). **^{13}C{^{1}H}-NMR (101 MHz, DMSO) δ (ppm)**: 136.77 (C-g), 135.75 (C-b), 118.42 (C-e),

117.48 (C-d), 114.98 (C-f), 110.67 (C-c), 53.61 (C-i), 42.18 (C-h). **FT-IR** (ATR) *v* (cm^{-1}): 3366 and 3299 (1° amine). **MP** (°C): 121.7 – 123.8.

*6.3.2 The synthesis of N^1-(2-(bis(2-((2-amino-4-(trifluoromethyl)phenyl)amino)ethyl)amino)ethyl)-4-(trifluoromethyl)benzene-1,2-diamine (**5**)*

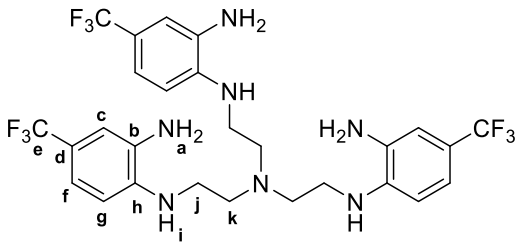

N^1-(2-nitro-4-(trifluoromethyl)phenyl)-N^2,N^2-bis(2-((2-nitro-4-(trifluoromethyl)phenyl)amino)ethyl)ethane-1,2-diamine (0.603 g, 0.842 mmol), ammonium chloride (1.35 g, 25.2 mmol) and zinc powder (3.32 g, 50.8 mmol) were reacted in anhydrous methanol at room temperature for 1 hour. The product (**5**) was isolated as a beige solid (0.660 g, 0.706 mmol). **R_f (1:1 EtOAc: Pet. Ether):** 0.97. **Yield:** 83.8%. **^{1}H NMR (300 MHz, DMSO) δ (ppm):** 6.83 (d, $^3J_{HH}$ = 2.0 Hz, 3H, H-c), 6.74 (d, $^3J_{HH}$ = 8.3 Hz, 3H, H-g), 6.45 (d, $^3J_{HH}$ = 8.2 Hz, 3H, H-f), 5.02 (t, $^3J_{HH}$ = 5.2 Hz, 3H, H-i), 4.84 (s, 6H, H-a), 3.19 (dd, $^3J_{HH}$ = 11.9 Hz, $^4J_{HH}$ = 6.0 Hz, 6H, H-j), 2.78 (t, $^3J_{HH}$ = 6.6 Hz, 6H, H-k). **^{13}C{^{1}H}-NMR (101 MHz, DMSO) δ (ppm)**: 139.03 (C-h), 135.08 (C-b), 124.07 (C-d), 116.46 (q, *J* = 31.0 Hz, C-e), 114.70 (C-g), 109.69 (C-c), 108.28 (C-f), 52.63 (C-j), 41.35 (C-k). **FT-IR** (ATR) *v* (cm^{-1}): 3342 and 3306 (1° amine). **MP** (°C): 183.9 – 185.6.

*6.3.3 Synthesis of N^1-(2-(bis(2-((2-amino-4-methylphenyl)amino)ethyl)amino)ethyl)-4-methylbenzene-1,2-diamine (**6**)*

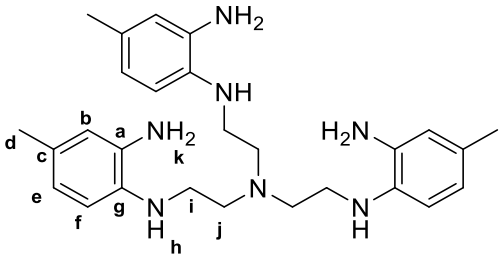

N^1-(4-methyl-2-nitrophenyl)-N^2,N^2-bis(2-((4-methyl-2-nitrophenyl)amino)ethyl)ethane-1,2-diamine (1.11 g, 2.01 mmol) was reacted with ammonium chloride (3.17 g, 59.3 mmol) and zinc powder (6.76 g, 103 mmol) in anhydrous methanol for 1 hour. The desired product (**6**) was isolated as a brown solid (0.668 g, 1.45 mmol). **R_f (EtOAc):** 0.14. **Yield**: 75.1%. **^{1}H NMR (300 MHz, DMSO) δ (ppm)**: 6.40 (d, $^3J_{HH}$ = 1.1 Hz, 3H, H-b), 6.32 (m, 6H, H-e, H-f), 4.32 (s, 6H, H-k), 4.25 (t, $^3J_{HH}$ = 5,0 Hz, 3H, H-h), 3.07 (d, $^3J_{HH}$ = 4.8 Hz, 6H, H-i), 2.74 (t, $^3J_{HH}$ = 6.4 Hz, 6H, H-j), 2.08 (s, 9H, H-d). **^{13}C{^{1}H}-NMR (101 MHz, DMSO) δ (ppm)**: 135.96 (C-g), 134.42 (C-a), 125.99 (C-c), 118.60 (C-e), 115.90 (C-f), 111.12 (C-b), 53.70 (C-i), 42.47 (C-j), 20.91 (C-d). **FT-IR** (ATR) *v* (cm^{-1}): 3373 and 3318 (1° amine). **MP** (°C): 128.3 – 130.2.

6.4 The general synthetic procedure for the 2,5-disubstituted benzimidazole-based trimeric ligands (7 – 12)

The appropriate tris-1,2-benzenediamine (1 eq.) was dissolved in anhydrous ethanol (6 mL), and allowed to stir for 5 minutes. Benzaldehyde or 2-pyridinecarboxaldehyde (3.6 eq.) was added to the reaction vessel. Thereafter, magnesium sulfate (18 eq.) and trifluoroacetic acid (0.3 eq.) were added to the reaction vessel. The reaction mixtures with benzaldehyde were refluxed at 80 °C for 24 hours and the reactions with 2-pyridinecarboxaldehyde were stirred at room temperature for 24 hours, open to air. TLC analysis confirmed the successful conversion of starting materials to a new product. The reaction mixture was subsequently filtered and the filtrate was collected, and excess solvent was removed by rotary evaporation. The resultant crude was redissolved in ethyl acetate (30 mL) and washed with a saturated sodium bicarbonate solution (30 mL) and a saturated brine solution (30 mL). The organic

extract was collected and dried over anhydrous sodium sulfate, and the excess solvent was removed *in vacuo.* The resultant residue was purified using column chromatography.

*6.4.1 Synthesis of tris(2-(2-phenyl-1H-benzo[d]imidazol-1-yl)ethyl)amine (**7**)*

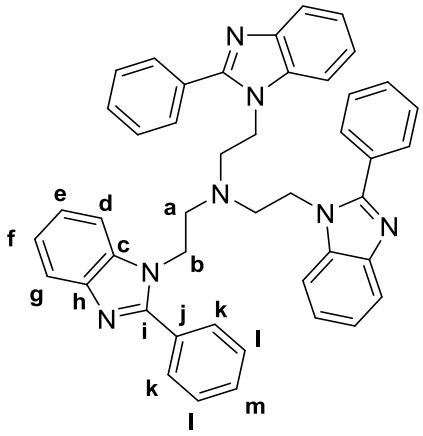

N[1]-(2-(bis(2-((2-aminophenyl)amino)ethyl)amino)ethyl)benzene-1,2-diamine (0.113 g, 0.246 mmol) was dissolved in ethanol. Benzaldehyde (0.0876 mL, 0.859 mmol), TFA (0.00547 mL, 0.0715 mmol) and magnesium sulfate (0.523 g, 4.83 mmol) were added to the reaction vessel. The desired product was isolated as a pale yellow solid (**7**) (0.0740g, 0.109 mmol). **R_f (7:3 EtOAc: Pet. Ether)**: 0.21. **Yield**: 51.1%. **^{1}H NMR (400 MHz, DMSO) δ (ppm)**: 7.68 – 7.62 (m, 3H, H-e), 7.59 – 7.53 (m, 6H, H-k), 7.48 – 7.40 (m, 9H, H-l and H-m), 7.29 – 7.22 (m, 6H, H-d and H-g), 7.20 – 7.15 (m, 3H, H-f), 3.79 (t, $^3J_{HH}$ = 7.1 Hz, 6H, H-a), 2.41 (t, $^3J_{HH}$ = 7.1 Hz, 6H, H-b). **^{13}C{^{1}H}-NMR (101 MHz, DMSO) δ (ppm):** 153.59 (C-i), 143.01 (C-h), 135.71 (C-c), 130.81 (C-m), 130.08 (C-i), 129.43 (C-l), 129.13 (C-k), 123.00 (C-f), 122.52 (C-e), 119.70 (C-g), 110.91 (C-d), 52.91 (C-a), 42.75 (C-b). **FT-IR** (ATR) *v* (cm^{-1}): 1695 (imine C=N). **MP** (°C): 193.6 – 196.2. **Purity**: 98% by LC (t_R: 2.823 min).

*6.4.2 Synthesis of tris(2-(2-phenyl-5-(trifluoromethyl)-1H-benzo[d]imidazol-1-yl)ethyl)amine (**8**)*

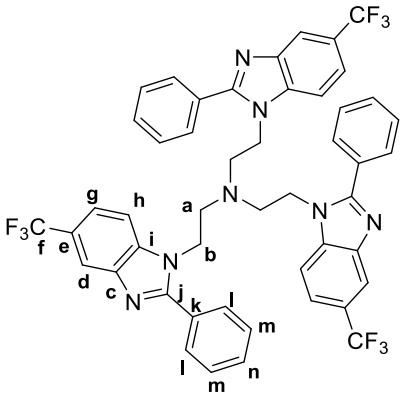

N[1]-(2-(bis(2-((2-amino-4-(trifluoromethyl)phenyl)amino)ethyl)amino)ethyl)-4-(trifluoromethyl)benzene-1,2-diamine (0.106 g, 0.165 mmol) was dissolved in ethanol. Benzaldehyde (0.0631 mL, 0.598 mmol), TFA (0.00371 mL, 0.0481 mmol) and magnesium sulfate (0.348 g, 2.88 mmol) were subsequently added to the reaction vessel. The pure product (**8**) was isolated as a cream solid (0.0952 g, 0.108 mmol). **R_f (1:1 EtOAc: Pet. Ether)**: 0.18. **Yield:** 70.3%. **^{1}H NMR (300 MHz, DMSO) δ (ppm):** 8.01 (s, 3H, H-d), 7.61 – 7.54 (m, 6H, H-g, H-h), 7.52 (dd, $^3J_{HH}$ = 8.7 Hz, $^4J_{HH}$ = 1.4 Hz, 3H, H-n), 7.48 – 7.39 (m, 12H, H-l, H-m), 3.88 (t, $^3J_{HH}$ = 6.6 Hz, 6H, H-a), 2.36 (t, *J* = 6.6 Hz, 6H, H-b). **^{13}C{^{1}H}-NMR (101 MHz, DMSO) δ (ppm)**: 155.87 (C-j), 142.41 (C-i), 138.00 (C-c), 130.51 (C-k), 130.11 (C-n), 129.49 (C-m), 129.21 (C-l), 126.78 (C-e), 123.55 (q, *J* = 35.9 Hz, C-f), 119.47 (C-g), 117.06 (C-d), 112.01 (C-h), 52.43 (C-b), 42.88 (C-a). **^{19}F{^{1}H}-NMR (377 MHz, DMSO) δ (ppm)**: -58.94 (d, J_{F-C} = 23.3 Hz). **FT-IR** (ATR) *v* (cm^{-1}): 1626 (imine C=N). **MP** (°C): 204.4 – 205.1. **Purity**: 94% by LC (t_R: 2.880 min).

*6.4.3 Synthesis of tris(2-(5-methyl-2-phenyl-1H-benzo[d]imidazol-1-yl)ethyl)amine (**9**)*

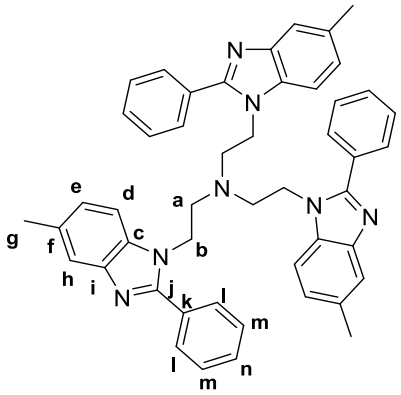

N[1]-(2-(bis(2-((2-amino-4-methylphenyl)amino)ethyl)amino)ethyl)-4-methylbenzene-1,2-diamine (0.0968 g, 0.198 mmol) was dissolve in ethanol. Thereafter, benzaldehyde (0.0796 mL, 0.780 mmol), TFA (0.00500 mL, 0.0650 mmol) and magnesium sulfate (0.469 g, 3.91 mmol) were added to the reaction vessel. The desired product was isolated as a white solid (**9**) (0.0723 g, 0.100 mmol). **R_f (1:1 Pet. Ether: EtOAc)**: 0.12. **Yield:** 46.4%. **^{1}H NMR (300 MHz, $CDCl_3$) δ (ppm):** 7.58 (s, 3H, H-h), 7.55 – 7.48 (m, 6H, H-l), 7.44 – 7.35 (m, 9H, H-m, H-n), 7.07 (dd, $^3J_{HH}$ = 8.2 Hz, $^4J_{HH}$ = 1.1 Hz, 3H, H-d), 6.78 (d, $^3J_{HH}$ = 8.2 Hz, 3H, H-e), 3.69 (t, $^3J_{HH}$ = 7.0 Hz, 6H, H-a), 2.50 (s, 9H, H-g), 2.37 (t, $^3J_{HH}$ = 7.0 Hz, 6H, H-b). **^{13}C{^{1}H}-NMR (101 MHz, $CDCl_3$) δ (ppm)**: 153.41 (C-j), 143.07 (C-i), 133.17 (C-f), 132.53 (C-c), 130.37 (C-k), 129.92 (C-m), 129.07 (C-n), 128.83 (C-l), 124.55 (C-d), 119.94 (C-h), 109.07 (C-e), 53.43 (C-b), 42.78 (C-a), 21.56 (C-g). **FT-IR** (ATR) *v* (cm^{-1}): 1625 (imine C=N). **MP** (°C): 197.6 – 199.8. **Purity**: 97% by LC (t_R: 2.703 min).

*6.4.4 Synthesis of tris(2-(2-(pyridin-2-yl)-1H-benzo[d]imidazol-1-yl)ethyl)amine (**10**)*

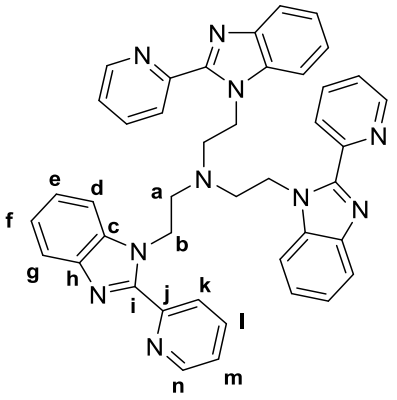

N[1]-(2-(bis(2-((2-aminophenyl)amino)ethyl)amino)ethyl)benzene-1,2-diamine (0.103 g, 0.238 mmol) was dissolved in ethanol. Thereafter, 2-pyridinecarboxaldehyde (0.0817 mL, 0.859 mmol), TFA (0.00547 mL, 0.0715 mmol) and magnesium sulfate (0.517 g, 4.29 mmol) were added to the reaction vessel. The desired product (**10**) was isolated as a pale brown solid (0.0300g, 0.0441 mmol). **R_f (7:3 EtOAc: Pet. Ether)**: 0.22. **Yield:** 34.8%. **^{1}H NMR (300 MHz, DMSO) δ (ppm)**: 8.30 (m, 6H, H-n and H-m), 7.92 (td, $^3J_{HH}$ = 7.8 Hz, $^4J_{HH}$ = 1.5 Hz, 3H, H-l), 7.76 – 7.69 (m, 3H, H-e),7.41 – 7.23 (m, 12H, H-k, H-d, H-f and H-g), 4.60 (t, $^3J_{HH}$ = 6.8 Hz, 6H, H-a), 2.97 (t, $^3J_{HH}$ = 6.9 Hz, 6H, H-b). **^{13}C{^{1}H}-NMR (101 MHz, DMSO) δ (ppm):** 149.81 (C-j), 149.37 (C-n), 148.39 (C-h), 142.04 (C-i), 137.26 (C-l), 136.22 (C-c), 124.17 (C-k), 124.02 (C-m), 123.13 (C-f), 122.32 (C-g), 119.53 (C-e), 110.42 (C-d), 53.64 (C-a), 43.38 (C-b). **FT-IR** (ATR) *v* (cm^{-1}): 1733 (imine C=N), 1586 (pyridyl C=N). **MP** (°C): 183.5 – 184.9. **Purity**: 99% by LC (t_R: 2.816 min).

*6.4.5 Synthesis of tris(2-(2-(pyridin-2-yl)-5-(trifluoromethyl)-1H-benzo[d]imidazol-1-yl)ethyl)amine (**11**)*

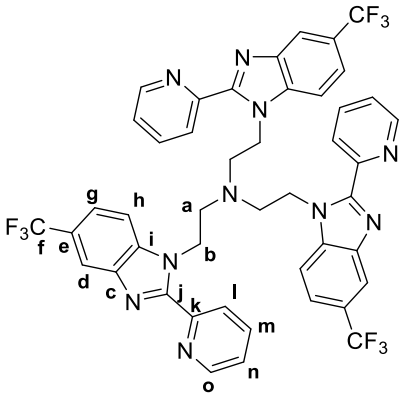

N[1]-(2-(bis(2-((2-amino-4-(trifluoromethyl)phenyl)amino)ethyl)amino)ethyl)-4-(trifluoromethyl)benzene-1,2-diamine (0.107 g, 0.169 mmol) was dissolved in ethanol. Thereafter, 2-pyridinecarboxaldehyde (0.0550 mL, 0.578 mmol), TFA (0.00371 mL, 0.0481 mmol) and magnesium sulfate (0.351 g, 2.93 mmol) were added to the reaction vessel. The desired product was isolated as a white solid (**11**) (0.0203 g, 0.0229 mmol). **R_f (2:1 Pet. Ether: EtOAc)**: 0.13. **Yield:** 40.3%. **^{1}H NMR (300 MHz, DMSO) δ (ppm)**: 8.35 (d, *J* = 4.2 Hz, 3H, H-o), 8.29 (d, $^3J_{HH}$ = 7.9 Hz, 3H, H-n), 8.10 (s, 3H, H-d), 7.95 (t, $^3J_{HH}$ = 7.4 Hz, 3H, H-l), 7.66 – 7.53 (m, 6H, H-g, H-h), 7.42 – 7.33 (m, 3H, H-m), 4.65 (t, $^3J_{HH}$ = 6.5 Hz, 6H, H-a), 3.03 (t, $^3J_{HH}$ = 6.3 Hz, 6H, H-b). **^{13}C{^{1}H}-NMR (151 MHz, DMSO) δ (ppm)**: 152.29 (C-k), 149.76 (C-j), 149.06 (C-o), 142.03 (C-c), 139.03 (C-i), 137.96 (C-e), 125.12 (C-f), 125.06 (C-n), 120.03 (C-g), 117.48 (C-h), 112.14 (C-d), 53.86 (C-b), 44.28 (C-a). **^{19}F{^{1}H}-NMR (377 MHz, DMSO) δ (ppm)**: -59.19 (s). **FT-IR** (ATR) *v* (cm^{-1}): 1620 (imine C=N), 1587 (pyridyl C=N). **MP** (°C): 201.3 – 202. **Purity**: 94% by LC (t_R: 3.038 min).

*6.4.6 Synthesis of tris(2-(5-methyl-2-(pyridin-2-yl)-1H-benzo[d]imidazol-1-yl)ethyl)amine (**12**)*

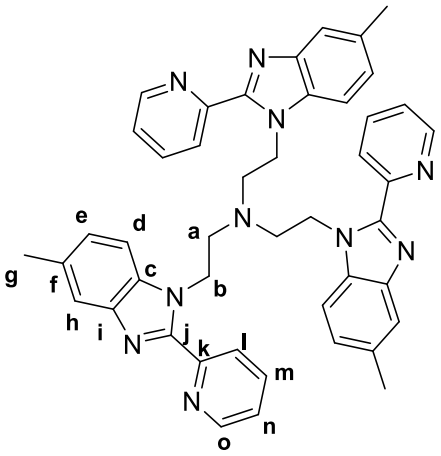

N^{1}-(2-(bis(2-((2-amino-4-methylphenyl)amino)ethyl)amino)ethyl)-4-methylbenzene-1,2-diamine (0.102 g, 0.217 mmol) was dissolve in ethanol. Thereafter, 2-pyridinecarboxaldehyde (0.0741 mL, 0.781 mmol), TFA (0.00500 mL, 0.0650 mmol) and magnesium sulfate (0.471 g, 4.01 mmol) were added to the reaction vessel. The desired product was isolated as a cream solid (**12**) (0.0530 g, 0.0733 mmol). **R_f (7:3 EtOAc: Pet. Ether)**: 0.27. **Yield:** 33.8%. **^{1}H NMR (400 MHz, $CDCl_3$) δ (ppm)**: 8.41 (d, $^{3}J_{HH}$ = 8.0 Hz, 3H, H-o), 8.30 (d, $^{3}J_{HH}$ = 4.5 Hz, 3H, H-l), 7.77 (td, $^{3}J_{HH}$ = 7.8 Hz, $^{4}J_{HH}$ = 1.8 Hz, 3H, H-m), 7.63 (s, 3H, H-h), 7.22 – 7.06 (m, 9H, H-d, H-e, H-n), 4.81 – 4.74 (m, 6H, H-a), 3.27 – 3.14 (m, 6H, H-b), 2.51 (s, 9H, H-g). **^{13}C{^{1}H}-NMR (101 MHz, $CDCl_3$) δ (ppm)**: 150.50 (C-j), 149.65 (C-k), 148.52 (C-o), 142.86 (C-i), 136.77 (C-m), 134.75 (C-f), 132.54 (C-c), 125.17 (C-e), 124.57 (C-d), 123.62 (C-l), 119.91 (C-h), 109.43 (C-n), 54.66 (C-b), 44.38 (C-a), 21.60 (C-g). **FT-IR** (ATR) *v* (cm^{-1}): 1726 (imine C=N), 1590 (pyridyl C=N). **MP** (°C):170.1 – 173.5. **Purity**: 99% by LC (t_R: 2.969 min).

6.5 The general synthesis of the 2-ferrocenyl tris-benzimidazole compounds (13 – 15)

The appropriate tris-1,2-benzenediamine (1 eq.) was dissolved in dry ethanol (6 mL), and allowed to stir for 5 minutes. Ferrocenecarboxaldehyde (3.6 eq.) was added to the reaction vessel. Thereafter, magnesium sulfate (18 eq.) and trifluoroacetic acid (0.3 eq.) were added to the reaction vessel. The reaction mixture was stirred at room temperature for 24 hours, open to air. Upon confirmation of reaction completion by TLC, the reaction mixture was subsequently filtered and the filtrate collected. The excess solvent was removed by rotary evaporation, and the resultant crude was redissolved in ethyl acetate (30 mL) and washed with a saturated sodium bicarbonate solution (30 mL) and a saturated brine solution (30 mL). The organic extracts were collected and dried over anhydrous sodium sulfate, and the excess solvent was removed under vacuum. The resultant residue was purified using column chromatography.

*6.5.1 The synthesis of tris(2-(2-ferrocenyl-1H-benzo[d]imidazol-1-yl)ethyl)amine (**13**)*

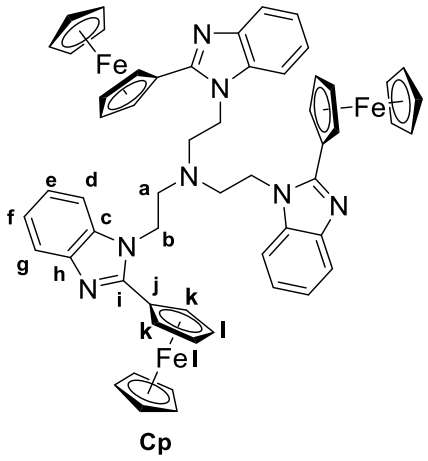

N[1]-(2-(bis(2-((2-aminophenyl)amino)ethyl)amino)ethyl)benzene-1,2-diamine (0.100 g, 0.230 mmol) was dissolved in ethanol. Thereafter, ferrocenecarboxaldehyde (0.228 g, 1.06 mmol), TFA (0.00600 mL, 0.0725 mmol) and magnesium sulfate (0.635 g, 5.27 mmol) were added to the reaction vessel. The desired product was isolated as a dark red solid (**13**) (0.0312 g, 0.0312 mmol). **R_f (1:1 EtOAc: Pet. Ether)**: 0.32. **Yield:** 13.1%. **^{1}H NMR (300 MHz, DMSO) δ (ppm)**: 7.63 – 7.53 (m, 3H, H-d), 7.40 – 7.33 (m, 3H, H-g), 7.25 – 7.14 (m, 6H, H-e and H-f), 4.83 (br s, 6H, H-k), 4.50 – 4.35 (m, 12H, H-l and H-a), 4.15 (s, 15H, H-Cp), 3.03 (t, *J* = 7.2 Hz, 6H, H-b). **^{13}C{^{1}H}-NMR (151 MHz, DMSO) δ (ppm)**: 152.86 (C-i), 143.24 (C-h), 136.30 (C-c), 122.23 (C-e

and C-f), 118.88 (C-d), 110.39 (C-g), 74.58 (C-j), 70.31 (C-k), 69.96 (C-Cp), 69.43 (C-l), 54.43 (C-b), 43.14 (C-a). **FT-IR** (ATR) *v* (cm^{-1}): 1611 (imine C=N).**MP** (°C): 168.3 – 170.1. **MS (HR-ESI, *m/z*)**: Calculated: 1002.2327, Found: 1002.2359 (100%, $[M+H]^+$).

*6.5.2 Synthesis of tris(2-(2-ferrocenyl-5-(trifluoromethyl)-1H-benzo[d]imidazol-1-yl)ethyl)amine (**14**)*

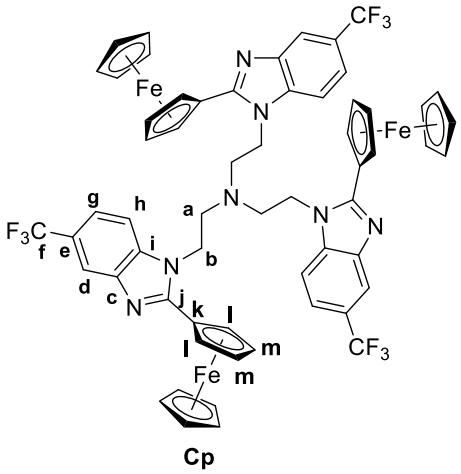

N^1-(2-(bis(2-((2-amino-4-(trifluoromethyl)phenyl)amino)ethyl)amino)ethyl)-4-(trifluoromethyl)benzene-1,2-diamine (0.103 g, 0.160 mmol) was dissolved in ethanol. Ferrocenecarboxaldehyde (0.124 g, 0.578 mmol), TFA (0.00369 mL, 0.0418 mmol) and magnesium sulfate (0.348 g, 2.89 mmol) were added to the reaction vessel. The pure product (**14**) was isolated as a pale orange solid (0.0616 g, 0.0511 mmol). **R_f (2:1 EtOAc: Pet. Ether)**: 0.22. **Yield:** 31.8%. **^{1}H NMR (600 MHz, DMSO) δ (ppm)**: 7.95 (s, 3H, H-d), 7.55 (d, *J* = 8.4 Hz, 3H, H-g), 7.49 (d, *J* = 8.4 Hz, 3H, H-h), 4.87 (br s, 6H, H-l), 4.48 (br s, 6H, H-m), 4.45 (t, *J* = 6.8 Hz, 6H, H-a), 4.15 (s, 15H, H-Cp), 3.03 (t, *J* = 6.8 Hz, 6H, H-b). **^{13}C{^{1}H}-NMR (151 MHz, DMSO) δ (ppm)**: 155.80 (C-j), 142.67 (C-c), 138.65 (C-i), 126.42 (C-e), 124.62 (C-f), 118.70 (C-g), 116.07 (C-d), 111.37 (C-h), 73.51 (C-k), 70.73 (C-m), 70.07 (C-Cp), 69.70 (C-l), 53.97 (C-b), 43.24 (C-a). **^{19}F{^{1}H}-NMR (377 MHz, DMSO) δ (ppm)**: -58.86 (d, J_{F-C} = 30.6 Hz). **FT-IR** (ATR) *v* (cm^{-1}): 1623 (imine C=N). **MP** (°C): 216.5 – 218.2. **MS (HR-ESI, *m/z*)**: Calculated: 1206.1956, Found: 1206.1980 (100%, $[M+H]^+$).

*6.5.3 Synthesis of tris(2-(5-methyl-2-ferrocenyl-1H-benzo[d]imidazol-1-yl)ethyl)amine (**15**)*

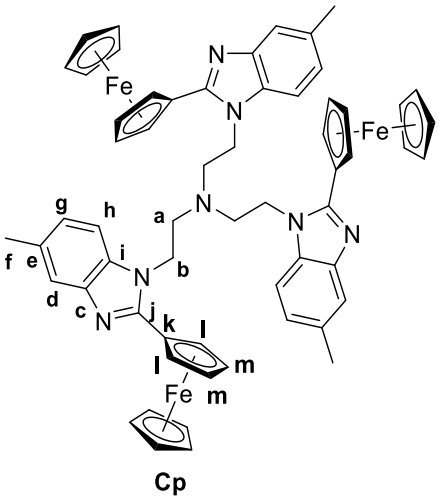

N^{1}-(2-(bis(2-((2-amino-4-methylphenyl)amino)ethyl)amino)ethyl)-4-methylbenzene-1,2-diamine (0.112 g, 0.231 mmol) was dissolve in ethanol. Ferrocenecarboxaldehyde (0.167 g, 0.701 mmol), TFA (0.00500 mL, 0.0650 mmol) and magnesium sulfate (0.483 g, 4.21mmol) were added to the reaction vessel. The desired product was isolated as a reddish-brown solid (**15**) (0.0480 g, 0.0460 mmol). **R_f (1:1 EtOac: Pet. Ether)**: 0.36. **Yield:** 22.0**%**. **^{1}H NMR (300 MHz, DMSO) δ (ppm):** 7.37 (s, 3H, H-d), 7.21 (d, *J* = 8.2 Hz, 3H, H-h), 7.02 (dd, *J* = 8.3, 1.2 Hz, 3H, H-g), 4.80 (br s, 6H, H-l), 4.43 (br s, 6H, H-m), 4.34 (t, *J* = 6.5 Hz, 6H, H-a), 4.13 (s, 15H, H-Cp), 2.98 (t, *J* = 6.2 Hz, 6H, H-b), 2.40 (s, 9H, H-g). **^{13}C{^{1}H}-NMR (101 MHz, DMSO) δ(ppm)**: 152.69 (C-j), 143.60 (C-i), 134.46 (C-c), 131.20 (C-e), 123.53 (C-h), 118.73 (C-d), 109.92 (C-g), 74.78 (C-k), 70.22 (C-l), 69.93 (C-Cp), 69.37 (C-m), 54.48 (C-b), 43.18 (C-a), 21.66 (C-f). **FT-IR** (ATR) *v* (cm^{-1}): 1620 (imine C=N). **MP** (°C): 139.1 – 141.7. **MS (HR-ESI, *m/z*)**: Calculated: 1044.2804, Found: 1044.2837 (100%, $[M+H]^{+}$).

6.6 The synthesis of *N*-ethyl-2-nitroaniline[3] (16)

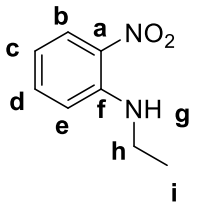

Ethylamine (0.630 mL, 9.48 mmol) was dissolved in DMF (5 mL) at room temperature. Thereafter, 1-fluoro-2-nitrobenzene (0.500 mL, 4.74 mmol) was added to the reaction vessel and the reaction was stirred at room temperature for 24 hours. After reaction completion was noted on TLC, the reaction mixture was diluted with a saturated brine solution (20 mL) and then extracted with two aliquots of ethyl acetate (2 x 20 mL). The organic extracts were collected and dried over anhydrous sodium sulfate, and excess solvent was reduced under vacuum. The resultant crude was purified using column chromatography (1: 19 EtOAc: Hexane) to afford the desired product (**16**) as a bright yellow oil (0.854 g, 5.14 mmol). **R_f (1:19 EtOAc: Hexane)**: 0.41. **Yield:** 90.1**%**. **^{1}H NMR (300 MHz, $CDCl_3$) δ (ppm)**: 8.15 (d, *J* = 7.8 Hz, 1H, H-b), 7.95 (s, 1H, H-g), 7.42 (t, *J* = 7.5 Hz, 1H, H-d), 6.84 (d, *J* = 8.6 Hz, 1H, H-e), 6.62 (t, *J* = 7.7 Hz, 1H, H-c), 3.44 – 3.25 (m, 3H, H-h), 1.37 (t, *J* = 7.2 Hz, 3H, H-i).

6.7 Synthesis of *N*^{1}-ethylbenzene-1,2-diamine[3] (17)

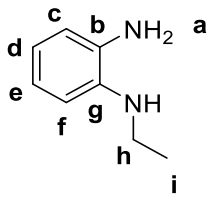

N-ethyl-2-nitroaniline (**16**) (0.800 g, 4.44 mmol) was added to a stirring solution of anhydrous methanol (10 mL). Ammonium chloride (2.37 g, 44.4 mmol) and zinc (5.81 g, 88.8 mmol) were subsequently added to the reaction vessel. The reaction mixture was stirred vigorously at room temperature for 1 hour. After 1 hour, TLC analysis showed the complete conversion of the starting materials to a new product. The reaction mixture was filtered through Celite® and rinsed with copious methanol. The filtrate was subsequently collected, and the excess solvent was reduced by rotary evaporation. The resultant residue was redissolved in ethyl acetate (30 mL) and washed with two aliquots of a saturated sodium

bicarbonate solution (2 x 30 mL) and thereafter deionized water (30 mL). The organic extract was collected, dried over anhydrous sodium sulfate and excess solvent was reduced *in vacuo* and the resultant crude was purified using column chromatography (100% ethyl acetate). The desired product (**18**) was isolated as a brown oil (0.541 g, 3.97 mmol). **R_f (100% EtOAc)**: 0.81. **Yield:** 89.5**%**. **^{1}H NMR (300 MHz, $CDCl_3$) δ(ppm)**: 6.90 – 6.81 (m, 1H, H-d), 6.77 – 6.65 (m, 3H, H-c, H-e, H-f), 3.26 (s, *J* = 12.0 Hz, 2H, H-a), 3.17 (q, *J* = 7.1 Hz, 2H, H-h), 1.32 (t, *J* = 7.1 Hz, 3H, H-i).

6.8 The synthesis of 1-ethyl-2-(pyridin-2-yl)-1*H*-benzo[*d*]imidazole[4] (18)

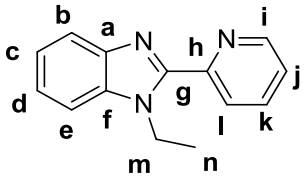

N[1]-ethylbenzene-1,2-diamine (**17**) (0.400 g, 2.94 mmol) was dissolved in anhydrous ethanol (5 mL) and stirred for 5 minutes. Thereafter, 2-pyridinecarboxaldehyde (0.420 mL, 4.41 mmol), magnesium sulfate (2.12 g, 17.6 mmol) and trifluoroacetic acid (0.023 mL, 0.294 mmol) were chronologically added to the reaction vessel. The reaction mixture was allowed to stir, open to air, for 24 hours at room temperature. TLC analysis confirmed the successful conversion of starting materials to a new product after 24 hours. The reaction mixture was subsequently filtered and the filtrate collected. The excess solvent was removed by rotary evaporation, and the resultant crude was redissolved in ethyl acetate (30 mL) and washed with a saturated sodium bicarbonate solution (30 mL) and a saturated brine solution (30 mL). The organic extract was collected and dried over anhydrous sodium sulfate, and the excess solvent was removed *in vacuo.* The resultant residue was purified using column chromatography (1: 2 EtOAc: Pet. Ether) and the desired product (**18**) was obtained as a dark brown viscous oil (0.337 g, 1.51 mmol). **R_f (1: 2 EtOAc: Pet. Ether)**: 0.33. **Yield:** 51.4**%**. **^{1}H NMR (300 MHz, $CDCl_3$) δ(ppm)**: 8.73 – 8.66 (m, 1H, H-i), 8.41 (d, *J* = 8.0 Hz, 1H, H-l), 7.88 – 7.76 (m, 2H, H-b, H-e), 7.50 – 7.40 (m, 1H, H-k), 7.38 – 7.28 (m, 3H, H-c, H-d, H-j), 4.87 (q, *J* = 7.1 Hz, 2H, H-m), 1.49 (t, *J* = 7.1 Hz, 3H, H-n).

6.9 The Synthesis of the cyclometallated *C,N*-Ru(II)-*p*-cymene metal complexes (19 – 21)

*6.9.1 Synthesis of cyclometallated Ru(II)-p-cymene metal complex (**19**)*

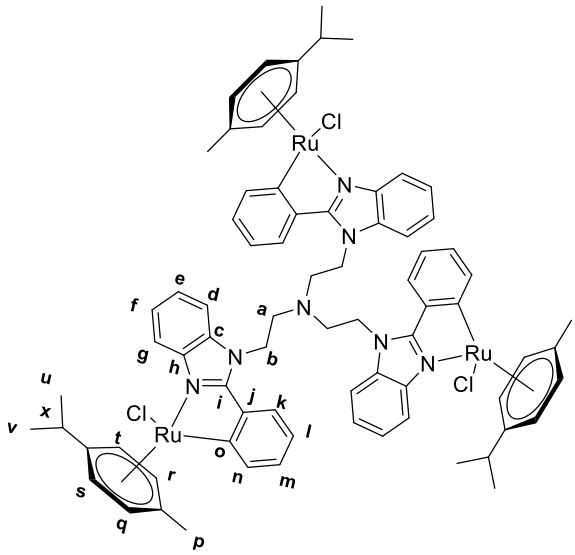

Tris(2-(2-phenyl-1*H*-benzo[*d*]imidazol-1-yl)ethyl)amine (0.0353 g, 0.0516 mmol) was dissolved in 1: 1 DCM: Ethanol (30 mL). To this brown solution, the dichloro (*p*-cymene)ruthenium(II) dimer (0.0474 g, 0.0774 mmol), sodium acetate (0.00853 g, 0.103 mmol) was added and the mixture was stirred at room temperature for 24 hours. After TLC analysis confirmed the conversion of the limiting reagent to a product spot, the reaction mixture was filtered through Celite®. The filtrate was collected, and excess solvent was reduced to *ca.* 1 mL, and this crude mixture was subjected to trituration in chloroform for 24 hours. A dark green crude was isolated by suction filtration, and this was re-dissolved in DCM (1 mL) and precipitated in pentane. The desired product (**19**) was isolated as a light green powder (0.0704 g, 0.0473 mmol) by suction filtration. **Yield**: 84.9%. **^{1}H NMR (300 MHz, DMSO) δ (ppm)**: 8.27 (d, $^{3}J_{HH}$ = 7.3 Hz, 3H, H-n), 7.97 (d, $^{3}J_{HH}$ = 8.0 Hz, 3H, H-g), 7.60 – 7.12 (m, 12H, H-d, H-e, H-f, H-k), 7.06 (t, $^{3}J_{HH}$ = 7.4 Hz, 3H, H-l), 6.86 (m, 3H, H-m), 5.97 (dd, $^{3}J_{HH}$ = 13.7 Hz, $^{4}J_{HH}$ = 6.9 Hz, 3H, H-r), 5.75 – 5.63 (m, 3H, H-q), 5.37 (dt, $^{3}J_{HH}$ = 11.2, 5.7 Hz, 3H, H-t), 5.19 (t, $^{3}J_{HH}$ = 5.8 Hz, 3H, H-s), 4.42 (s, 6H, H-a), 2.92 (br s, 6H, H-b), 1.63 (s, 9H, H-p), 0.70 – 0.54 (m, 9H, H-u), 0.53 – 0.36 (m, 9H, H-v). **^{13}C{^{1}H}-NMR (101 MHz, DMSO) δ (ppm)**: 141.34 (C-n), 124.11 (C-l), 123.63 (C-d, C-e, C-f), 122.54 (C-m), 117.91 (C-g), 111.05 (C-k), 89.75 (C-q), 89.88 (C-r), 82.56 (C-t), 81.06 (C-s), 53.93 (C-b), 43.59 (C-x), 30.69 (C-u), 22.42 (C-v), 21.70 (C-p),

18.84 (C-a). **FT-IR** (ATR) *v* (cm^{-1}): 1580 (imine C=N). **MP** (°C): 275.1 (decomp.). **MS (HR-ESI, *m/z*)**: Calculated: 1488.2580, Found: 1488.2526 (100%, $[M + H]^+$).

*6.9.2 Synthesis of the trifluoromethyl substituted Ru(II) cyclometallated complex (**20**)*

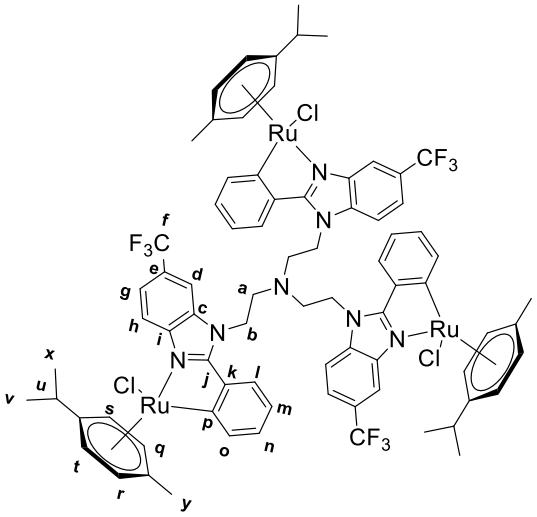

Tris(2-(2-phenyl-5-(trifluoromethyl)-1*H*-benzo[*d*]imidazol-1-yl)ethyl)amine (0.0210 g, 0.0227 mmol) was dissolved in dry acetonitrile (10 mL). The dichloro(*p*-cymene)ruthenium(II) dimer (0.0222 g, 0.0363 mmol) and sodium acetate (0.0112 g, 0.136 mmol) were then added to the reaction vessel. The reaction mixture was then allowed to stir at room temperature for 24 hours, after which the complete reaction of the limiting reagent was observed upon TLC analysis. The reaction mixture was then filtered through Celite ® and the filtrate was collected. Excess solvent was removed by rotary evaporation and the resulting crude was re-dissolved in DCM (*ca.* 1 mL). Hexane was subsequently added to the vessel, resulting in a dark yellow precipitate (**20**) which was isolated by suction filtration (0.0479 g, 0.0283 mmol). **Yield:** 83.3%. **^{1}H NMR (300 MHz, $CDCl_3$) δ(ppm)**: 8.30 (d, *J* = 7.5 Hz, 3H, H-o), 7.99 (m, 3H, H-h), 7.59 – 7.23 (m, 15H, H-g, H-d, H-l), 6.99 – 6.69 (m, 6H, H-m, H-n), 5.77 (t, $^3J_{HH}$ = 5.7 Hz, 3H, H-q), 5.66 (t, $^3J_{HH}$ = 5.4 Hz, 3H, H-s), 5.36 – 5.16 (m, 3H, H-r), 5.02 (t, $^3J_{HH}$ = 5.3 Hz, 3H, H-t), 3.67 (s, 6H, H-a), 2.33 – 2.08 (m, 9H, H-b, H-u), 1.98 (dd, *J* = 5.4, 2.4 Hz, 9H, H-y), 0.80 (dd, $^3J_{HH}$ = 13.8 Hz, $^4J_{HH}$ = 8.4 Hz, 9H, H-x), 0.64 (dd, $^3J_{HH}$ = 12.6 Hz, $^4J_{HH}$ = 6.0 Hz, 9H, H-v). **^{13}C{^{1}H}-NMR (151 MHz, $CDCl_3$) δ (ppm)**: 161.05, 142.17, 138.99, 135.47 – 133.80 , 131.85, 130.41, 126.40, 123.88, 121.63, 116.83 – 114.65 (m), 113.66, 103.81 – 103.05 (m), 101.64 – 100.21 (m), 91.49, 90.30, 83.33, 81.98, 53.39, 45.73 (d, J = 37.0 Hz), 44.24, 32.30, 31.09, 23.86, 23.17, 20.37, 15.50. **FT-IR** (ATR)

v (cm^{-1}): 1581 (imine C=N). **MS (HR-ESI, *m/z*)**: Calculated: 1156.9920, Found: 1157.3227 (40% [M + Na^+ - $C_{26}H_{25}ClF_3N_2Ru]^+$). **Elemental Analysis** for $C_{78}H_{75}Cl_3F_9N_7Ru_3{\cdot}3H_2O$ (1745.098 $g.mol^{-1}$): Found (%) C, 53.95%; H, 4.31%; N, 6.12%; Calculated (%) C, 53.69%; H, 4.68%; N, 5.62%.

*6.9.3 Synthesis of the methyl substituted Ru(II) cyclometallated complex (**21**)*

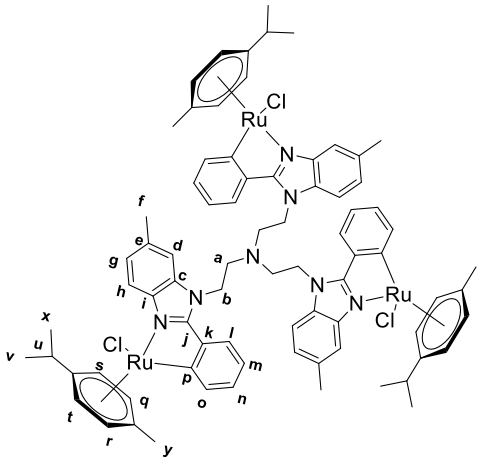

Tris(2-(5-methyl-2-phenyl-1*H*-benzo[*d*]imidazol-1-yl)ethyl)amine (0.0291 g, 0.0405 mmol) was dissolved in anhydrous acetonitrile (8 mL). To this solution, dichloro(*p*-cymene)ruthenium(II) dimer (0.0384 g, 0.0627 mmol), sodium acetate (0.0350 g, 0.427 mmol) was added and the mixture was stirred at room temperature for 24 hours. After TLC analysis (in 100% ethyl acetate) confirmed the complete conversion of the limiting reagent to a product spot, the reaction mixture was filtered through Celite®. The filtrate was collected, and excess solvent was removed, and the resultant crude was re-dissolved in *ca.* 1 mL DCM and hexane (12 mL) was subsequently added to the solution. This resulted in the precipitation of a dark yellow-brownish precipitate (**21**) which was isolated *via* suction filtration (0.0638 g, 0.0417 mmol). **Yield:** 88.3%. **^{1}H NMR (300 MHz, DMSO) δ (ppm):** 8.26 (t, $^3J_{HH}$ = 6.7 Hz, 3H, H-o), 7.72 (d, $^3J_{HH}$ = 4.4 Hz, 3H, H-h), 7.61 – 6.73 (m, 18H, H-n, H-m, H-l, H-g, H-d), 6.11 – 5.88 (m, 3H, H-q), 5.68 (t, $^3J_{HH}$ = 6.0 Hz, 3H, H-s), 5.47 – 5.27 (m, 3H, H-r), 5.23 – 5.12 (m, 3H, H-t), 4.54 – 4.23 (m, 6H, H-a), 2.84 – 2.74 (m, 6H, H-b), 2.65 – 2.55 (m, 6H, H-f), 2.42 (d, $^3J_{HH}$ = 3.9 Hz, 3H, H-f), 1.95 – 1.62 (m, 12H, H-y, H-u), 0.72 – 0.54 (m, 9H, H-x), 0.51 – 0.35 (m, 9H, H-u). **^{13}C{^{1}H}-NMR (151 MHz, DMSO) δ(ppm)**: 157.46,

146.16, 145.41, 141.62, 141.32, 135.00, 134.15, 134.05, 133.00, 129.25, 128.10, 126.53, 124.91, 123.93, 122.46, 89.88, 88.88, 82.93, 80.84, 33.43, 30.78, 24.43, 22.38, 21.79, 21.01, 18.94. **FT-IR** (ATR) *v* (cm^{-1}): 1578 (imine C=N). **MS (HR-ESI, *m/z*)**: Calculated: 1493.9860, Found: 1494.3296 (70% [M - Cl]$^{+}$). **Elemental Analysis** for $C_{78}H_{84}Cl_3N_7Ru_3{\cdot}3H_2O$ (1583.184 $g.mol^{-1}$): Found (%) C, 59.36%; H, 5.82%; N, 5.85%; Calculated (%) C, 59.18%; H, 5.73%; N, 6.19%.

6.10 General synthetic procedure for the cationic *N,N*-Ru(II)-*p*-cymene metal complexes (22 – 24)

The ruthenium dimer [Ru(η^6-*p*-Pr^iC_6H_4Me)Cl_2]$_2$ (1.5 eq.) was added to a stirring solution of the appropriate 2-pyridyl tris-benzimidazole ligand (1 eq.) in a 1: 1 *v/v%* solution of DCM: Ethanol. The reaction mixture was stirred at room temperature for 24 hours. After TLC analysis confirmed the complete reaction of the limiting reagent, the contents of the reaction flask were filtered through Celite® and the filtrate was collected. NH_4PF_6 (4 eq.) was added to the filtrate and was allowed to stir for at room temperature for 1 hour. The DCM was removed from the reaction mixture under reduced pressure, which resulted in the precipitation of a yellow solid. The solid was isolated by suction filtration, washed with cold ethanol and dried.

*6.10.1 Synthesis of the cationic N,N-Ru(II)-p-cymene metal complex (**22**)*

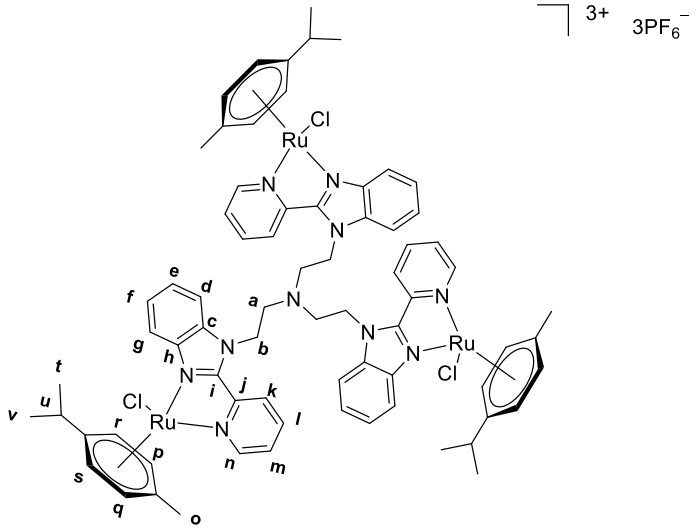

Tris(2-(2-phenyl-1*H*-benzo[*d*]imidazol-1-yl)ethyl)amine (0.0354 g, 0.0520 mmol) was reacted with dichloro(*p*-cymene)ruthenium(II) dimer (0.0478 g, 0.0780 mmol) at room temperature for 24 hours. Thereafter, NH_4PF_6 (0.0487 g, 0.299 mmol) was added to the reaction mixture and stirred for an additional hour. The desired product (**22**) was isolated by vacuum filtration as a dark yellow solid (0.0435 g, 0.0265 mmol). **Yield:** 51.1%. **^{1}H NMR (300 MHz, DMSO) δ (ppm):** 9.69 – 9.55 (m, 3H, H-n), 8.14 – 7.92 (m, 9H, H-m, H-l, H-e), 7.83 – 7.40 (m, 12H, H-k, H-d, H-f, H-g), 6.31 (d, $^3J_{HH}$ = 6.0 Hz, 3H, H-p), 6.27 (d, $^3J_{HH}$ = 6.0 Hz, 3H, H-q), 6.13 (d, $^3J_{HH}$ = 5.1 Hz, 3H, H-r), 6.05 (d, J^3J_{HH} = 5.8 Hz, 3H, H-s), 4.60 – 4.23 (m, 6H, H-a), 3.11 – 2.80 (m, 6H, H-b), 2.42 – 2.24 (m, 3H, H-u), 2.13 (s,9H, H-o), 0.91 – 0.73 (m, 9H, H-v, H-t). **^{13}C{^{1}H}-NMR (101 MHz, DMSO) δ (ppm)**: 157.98 (C-n), 148.39 (C-j), 145.46 (C-h), 140.23 (C-i), 127.64 (C-l), 126.90 (C-c), 126.18 (C-m), 124.69 (C-k), 119.46 (C-e), 119.31 (C-f) ,119.19 (C-g), 112.94 (C-d), 84.53 (C-p), 83.16(C-q), 80.72 (C-r), 79.64 (C-s), 52.32 (C-b), 44.36 (C-a), 30.96 (C-u), 22.25 (C-t), 22.13 (C-v), 19.09 (C-o). **^{31}P{^{1}H}-NMR (162 MHz, DMSO) δ (ppm)**: -144.13 (sep, *J* = 711.2 Hz, PF_6). **FT-IR** (ATR) *v* (cm^{-1}): 1599 (imine C=N), 1481 (pyridyl C=N). **MP** (°C): 225.2 (decomp.). **MS (HR-ESI, *m/z*)**: Calculated: 1783.9759, Found: 1784.1482 (70%, $[M - PF_6 + H]^{2+}$).

*6.10.2 Synthesis of the cationic N,N-Ru(II)-p-cymene metal complex (**23**)*

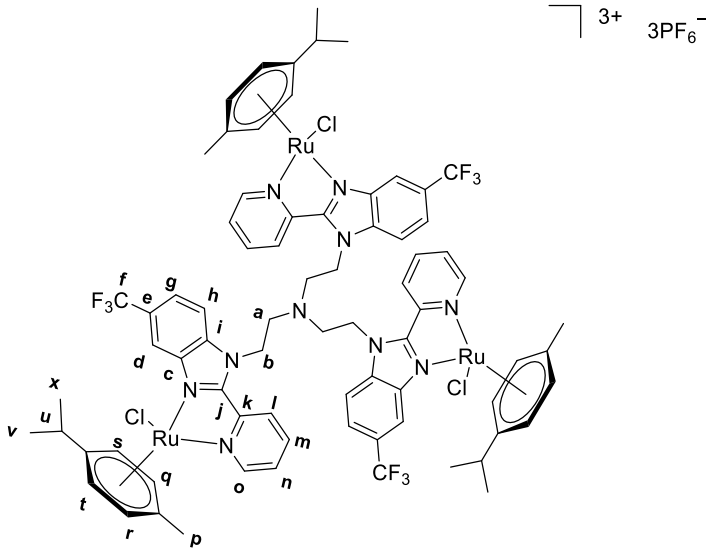

The ruthenium dimer $[Ru(\eta^6\text{-}p\text{-}Pr^iC_6H_4Me)Cl_2]_2$ (0.0636 g, 0.104 mmol) was reacted with tris(2-(2-(pyridin-2-yl)-5-(trifluoromethyl)-1*H*-benzo[*d*]imidazol-1-yl)ethyl)amine (0.0529 g, 0.0735 mmol) at room temperature. NH_4PF_6 (0.0356 g, 0.434 mmol) was added to the reaction mixture and stirred for an additional hour. The desired product (**24**) was isolated as a bright yellow solid (0.0523 g, 0.0293 mmol). **Yield**: 69.3%. **^{1}H NMR (600 MHz, DMSO) δ (ppm)**: 9.68 – 9.60 (m, 3H, H-o), 8.17 – 7.99 (m, 9H, H-n, H-l and H-d), 7.94 – 7.83 (m, 6H, H-g and H-h), 7.82 – 7.70 (m, 3H, H-m), 6.37 – 6.26 (m, 6H, H-q and H-s), 6.13 (dd, $^3J_{HH}$ = 13.1 Hz, $^4J_{HH}$ = 6.5 Hz, 3H, H-r), 6.07 – 5.99 (m, 3H, H-t), 4.68 – 4.32 (m, 6H, H-a), 3.12 – 2.89 (m, 6H, H-b), 2.47 – 2.40 (m, 3H, H-u), 2.13 – 2.08 (m, 9H, H-p), 0.91 – 0.83 (m, 18H, H-x and H-v). **^{13}C{^{1}H}-NMR (151 MHz, DMSO) δ (ppm)**: 158.13 (C-o), 150.88 (C-j), 144.84 (C-k), 140.91 (C-d), 139.88 (C-i), 138.47 (C-c), 128.22 (C-m),125.76 (C-e), 123.38 (C-l), 116.14 (C-*p*-cye), 115.05 (C-h), 104.51 (C-f), 87.20 (C-q), 84.96 (C-s), 83.41 (C-t), 81.69 (C-r), 52.48 (C-b), 45.20 (C-a), 31.46 (C-u), 22.31 (C-x), 22.16 (C-v), 19.34 (C-p). **^{31}P{^{1}H}-NMR** (162 MHz, DMSO) δ (ppm): -144.10 (sep, *J* = 711.1 Hz, PF_6). **^{19}F NMR (377 MHz, DMSO) δ (ppm)**: -59.32 (s, *J* = 7.4 Hz), -70.34 (dd, *J* = 711.0, 13.7 Hz). **FT-IR** (ATR) *v* (cm^{-1}): 1572 (imine C=N), 1490 (pyridyl C=N). **MP** (°C): 231.2 (decomp.). **MS (HR-ESI, *m/z*)**: Calculated: 1823.0329, Found: 1823.1600 (80%, $[M - PF_6 + 2H]^{3+}$).

*6.10.3 Synthesis of the cationic N,N-Ru(II)-p-cymene metal complex (**24**)*

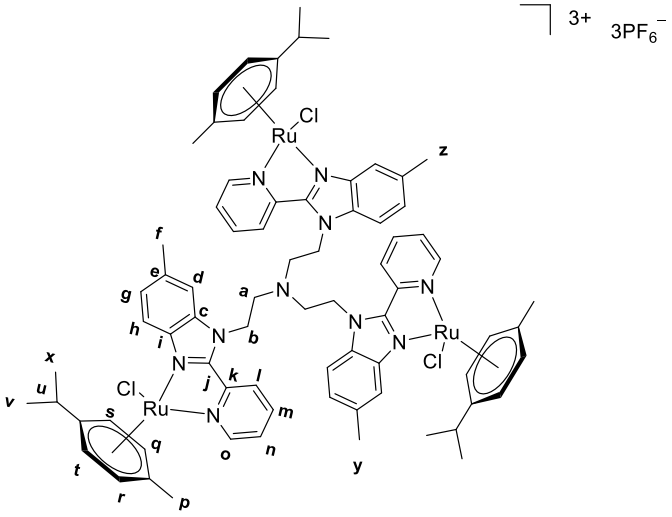

The ruthenium dimer [Ru(η^6-*p*-Pr^{i}C$_6$H$_4$Me)Cl$_2$]$_2$ (0.0382 g, 0.0624 mmol) was reacted with tris(2-(5-methyl-2-(pyridin-2-yl)-1H-benzo[*d*]imidazol-1-yl)ethyl)amine (0.0292 g, 0.0404 mmol)in a at room temperature. NH_4PF_6 (0.0487 g, 0.299 mmol) was addeds to the reaction mixture and stirred for 1 hour. The desired product (**23**) was isolated as a bright yellow solid (0.0597 g, 0.0303 mmol). **Yield**: 75.0%. **^{1}H NMR (400 MHz, DMSO) δ (ppm)**: 9.67 – 9.53 (m, 3H, H-o), 8.10 – 7.87 (m, 6H, H-n and H-d), 7.71 (ddd, $^2J_{HH}$ = 28.5 Hz, $^3J_{HH}$ = 16.6 Hz, $^4J_{HH}$ = 10.1 Hz, 6H, H-m and H-l), 7.54 – 7.27 (m, 6H, H-g and H-h), 6.33 (t, $^3J_{HH}$ = 7.3 Hz, 3H, H-q), 6.25 (d, $^3J_{HH}$ = 6.0 Hz, 3H, H-s), 6.15 (dd, $^3J_{HH}$ = 13.2 Hz, $^4J_{HH}$ = 6.5 Hz, 3H, H-r), 6.04 (d, $^3J_{HH}$ = 5.9 Hz, 3H, H-t), 4.53 – 4.17 (m, 6H, H-a), 2.95 (d, $^3J_{HH}$ = 22.9 Hz, 6H, H-b), 2.65 (s, 3H, H-f), 2.62 (s, 3H, H-y), 2.57 (s, 3H, H-z), 2.39 – 2.26 (m, 3H, H-u), 2.13 (t, $^3J_{HH}$ = 7.1 Hz, 9H, H-p), 0.85 – 0.75 (m, 18H, H-x and H-v). **^{13}C{^{1}H}-NMR (101 MHz, DMSO) δ (ppm)**: 157.85 (C-o), 148.01 (C-k), 145.52 (C-j), 140.59 (C-i), 140.23 (C-n), 136.25 (C-c), 134.35 (C-e), 128.58 (C-h), 127.44 (C-l), 124.31 (C-d), 118.31 (C-m), 112.51 (C-g), 87.07 (C-s), 84.72 (C-q), 82.96 (C-t), 80.27 (C-r), 55.35 (C-*p-cye*), 53.07 (C-*p-cye*), 52.53 (C-b), 44.24 (C-a), 30.97 (C-u), 22.31 (C-x, C-v), 22.10 (C-f, C-y), 21.64 (C-z), 19.13 (C-p). **^{31}P{^{1}H}-NMR (162 MHz, DMSO) δ (ppm)**: -144.16 (sep, *J* = 711.2 Hz, PF_6). **FT-IR** (ATR) *v* (cm^{-1}): 1674 (imine C=N), 1464 (pyridyl C=N). **MP** (°C): 236.8 (decomp.). **MS (HR-ESI, *m/z*)**: Calculated: 1986.4225, Found: 1986.0101 (20%, [M – PF_6]$^+$).

*6.10.4 Mononuclear cationic N,N-Ru(II)-p-cymene complex (**25**)*

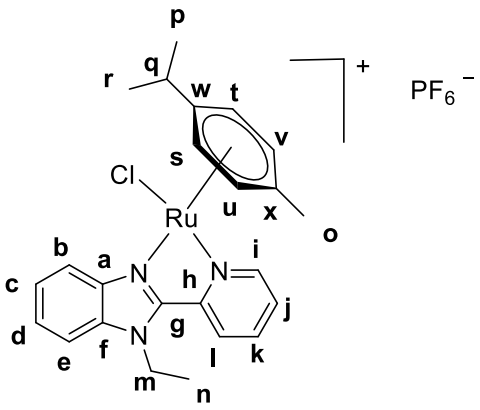

1-Ethyl-2-(pyridin-2-yl)-1*H*-benzo[*d*]imidazole (0.0784 g, 0.352 mmol) was reacted with dichloro(*p*-cymene)ruthenium(II) dimer (0.107 g, 0.176 mmol) at room temperature for 24 hours. NH_4PF_6 (0.0494 g, 0.301 mmol) was added to the reaction mixture and stirred for 1 hour. The desired product (**22**) was isolated by vacuum filtration as a yellow solid (0.0899 g, 0.141 mmol). **Yield**: 81.3%. **^{1}H NMR (300 MHz, DMSO) δ(ppm)**: 9.72 (d, *J* = 5.1 Hz, 1H, H-i), 8.52 (d, *J* = 8.1 Hz, 1H, H-j), 8.36 (t, *J* = 7.4 Hz, 1H, H-l), 8.13 (dd, *J* = 6.9, 1.8 Hz, 1H, H-k), 8.09 – 8.03 (m, 1H, H-b), 7.90 – 7.82 (m, 1H, H-e), 7.75 – 7.62 (m, 2H, H-c, H-d), 6.38 (d, *J* = 6.1 Hz, 1H, H-t), 6.33 (d, *J* = 6.2 Hz, 1H, H-s), 6.21 (d, *J* = 6.1 Hz, 1H, H-u), 6.11 (d, *J* = 6.1 Hz, 1H, H-v), 5.04 – 4.76 (m, 2H, H-m), 2.48 – 2.38 (m, 1H, H-q), 2.24 (s, 3H, H-o), 1.43 (t, *J* = 7.1 Hz, 3H, H-n), 0.92 – 0.85 (m, 6H, H-p, H-r). **^{13}C{^{1}H}-NMR (151 MHz, DMSO) (ppm)**: 157.91 (C-i), 148.30 (C-h), 145.64 (C-g), 140.86 (C-a), 140.45 (C-k), 135.78 (C-f), 127.70 (C-l), 126.81 (C-c), 126.02 (C-d), 125.15 (C-j), 119.10 (C-b), 112.88 (C-e), 104.79 (C-x), 103.27 (C-w), 86.90 (C-u), 84.54 (C-v), 83.16 (C-t), 80.57 (C-s), 40.93 (C-m), 30.97 (C-q), 22.13 (C-r), 22.10 (C-p), 19.10 (C-o), 15.19 (C-n). **MS (HR-ESI, *m/z*)**: Calculated: 494.0937, Found: 494.0948 (100% $[M - PF_6]^+$). **FT-IR** (ATR)*v* (cm^{-1}): 1592 (imine C=N), 1493 (pyridyl C=N). **MP** (°C): 186.3 (decomp.).

6.11 Single crystal X-ray crystallography

Single crystal X-ray diffraction data were collected on a Bruker KAPPA APEX II DUO diffractometer using graphite-monochromated Mo-Kα radiation (χ = 0.71073 Å). Data collection was carried out at 173(2) K. Temperature was controlled by an Oxford Cryostream cooling system (Oxford Cryostat). Cell refinement and data reduction were performed using the program SAINT.[5] The data were scaled, and absorption correction performed using SADABS.[6] The structure was solved by direct methods using SHELXS-97[6] and refined by full-matrix least-squares methods based on F^2 using SHELXL-2014[6] and using the graphical interface program X-Seed.[7] The programs X-Seed and POV-Ray[8] were used to prepare molecular graphic images. All non-hydrogen atoms were refined anisotropically. All hydrogen atoms were placed in idealized positions and refined in riding models with U_{iso} assigned 1.2 or 1.5 times U_{eq} of their parent atoms and the bond distances were constrained in the range from 0.95 Å to 0.99 Å.

6.12 Cell culture

The human breast adenocarcinoma cell line, MCF-7 (oestrogen-receptor positive, ER+) and the human melanoma cell line 501mel were maintained in Roswell Park Memorial Institute (RPMI) 1640 medium (Sigma Aldrich, USA). The human breast adenocarcinoma cell line, MDA-MB-231 (triple-negative, TNBC) was maintained in Dulbecco's Modified Eagle's Medium (DMEM) (Sigma Aldrich, USA). All culture medium was supplemented with 10% heat-inactivated foetal bovine serum (FBS), 100 U/mL penicillin and 100 µg/mL streptomycin. The non-tumorigenic human breast epithelial MCF-12A cells were maintained in complete media consisting of DMEM/ Ham's F12 supplemented with 10% heat-inactivated fetal bovine serum (FBS), 100 U/ml penicillin, 0.1 µg/ml cholera toxin (Sigma, St. Louis, MO, USA), 0.5 µg/ml hydrocortisone (Calbiochem, Billerica, MA), 10 µg/ml insulin (Novorapid; Novo Nordisk, Copenhagen, Denmark), 20 ng/ml epidermal growth factor (Gibco, Life Technologies, Carlsbad, CA), and 5% horse serum (Highveld Biological, Lyndhurst, South Africa). Cells were maintained at 37 °C in a 95% air and 5% CO_2 humidified incubator and medium was replaced every 2 to 3 days.

6.13 Cytotoxicity studies

Cells (MCF-7, MDA-MB-231, 501mel and MCF-12A) were seeded in a 96-well plate at a density of 4500 cells/well, 3000 cells/well, 4000 cells/well and 6000 cells/well, respectively, and were incubated for either 48 hours (MCF-7, 501mel and MCF-12A cell lines) or 24 hours (MDA-MB-231 cell line), respectively, to allow adhesion. After adhesion, the cells were treated with either the vehicle (0.1% DMSO) or 10 µM or 20 µM of the test compounds for 48 hours. The impact of the test compounds on cell viability of cancer cells was determined using the 3-(4,5-dimethylthiazol-2-yl)-2,5 diphenyltetrazolium bromide (MTT) assay as described in literature.[9] The absorbance at 600 nm was determined for each well using a spectrophotometer (GloMax® Explorer Multimode Microplate Reader GM3500, Promega) and normalized to the RPMI medium (for the MCF-7 cell line) absorbance. For IC_{50} (concentration required for 50% viability) determination of selected compounds, cells were treated using concentrations 5 – 35 µM. These experiments were performed twice in quadruplicate, and the mean cell viability determined using GraphPad Prism V.5.01 software.

6.14 Solution stability and 5'-GMP binding study

The solvent stability of the trimetallic complexes (**22** – **24**) was assessed using UV/ Vis spectroscopy, in which 5.00 mg of each complex was dissolved in 1 mL of DMSO. The samples were heated and maintained at 37 °C for the duration of sampling. UV/ Vis spectra were recorded at 0, 2.5, 5, 24, 26.5 29, 31.5 and 48 hours after the initial sample preparation. The UV/ Vis spectra were recorded on a Shimadzu UV-1800 spectrophotometer which was set to measure absorbance at wavelengths between 250 and 800 nm. The interaction of the complex **22** was investigated by ^{1}H NMR experiments in which 3.00 mg of **22** and 3.00 mg of 5'-GMP was dissolved in a mixture of 0.5 mL of H_2O and 0.5 mL of DMSO (d_6). The samples were heated and maintained at 37 °C for the duration of the experiment. The ^{1}H NMR spectra were recorded at 0 and 24 hours after initial sample preparation.

6.15 References

1 M. A. Bennett and A. K. Smith, *Dalton Trans.*, 1974, 233–241.

2 R. Hernández Sánchez, A. M. Willis, S.-L. Zheng and T. A. Betley, *Angew. Chem. Int. Ed. Engl.*, 2015, **54**, 12009–12013.

3 E. J. Hennessy, V. Oza, A. Adam, K. Byth, L. Castriotta, G. Grewal, G. A. Hamilton, V. M. Kamhi, P. Lewis, D. Li, P. Lyne, L. Öster, M. T. Rooney, J. C. Saeh, L. Sha, Q. Su, S. Wen, Y. Xue and B. Yang, *J. Med. Chem.*, 2015, **58**, 7057–7075.

4 L. Huang, K. Z. Wang, C. H. Huang, F. Y. Li and Y. Y. Huang, *J. Mater. Chem.*, 2001, **11**, 790–793.

5 A. Bruker and A. X. S. Saint, *Acta Crystallogr. Sect. A Fundam. Crystallogr.*, 2008, **64**, 112–122.

6 G. M. Sheldrick, *Acta Crystallogr. Sect. C Struct. Chem.*, 2015, **71**, 3–8.

7 L. J. Barbour, *J. Supramol. Chem.*, 2001, **1**, 198–191.

8 http://www.povray.org., http://www.povray.org.

9 T. Mosmann, *J. Immunol. Methods*, 1983, **65**, 55–63.